THE INFLUENCE OF TEMPERATURE STRATIFICATION IN THE LOWER ATMOSPHERIC BOUNDARY LAYER ON THE OPERATING POINT OF A NATURAL DRAFT DRY-COOLING TOWER

by

Jacob Elisa Hoffmann

Dissertation presented for the degree Doctor of Philosophy
(Mechanical Engineering) at the University of Stellenbosch

Promoter: Prof. D.G. Kröger

Department of Mechanical Engineering
University of Stellenbosch
November 1997

Declaration

I, the undersigned, declare that the work contained in this dissertation is my own original work, and has not previously in its entirety or in part been submitted at any university for a degree.

Date: 17 November 1997

ABSTRACT

Natural draft dry-cooling towers for power stations are designed to reject heat at a prescribed rate under specified atmospheric conditions. In the past, cooling tower designs were based on the annual average ambient air temperature, measured at 1.5 m above the ground (the reference temperature). Furthermore, the air flow through the tower was calculated according to an adiabatic temperature lapse rate in the atmosphere. However, the air inlet temperature at the heat exchanger may deviate significantly from the reference temperature due to temperature stratification in the atmosphere and the fact that the tower draws in air from considerable heights above the ground. Furthermore, the buoyancy force that drives the air through a natural draft cooling tower is also affected by ambient air temperature stratifications. In this thesis, a logical build-up to a final numerical model is followed. The physics of the formation of atmospheric temperature profiles and their relation to large scale weather patterns are discussed first, followed by a section on the heat and momentum transfer processes encountered in a natural draft dry-cooling tower. This is followed by a discussion of field data, and it all culminates in the application of this theory and data in a numerical example, illustrating the usefulness of the proposed model.

Keywords:

Temperature stratification, temperature lapse rate, atmospheric temperature profiles, dry-cooling tower, cooling tower design.

OPSOMMING

Natuurlike trek droë koeltorings vir kragstasies word ontwerp om van 'n gegewe warmtelas ontslae te raak onder heersende atmosferiese toestande. Huidiglik word die jaarlikse gemiddelde omgewingstemperatuur as verwysingspunt gebruik in koeltoringontwerp. Dit is internasionaal die standaard om dié temperatuur 1.5 m bokant die grond te meet. Verder word 'n adiabatiese temperatuurverdeling in die atmosfeer aanvaar vir gebruik in die trekvergelyking. Op enige spesifieke oomblik kan die luginlaattemperatuur by die warmte-uitruiler egter beduidend van die gemete omgewingstemperatuur verskil. Die rede hiervoor is dat sterk temperatuurgradiënte dikwels in die eerste paar meter van die atmosfeer voorkom. Groot natuurlike trek droë koeltorings suig lug in wat hierdie gebied insluit, vandaar die verskil. Verder beïnvloed die temperatuurgradiënte ook boonop die lugvloei deur die toring, met verdere implikasies vir die warmteoordrag. In hierdie tesis word 'n logiese opbou tot 'n voorgestelde numeriese model gevolg. Eerstens word die fisiese prosesse in die atmosfeer wat aanleiding tot temperatuurgradiënte gee, en hul verhouding met makro-skaal weerstoestande, aangespreek. Dit word opgevolg met 'n bespreking van die warmte- en momentumoordragsprossesse in 'n natuurlike trek droë koeltoring.. Hierdie teorië word daarna getoets teen eksperimentele data wat by 'n kragstasie gemeet is. Ten slotte word die toepassing van die voorgestelde model aan die hand van 'n numeriese voorbeeld geïllustreer.

Sleutelwoorde:

Atmosferiese grenslaag, temperatuurgradiënt, temperatuurprofiel, droë koeltoring, koeltoring ontwerp.

ACKNOWLEDGEMENT

The author is indepted to the following individuals and institutions for their valuable contributions to this thesis:

Prof. D.G. Kröger, promoter.

Prof. G. Ernst and Dr. J. Madadnia, external examiners, and Dr. T. Harms, internal examiner.

Dr. M. Jury, for his contribution on atmospheric science.

Dr. C.G. du Toit, for his guidance with the numerical work.

My wife Tanya, for her love, patience, encouragement, and also typing and proofreading the text.

The FRD and Water Research Commission for their financial support.

INDEX

CHAPTER 4: FULL SCALE TESTS

CHAPTER 5: NUMERICAL ANALYSIS

CHAPTER 6: ILLUSTRATIVE EXAMPLES

NOMENCLATURE

A	Area	m^2
	Hour angle	
	Series of constants	
a	Extinction coefficient	
	Entrainment coefficient	
	Coefficient	
b	Exponent	
	Plume width	m
C_d	Drag coefficient	
c	Specific heat	J/kg K
	Arbitrary constant	
d	Diameter	m
F	Force	N
	Temperature correction factor	
f	Friction factor	
g	Gravitational acceleration	m/s^2
H	Height	m
h	Heat transfer coefficient	W/m^2 K
I	Radiative heat flux	W/m^2
K	Pressure loss coefficient	
k	Linear heat transfer coefficient	W/m K
L	Length	m
	Monin-Obukhov scaling length {defined by equation (2.5-8)}	m
M	Source (or sink) strength	
m	Mass flow rate	kg/s
N	Cloud cover factor	
Ny	Heat transfer number	m^{-1}
n	Number	
	Degrees of freedom (Legendre functions)	

P	Legendre function	
p	Pressure	N/m^2
Q	Heat transfer rate	W
q	Heat transfer rate per unit volume	W/m^3
R	Gas constant for air	J/kg K
	Radius of sphere	m
r	Radius of circle or cylinder	m
Ry	Characteristic flow number	m^{-1}
S	Source term in generalised transport equation	
s	Stability class	
T	Temperature	K
t	Time	s
U	Overall heat transfer coefficient	W/m^2 K
v	Velocity component (subscript indicates direction)	m/s
v	Velocity vector	m/s
X	Meteorological parameter {defined by equation (4.5-1)}	K/m
x	Space co-ordinate (length)	m
y	Space co-ordinate (width)	m
z	Space co-ordinate (height)	m

Greek symbols

α	Albedo	
Γ	Diffusion coefficient	m^2/s
γ	Isentropic index	
Δ	Difference	
δ	Thickness	m
ε	Effectiveness	
	Roughness length	m
η	Efficiency	

Θ	Solar altitude angle	
θ	Potential temperature	K
	Latitude angle (Legendre functions)	
θ_*	Scaling temperature {defined by equation (2.5-6)}	K
κ	Von Karman's constant	
λ	Separation constant	
μ	Dynamic viscosity	kg/m s
ξ	Similarity variable {defined by equation 2.5-9)}	
π	Mathematical constant pi	
ρ	Density	kg/m^3
σ	Stefan-Boltzmann constant	$W/m^2 K^4$
	Porosity	
τ	Shear stress	N/m^2
Φ	Solar declination angle	
ϕ	Longitude angle (Legendre functions)	
	General variable	
	General function	
Ψ	Latitude	
ψ	Stream function	
Ω	Rotational speed of the earth	s^{-1}

Subscripts

0	Reference state or position
1	Defined by figure 3-2
2	Defined by figure 3-2
3	Defined by figure 3-2
4	Defined by figure 3-2
5	Defined by figure 3-2
6	Defined by figure 3-2

10	At 10 m above ground level
1.2	At 1.2 m above ground level
a	Air
ae	Effective air side
ai	Air inlet
ao	Air outlet
B	Boundary node
b	Bulk
c	Constant flux layer
ct	Cooling tower
ctc	Cooling tower contraction
cte	Cooling tower expansion
d	Drag
E	Eastern neighbor
e	Eastern boundary
	Entrainment
f	Fin
fr	Frontal
geo	Geometric
gx	Geostrophic in x-direction
gy	Geostrophic in y-direction
h	Heat
he	Heat exchanger
ht	Heat transfer
I	Internal node
I	Inlet
	Internal node boundary
iso	Isothermal
k	Belonging to the k^{th} cell
lm	Logarithmic mean
LW	Long wavelength
m	Momentum

	Mean
n	n^{th} degree of freedom (Legendre functions)
Ny	Belonging to the heat transfer number
o	Outlet
p	Planetary boundary layer
	Constant pressure
r	Root
Ry	Belonging to the flow parameter
s	Solar
sens	Sensible
soil	Soil
t	Tube
	Throat
ts	Tower supports
W	Western neighbor
w	Water
	Wall
	Western boundary
wi	Water inlet
wo	Water outlet
x	In the x-direction
y	In the y-direction
z	In the z-direction
*	Scaling
∞	Far away
	Free stream
ϕ	Belonging to the general variable ϕ

Dimensionless groups

Fr	Froude number
Nu	Nusselt number
Pe	Peclet number
Pr	Prandtl number
Re	Reynolds number

CHAPTER 1

INTRODUCTION

The demand for electricity in South Africa shows clear seasonal and diurnal patterns. High demand in winter necessitates maximum generation, while in summer, the demand for electricity is greatly reduced. Furthermore, the demand shows two distinct daily peaks, one from approximately 04:00 to 10:00, and the other from 16:00 to 22:00. Of significance here, is that these peaks partially overlap the time when ambient temperature inversions are formed (18:00 - 07:00). Two characteristics of the general winter weather patterns in South Africa are responsible for these inversions. The winters in the interior, where most of the power stations are located, are dry and cloudless, resulting in substantial radiation losses from the earth's surface during the night. This causes strong temperature inversions to develop in the atmosphere close to the ground. Furthermore, once formed, an inversion is maintained, since there is virtually no wind during this time of the year, and consequently little turbulent disruption of the inversion layer. Clearly, the influence of temperature inversions on cooling tower performance is important from a South African power generation perspective, and a review of the literature shows that this is also the case in other countries.

Figure 1-1 explains schematically how a temperature inversion influences the performance of a natural draft dry-cooling tower. As shown in the figure, the tower draws in air from different heights up to approximately half the tower height. Thus, the air inlet temperature measured at the heat exchanger will be a composite of the ambient air temperature at the different layers. In the case of a temperature inversion, the ambient air temperature increases with height, and this means that the air inlet temperature will be higher than the ambient temperature that is normally measured at 1.5 m above the ground. In a cooling tower, the cold water temperature increases almost linearly with an increase in the air inlet temperature, and in power generation, this translates into a lower unit efficiency, and hence a higher heat rejection rate at the tower if the unit is to generate the same load. This in turn raises the temperature of the hot

water entering the tower, and subsequently the cold water temperature will increase further. Eventually, a new equilibrium will be established at a higher cold water temperature.

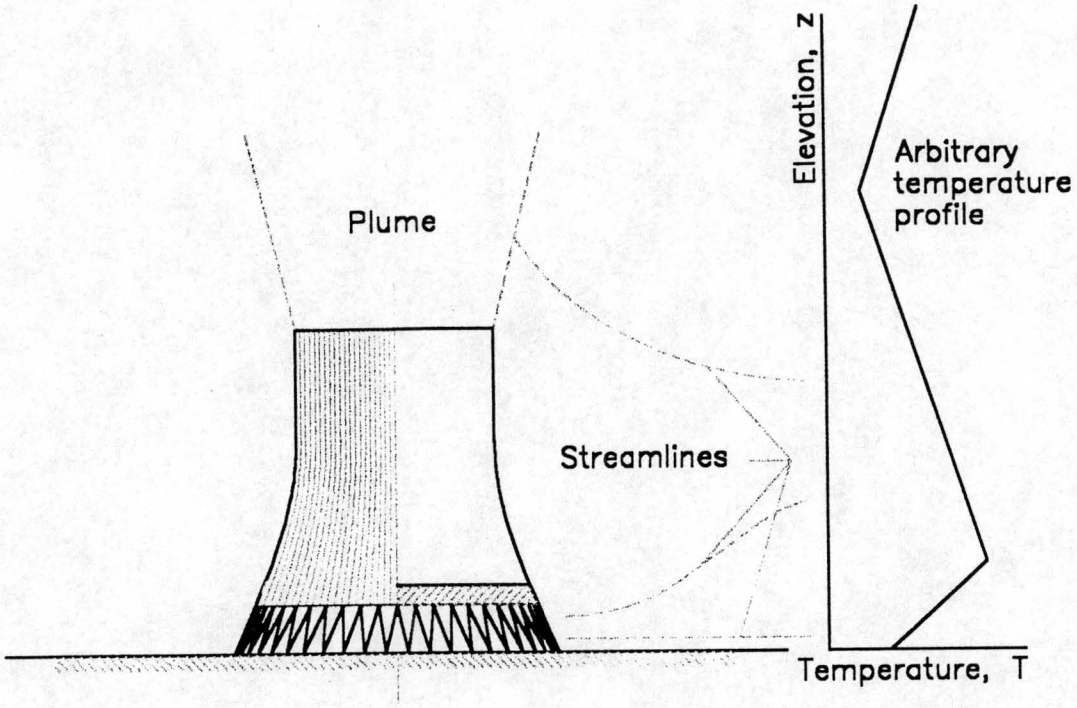

Figure 1-1. Schematic presentation of the air flow pattern in the vicinity of a large natural draft dry-cooling tower, illustrating how the air inlet temperature at the heat exchanger is influenced by an ambient temperature inversion.

Furthermore, the higher temperature of the ambient air column next to the tower also means that the density difference between the column of warm air inside the tower shell and the ambient air is reduced. Since this density difference is the driving force for air flow through the tower, it means that the air flow through the tower is reduced. Of course, a lower air flow rate will decrease the heat rejection rate, and increase the cold water temperature, with the same consequences as outlined above.

Since both these effects tend to reduce the performance of the tower, they are of particular importance in cooling tower design and acceptance tests. It seems that ambient temperature inversions have received the most attention in the latter application,

at least from a contractually guaranteed performance point of view, while cooling tower designs are still based on an annual average ambient air temperature and the adiabatic temperature lapse rate.

Merkel [26ME1] has identified ambient air temperature inversions as detrimental to cooling tower performance as early as 1926. However, this topic received little attention until the late 1970's, when Buxmann [77BU1] and Tesche [81TE1] published a series of papers on the effect of temperature inversions on cooling tower performance. Both addressed the influence of a temperature inversion on the air flow through the tower, but assumed that the temperature of the air entering the heat exchanger will not be affected. Lauraine et al [88LA1] proposed an easy method to detect the presence of a temperature inversion during cooling tower acceptance tests. They suggested that a second air temperature is measured at the inlet height of the tower, and if this temperature differs by more than 2 °C from the air temperature measured 1.5 m above the ground, the test should be discarded. Unfortunately, they did not expand their work to cooling tower design. Benton and Mirsky [93BE1] measured ambient air temperatures at 10 m, 45 m and 91 m, and derived a linear temperature lapse rate from these measurements. These lapse rates were then correlated against measured cooling tower performance. They were also successful in developing a computer model to predict cooling tower performance in the presence of atmospheric temperature lapse rates. However, their model is based on an air inlet temperature measured at ground level, and a linear temperature lapse rate. As such, it does not take the effect of strong ground based atmospheric temperature gradients (typically in the 0 m to 10 m range) into account.

A superadiabatic air temperature profile enhances the tower's performance and is not perceived as a problem, and therefore it has not received any attention in the literature. This thesis deals with both temperature inversions and superadiabatic temperature profiles. In summer, the effect of high ambient air temperatures on tower performance will be tempered by the presence of a superadiabatic temperature profile, since the air inlet temperature should be a few degrees lower than the air temperature measured closer to the ground. This lower upper extreme air inlet temperature holds an inherent design benefit in a highly competitive cooling tower design environment.

The objective of this thesis is to develop a model that will accurately quantify the effect that ambient temperature stratification (an inversion as well as a superadiabatic temperature profile) has on cooling tower performance. As such, the model must be able to predict the correct air inlet temperature at the heat exchanger, as well as quantify its effect on the air flow through the tower from the prevailing ambient conditions. This requires that the ambient temperature profile is characterised in a way that captures both the profile strength (i.e. the maximum deviation from the reference temperature measured at 1.5 m above the ground) and depth (the height at which the maximum deviation occurs). With proper verification, this model can then be applied to cooling tower design and evaluation.

Model verification was done through extensive field tests done during July and August 1990 at the Kendal power station in South Africa. Air temperatures, wind speeds and wind directions were continuously measured at different elevations on a 96 m tall weather mast. At the same time, all the parameters relating to cooling tower performance, including the heat rejection rate, was measured on the number 1 cooling tower. These measurements will be discussed in detail in chapter 4.

Of course, the effect of temperature stratification on cooling tower performance has to be measured against an acceptable reference condition. The most appropriate choice of reference proved to be the performance of the tower in an adiabatic atmosphere. Unfortunately, perfect adiabatic conditions are extremely rare in nature. When they do occur, they are accompanied by moderate to strong winds, a condition that falls outside the scope of this work[1]. This limitation is easily overcome in computational fluid dynamics, since one can artificially create a corresponding reference case for any ambient condition. Therefore, the final adjudication of the effect of ambient air temperature stratification on cooling tower performance was done numerically. A detailed discussion is left to chapter 5.

---

1 Golder [72GO1] proposed that the ambient temperature profile will be approximately adiabatic for wind speeds above 8 m/s, while Du Preez [92DU1] suggested that tower performance is subject to wind influence at wind speeds as low as 2 m/s.

CHAPTER 2

PHYSICS OF THE WIND AND TEMPERATURE PROFILES IN THE ATMOSPHERIC BOUNDARY LAYER

2.1 INTRODUCTION

A temperature inversion impairs the performance of a natural draft dry-cooling tower, while a superadiabatic temperature lapse rate enhances it, but the interaction between the tower and its environment is not fully understood. The standard procedure for measuring atmospheric variables consists only of a temperature measurement at 1.5 m, and wind speed and direction measurements at 10 m above ground level [96AN1]. Data on atmospheric temperature profiles in the planetary boundary layer is scarce. The objective of this chapter is to establish the physical relationship(s) between the various atmospheric parameters required to determine the formation and nature of a temperature profile in the lower atmosphere. Once determined, these profiles can be used to determine the performance of a natural draft dry-cooling tower under different ambient conditions.

Temperature inversions occur quite frequently at night during the winter months in the South African midlands. During this time of the year, clear skies and very dry conditions prevail, primarily due to the presence of a cell of high pressure that dominates the weather of the southern tip of the African continent during winter [89JU1].

Cooling towers are designed to reject heat at a predetermined rate under given atmospheric conditions such as the air temperature, wind speed and atmospheric pressure. For atmospheric parameters, design conditions normally correspond to their annual mean values, with some guarantees attached to the tower's thermal performance under extreme conditions. In a natural draft dry-cooling tower, the ambient air temperature (combined with a number of other parameters, such as the heat rejection rate, type of heat exchanger and tower geometry) also determines the air flow through

the tower, since the draft is based on the density difference between the atmospheric air outside the tower, and the warm air inside the tower shell. In figure 2-1, the interaction between the physical variables influencing the performance of the tower is shown.

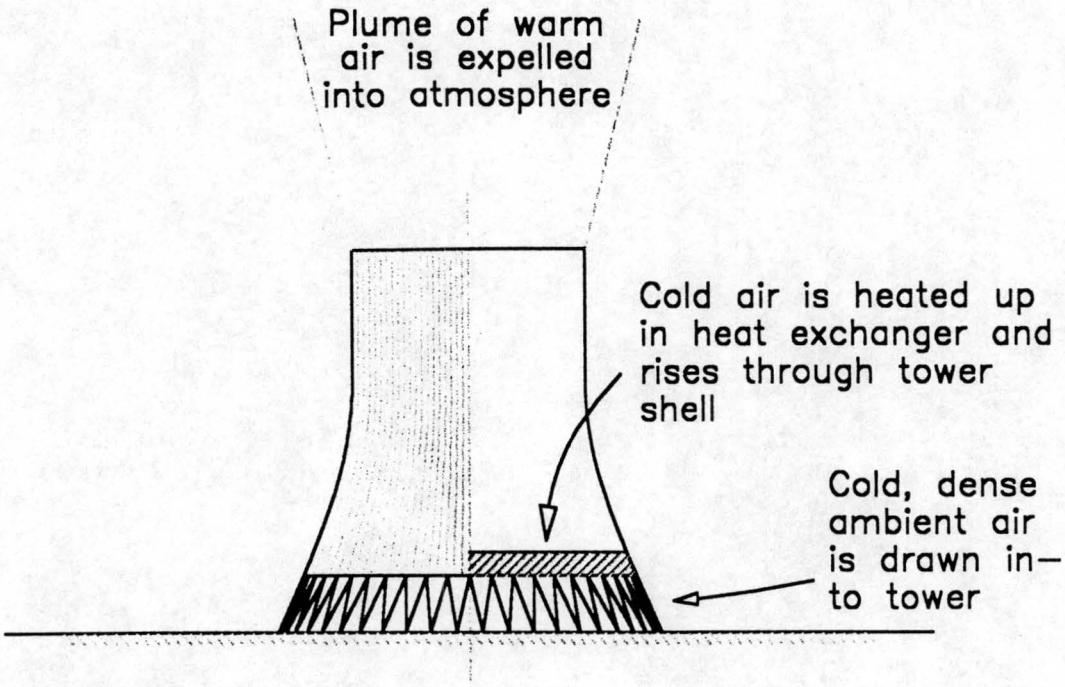

Figure 2-1. Schematic presentation of a natural draft dry-cooling tower.

A parcel of air brought down from any height, will be compressed adiabatically, and experience an increase in temperature. If adiabatic ambient conditions prevail, the parcel will remain in equilibrium with its immediate environment. This means that in the case of a cooling tower that draws in air from different heights, the air inlet temperature at the heat exchanger will be essentially the same as the temperature measured at 1.5 m above ground level. On the other hand, under thermally stable (inversion) or unstable (superadiabatic) conditions, the air inlet temperature will be respectively higher or lower than the temperature measured at 1.5 m. This is further aggravated by the occurrence of strong local temperature gradients within the first few metres above the ground, a phenomenon that will be explained in greater detail.

A surface temperature inversion impairs the vertical movement of air. Since the atmosphere is thermally stable, any downward movement of the air induced by the tower inlet will be opposed by a buoyancy force acting on the displaced air. Normally, the tower will be high enough to penetrate a surface inversion (typically confined to a 20-100 m thick layer next to the surface), and the plume will not be affected. During a surface inversion, the tower will draw in air from lower altitudes than under adiabatic conditions. Furthermore, the air temperature in the higher layers may be significantly higher than the temperature measured at ground level, leading to a higher effective air inlet temperature. Combined with the reduction in draft, caused by the lower density difference between ambient air and the air inside the tower, a temperature inversion can reduce the air flow through the tower significantly [81TE1]. Hence, a tower designed for adiabatic conditions will experience a shift in operating point in the presence of a temperature inversion.

In the South African power generating industry, this does not pose a serious problem, since the demand for electricity follows a diurnal pattern, with peaks in midmorning and early evening. Since cooling towers are designed to cope with high daytime temperatures in summer (30 °C and higher), tower performance in winter, although impaired, is usually not problematic. This, of course, may not be the case in other industries or countries with significantly different electricity consumption profiles.

During adiabatic (or superadiabatic) conditions, the plume of warm air emitted from a cooling tower is accelerated by buoyancy forces, and the plume will rise indefinitely. However, if a subsidence temperature inversion (typically at heights between 200 m and 500 m [88PR1]) forms in the atmosphere, the plume is sometimes trapped in this inversion layer, and plume dispersion is greatly reduced. This may lead to severe fog formation, and even precipitation in the case of a wet-cooling tower. Such an occurrence is highly unlikely in South Africa with its dry and mild winters. However, in colder countries, precipitation may cause the formation of ice on roads, which combined with the reduced visibility, may lead to serious road hazards.

The highly competitive nature of the electricity supply industry has greatly reduced the margin of error in power plant designs. It has become necessary to consider temperature inversions in the design of large cooling towers. Failure to do so, will lead to deterioration of cooling tower performance under unfavourable conditions, that, in the case of power plants, will cause load losses.

2.2 SOLAR RADIATION

The earth moves around the sun in an approximately circular path, with the sun located slightly off the centre of the circle. This eccentricity is such that the earth is closest to the sun on January 1, and furthest from the sun on July 1. The earth's axis of rotation is tilted 23.5 ° with respect to the plane of its orbit around the sun. This tilt is the cause of the seasons. When it is winter in the southern hemisphere, the south end of the axis of the rotation is tilted away from the sun, while in summer, it is tilted towards the sun. The day when the axis is tilted exactly towards the sun is called the summer solstice, i.e. December 23. On June 21, the axis of rotation is tilted directly away from the sun, and this day is called the winter solstice. On March 22 and September 22, the tilt is in a plane tangential to the earth's orbit around the sun. These days are called the autumn and spring equinoxes, respectively. Due to the eccentricity of the sun with respect to the earth's orbit, the earth is closer to the sun when it is summer in the southern hemisphere, and there is a tendency for the seasonal differences in temperature to be greater in the southern hemisphere than in the northern hemisphere.

The amount of radiation falling on a surface of unit area normal to the rays of the sun at the outer limit of the atmosphere, when the distance between the sun and the earth is at its mean value, is called the solar constant, I_0. The average value of the solar constant is 1 377 W/m^2. When radiation passes through the atmosphere, it is depleted due to scattering and absorption by atmospheric gases, especially carbon dioxide and water vapor, and air-borne particles. Although the thickness of the atmosphere will vary somewhat with location, this variation is small, and the relative thickness of the

atmosphere, δ_0, approaches unity. The effective path length for radiation through the atmosphere at any time, and for any location, is given by

$$\delta = \delta_0 \operatorname{cosec}\Theta \qquad \ldots (2.2\text{-}1)$$

The atmosphere absorbs radiation selectively in quite narrow wavelength bands, as shown in figure 2-2. Solar radiation, which is concentrated at short wavelengths(0.4 - 0.7 μm), is mostly transmitted, whereas thermal radiation (at wavelengths 3-80 μm) is absorbed to a fairly large extent. Therefore, the atmosphere acts effectively as a greenhouse, trapping much of the incoming solar radiation to provide the necessary heat for life on earth.

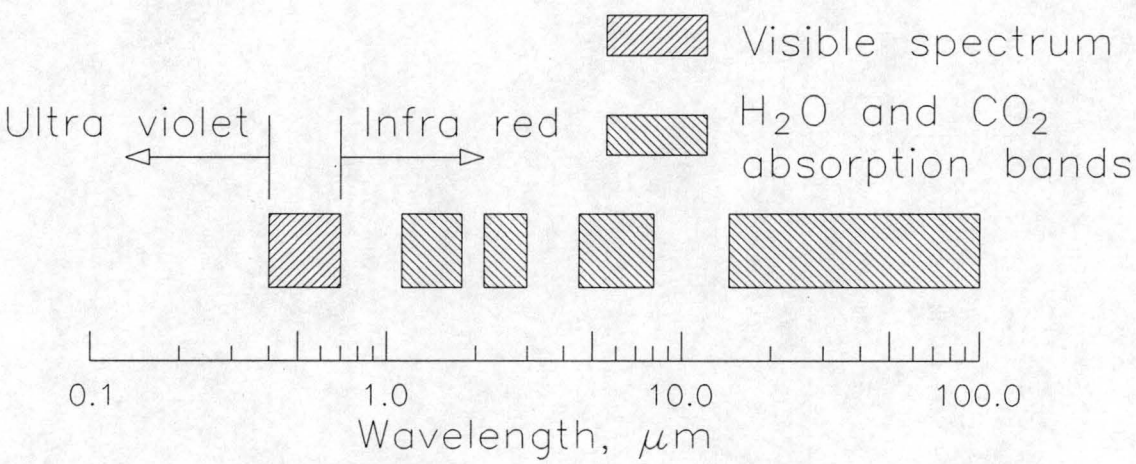

Figure 2-2. Radiation absorption bands of atmospheric gases.

The amount of solar radiation, I_s, that reaches the earth's surface depends on the latitude, season, solar time, cloud cover and pollutants in the atmosphere. The molecular absorption of the incoming solar radiation by atmospheric gases may be described by Beer's law

$$I = I_0 \exp(-a\delta) \qquad \ldots (2.2\text{-}2)$$

with a the average extinction coefficient for all wavelengths. An approximate value for a is 0.431, which neglects the small influences of atmospheric pressure and the height above sea level on the optical mass of the atmosphere.

The angle between the sun's rays and a plane through the equator at solar noon is called the sun's angle of declination, Φ. This angle varies from 23.5 ° on the summer solstice, to -23.5 ° on the winter solstice. During this time the sun has advanced through 180 ° along its orbit. The time elapsed between the summer and winter solstices is exactly half a year, or 182.6 days. Hence, the declination angle for any day of the solar year (which starts on December 23) is given by

$$\sin\Phi = -\cos\left\{(n_s - 1)\frac{180°}{182.6}\right\}\sin(23.5°) \qquad \ldots (2.2\text{-}3)$$

with n_s the number of days that have elapsed since the summer solstice.

At an arbitrary point p on the surface of the earth, a line connecting point p with the centre of the sun, as shown in figure 2-3, may be drawn for any solar day n_s , at any solar time t_s.[1] The latitude angle of point p is Ψ degrees. A line from the centre of the earth to the sun passes through the surface of the earth at point q, where it will be solar noon. The projections of points p and q on the equatorial plane are p_0 and q_0 respectively. By definition, the hour angle A is the angle in the equatorial plane between the two meridians passing through p_0 and q_0 respectively. For convenience, it is assumed that the sun's rays are parallel to each other. Although this is not exactly true, considering the great distance between the earth and the sun compared to the diameter of the earth, no significant errors will enter the calculations through this assumption. Consider the spherical triangle Spq, with S the south pole, which is made up of segments of circles on the earth's surface. For any general spherical triangle made up of segments of great circles, the law of cosines holds. Thus, for the spherical triangle Spq, the solar altitude angle Θ , is found from

---

1 The solar time is unique to any longitude on earth, and it is chosen such that solar noon corresponds to the time that the sun is at its highest position in the sky. In terms of the solar time, the time from sunrise to noon will be equal to the time from noon to sunset.

$$\cos(90^\circ - \Theta) = \sin\Phi\sin\Psi + \cos\Phi\cos\Psi\cos A \qquad \ldots (2.2\text{-}4)$$

with the latitude Ψ of point p presumably known.

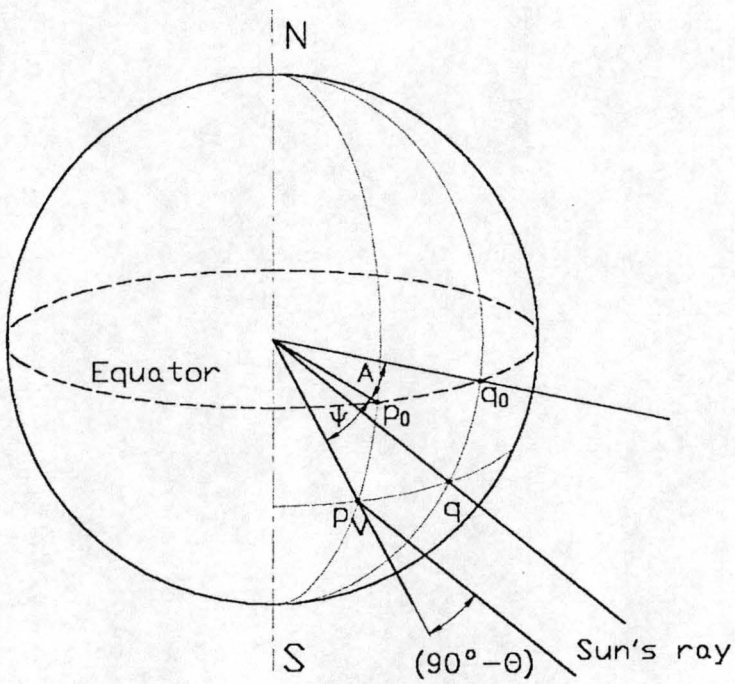

Figure 2-3. Diagram for calculating the solar altitude angle, Θ.

The angle of declination, Φ, is given by equation (2.2-3). Noting that it takes the earth 24 hours to rotate through 360 °, the hour angle A can be derived from the solar time through

$$A = (t_s - 12) \times 15^\circ \qquad \ldots (2.2\text{-}5)$$

with t_s the local solar time. Thus, the solar altitude angle Θ for any point p, at any time of the day t_s, for any day of the year n_s, may be calculated from equation (2.2-4), and accordingly, the incident solar radiation received at the earth's surface from equations (2.2-1) and (2.2-2).

The reflective properties of a surface is described in terms of the albedo, α_r of that surface, which is defined as

$$\alpha_r = \frac{\text{reflected energy}}{\text{total incident energy}} \qquad \ldots (2.2\text{-}6)$$

The albedo of the earth's surface depends mainly on the surface geometry, vegetation and ground cover (such as dew, frost, or snow), but the wind velocity may also enter the expression for the local albedo. On a plain covered with tall grass, for example, the wind will cause the grass to bend over in the direction it is blowing, and change the reflective properties of the surface. Baer [78BA1] proposed an average value of $\alpha_r = 0.25$. This should only be used in the absence of more detailed information on the albedo.

2.3 THE ADIABATIC ATMOSPHERE

Consider a small parcel of air that may be displaced vertically in the atmosphere. If the process is adiabatic, the parcel will experience a change in temperature as a result of the change in pressure. The hydrostatic variation in pressure is given by

$$\frac{dp}{dz} = -\rho g \qquad \ldots (2.3\text{-}1)$$

If the process is also isentropic, the following relation holds

$$\frac{p}{\rho^{\gamma}} = \text{constant} \qquad \ldots (2.3\text{-}2)$$

However, for all practical purposes, atmospheric air may be considered as an ideal gas, hence

$$\frac{p}{\rho} = RT \qquad \ldots (2.3\text{-}3)$$

Substitute equation (2.3-3) into equation (2.3-2), differentiate with respect to the altitude z and re-arrange to find

$$\frac{(1-\gamma)}{\gamma}\frac{dp}{dz} + \frac{1}{T}\frac{dT}{dz} = 0 \qquad \ldots (2.3\text{-}4)$$

By substituting equation (2.3-1) into equation (2.3-4) and invoking the ideal gas law, the adiabatic temperature lapse rate is obtained

$$\frac{dT}{dz} = \frac{g(1-\gamma)}{\gamma R} \qquad \ldots (2.3\text{-}5)$$

For dry air with γ=1.4 and R=287.08 J/kg °C, the adiabatic lapse rate is 0.00975 °C/m. This temperature lapse rate is seldom observed in the stratosphere, due to the absorption of radiation by the atmospheric gases, especially carbon dioxide and water vapor. As a result, the observed temperature gradient will be weaker than the adiabatic temperature lapse rate. This deviation will vary from a minimum at the equator, where the sun's rays follow the shortest path through the atmosphere, to a maximum at the poles.

An International Standard Atmosphere (ISA), intended to approximate the atmospheric conditions for most of the year in the temperate latitudes is defined as having a mean sea level pressure of 101.325 kPa, an average sea level temperature of 15 °C, and a temperature lapse rate of 0.0065 °C/m up to a height of 11 000 m.

2.4 THE GEOSTROPHIC WIND

Geostrophic winds are caused by the combined effect of a pressure distribution in the upper atmosphere and the Coriolis force due to the rotation of the earth at a height where surface effects are negligible.

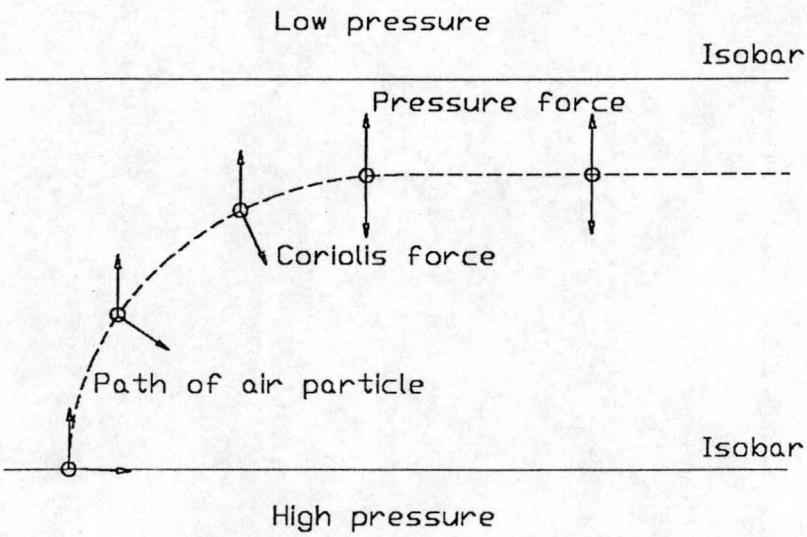

Figure 2-4. Forces exerted on an air parcel in a pressure field.

Consider a parcel of air, initially at rest relative to the surface of the earth, in an arbitrary pressure field, as shown in figure 2-4. Due to the presence of a pressure gradient, a net force is exerted on the parcel, and the parcel is accelerated from the high pressure to the low pressure zone. As soon as the parcel starts moving relative to the rotating earth, a Coriolis force is exerted on it. This causes the particle to change direction until the Coriolis force counterbalances the force exerted by the pressure field. When equilibrium is attained, the parcel will move in a straight line parallel to the isobars, and it is said that the geostrophic movement is established. The components of the geostrophic wind velocity are given by the following implicit expressions

$$-\frac{1}{\rho}\frac{\partial p}{\partial x} = 2\Omega v_{gx} \sin\Psi \qquad \ldots (2.4\text{-}1)$$

and

$$-\frac{1}{\rho}\frac{\partial p}{\partial y} = 2\Omega v_{gy} \sin\Psi \qquad \ldots (2.4\text{-}2)$$

for the x- and y-directions respectively, with north the default y-direction.

From equations (2.4-1) and (2.4-2), it is clear that the geostrophic wind varies with latitude, reaching a maximum at the poles and dropping to zero at the equator, where the direction of the geostrophic wind will also change sign, from being positive in the northern hemisphere to negative in the southern hemisphere under influence of the same pressure field.

2.5 THE ATMOSPHERIC BOUNDARY LAYER

2.5.1 TRANSPORT IN THE ATMOSPHERIC BOUNDARY LAYER

The atmospheric boundary layer is characterized by large vertical gradients in the wind velocity, air temperature and humidity. Transport through the boundary layer is by virtue of eddy diffusion, and the physical condition of the atmosphere depends on the momentum, heat and moisture fluxes.

Significant diurnal variations of temperature near the earth's surface will result due to radiative heating and cooling of the surface. In the afternoon the sun has heated the ground sufficiently to cause a net heat flux towards the atmosphere. This will result in unstable conditions in the atmosphere, with a corresponding sharp decrease in temperature in the lowest few meters. As the sun sets, the ground cools by radiation, and a surface inversion may be formed, as shown in figure 2-5. This layer will thicken during the night. After sunrise, the surface temperature will gradually increase, until the unstable late afternoon profile is once more established.

In order to interpret the diurnal temperature and wind profiles, a one-dimensional numerical model was derived. The model consists of four layers as shown in figure 2-6, namely a soil layer, a viscous sub-layer, a constant flux layer, in which the fluxes of heat and momentum remain constant, and an outer layer called the Ekman layer. Of course, this is an adaptation of classical turbulent boundary layer theory often encountered in fluid dynamics [79SC1], [74WH1], with the soil the equivalent of the wall, the viscous sub-layer corresponds to the inner layer, the constant flux layer to the overlap layer, and the Ekman layer to the outer layer respectively. The depth of these layers can vary greatly, and are determined by the scale of the various transport processes in the atmospheric boundary layer.

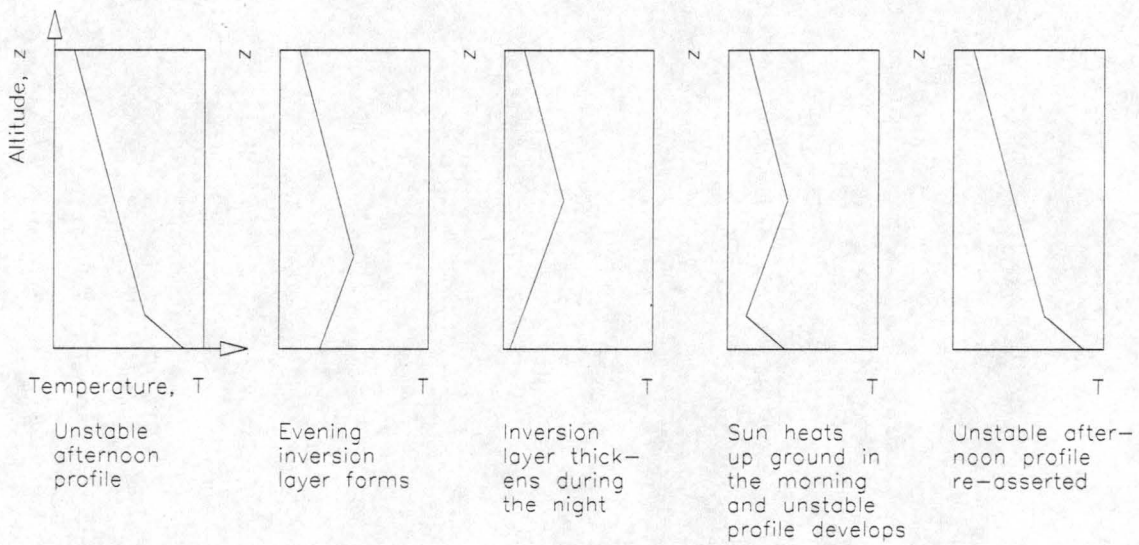

Figure 2-5. Diurnal change of the temperature profile in the atmospheric boundary layer.

To derive a mathematical model for heat, mass and momentum transfer in the atmospheric boundary layer, the following assumptions are made:

a) Eddy diffusion coefficients for heat and mass transfer are of the same general form

b) The soil is completely void of any moisture

c) Dew formed during the night will not enter the soil, but will evaporate after sunrise

d) Topographical effects and advection may be neglected

e) Earth's albedo is known and constant

f) Wind at top of planetary boundary layer is geostrophic and constant

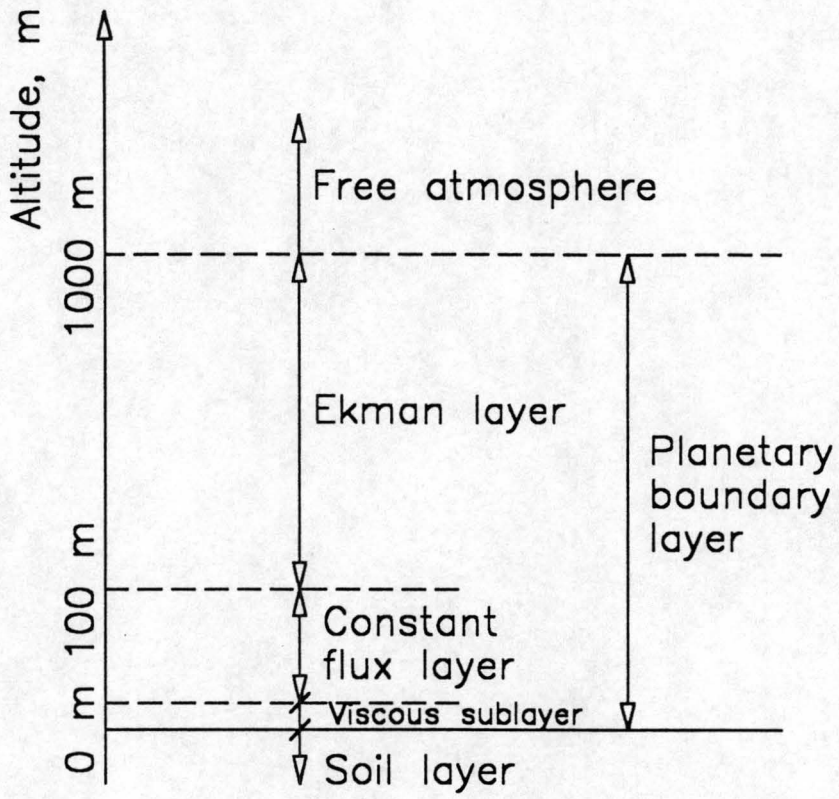

Figure 2-6. Sketch of calculation domain for model of atmospheric boundary layer.

The soil temperature at a depth of one meter does not change significantly within the span of a few days, and may be assumed to remain constant. Heat transfer in the soil layer is by virtue of conduction, and the governing equation for heat transfer in this layer is given by

$$\rho c \frac{\partial T}{\partial t} = \frac{\partial}{\partial z}\left(k \frac{\partial T}{\partial z}\right) \qquad \ldots (2.5\text{-}1)$$

The potential temperature θ is frequently used in atmospheric sciences, and it is defined as the temperature that a parcel of air will attain if it is brought down adiabatically to a reference height at the surface from any altitude. The potential temperature is preferred, since its gradient is a true reflection of the actual heat flux in the atmospheric boundary layer. By definition, the potential temperature is

$$\theta = T\left(\frac{p_{a1}}{p_a}\right)^{(\gamma-1)/\gamma} \qquad \ldots (2.5\text{-}2)$$

with p_{a1} the barometric pressure at the reference height.

The vertical fluxes of heat and momentum in the constant flux layer remain virtually unchanged. This layer varies in depth from about 10 m during stable conditions up to 100 m under unstable conditions, that is thin compared to the planetary boundary layer thickness, and it may be considered a quasi-steady layer. Hence, the governing equations for heat and momentum transfer in the constant flux layer are respectively

$$\frac{\partial}{\partial z}\left(\Gamma_h \frac{\partial \theta}{\partial z}\right) = 0 \qquad \ldots (2.5\text{-}3)$$

for heat transfer, and

$$\frac{\partial}{\partial z}\left(\Gamma_m \frac{\partial v}{\partial z}\right) = 0 \qquad \ldots (2.5\text{-}4)$$

for momentum transfer.

Transport of fluid properties through the constant flux layer is by virtue of small turbulent eddies. A fluid parcel is engulfed by the eddy, which transports it through the surrounding fluid, and upon break-up of the eddy, the fluid parcel is mixed intimately with its surroundings. In nature, eddy diffusion is like molecular diffusion, only on a

much larger scale. The eddy diffusion coefficient for heat transfer, Γ_h, depends on the atmospheric stability, the height above the ground and the surface roughness, leading to

$$\Gamma_h = \frac{\kappa z}{\theta_* \phi_h (z/L)} \qquad \ldots (2.5\text{-}5a)$$

Similarly, for momentum transfer, one has

$$\Gamma_m = \frac{\kappa z}{v_* \phi_m (z/L)} \qquad \ldots (2.5\text{-}5b)$$

with κ von Kármán's constant ($\kappa \approx 0.4$).

The symbol θ_* represents a scaling temperature, a parameter of the temperature profile that is defined in terms of the sensible heat flux at the surface

$$\theta_* = \frac{-q_{sens}}{\rho c_p \kappa v_*} \qquad \ldots (2.5\text{-}6)$$

The scaling or friction velocity v_* in turn is a parameter of the wind profile, and is defined in terms of the surface shear stress τ_0 as

$$v_* = \sqrt{\frac{\tau_0}{\rho}} \qquad \ldots (2.5\text{-}7)$$

No attempt will be made to determine τ_0, and the scaling velocity will be extracted from the wind profile instead.

L is Monin and Obukhov's [54MO1] scaling length, which is defined in terms of the other parameters as

$$L = \frac{T_{1.5}\, v_*^2}{g\kappa^2 \theta_*} \qquad \ldots (2.5\text{-}8)$$

with $T_{1.5}$ the air temperature measured at 1.5 m above the ground. The functions ϕ_h and ϕ_m in equations (2.5-5a) and (2.5-5b) are both equal to unity in an adiabatic atmosphere. Furthermore, ϕ_h and ϕ_m are used to modify the eddy diffusion coefficients for non-adiabatic cases, and are different for momentum and heat. They are usually written in terms of a similarity variable ξ for convenience. ξ is defined as

$$\xi = \frac{z}{L} \qquad \ldots (2.5\text{-}9)$$

Kondo and Yamazawa [86KO1] suggested the values listed in table 2-1 for the empirical functions ϕ_h and ϕ_m based upon experimental data:

Table 2-1. Eddy diffusion coefficients for stratified atmosphere.

Stability Class	Momentum ϕ_m	Heat ϕ_h
$-\infty < \xi < -10$	$[1 - 16\xi]^{-1/4}$	$[1 - 16\xi]^{-1/2}$
$-10 \le \xi < 0$	$[1 - 16\xi]^{-1/3}$	$[1 - 16\xi]^{-1/2}$
$0 \le \xi < 0.3$	$[1 + 6\xi]$	$[1 + 6\xi]$
$0.3 \le \xi < 10$	$[1 + 22.8\xi]^{1/2}$	$[1 + 22.8\xi]^{1/2}$

The Monin-Obukhov length may be interpreted as the height at which the magnitudes of mechanical and thermal production of turbulence are equal. Furthermore, it provides a measure of the stability of the atmospheric boundary layer

$$L^{-1} \begin{cases} < 0; & \text{unstable} \\ = 0; & \text{adiabatic} \\ > 0; & \text{stable} \end{cases} \qquad \ldots (2.5\text{-}10)$$

Due to roughness elements, the earth's surface is shielded from momentum transfer. The roughness length z_0 is defined as the height at which it is presumed that the mean wind speed vanishes. The roughness length is a function of surface irregularities, such as topography, vegetation and buildings, and the mean wind speed. The roughness length increases with increasing length of the roughness elements, but may either increase or decrease with increasing wind velocity. A strong wind blowing over a plain covered with tall grass will cause the grass to bend over and thus decrease the roughness length, whereas the same wind blowing over an open body of water will make the water surface choppy, thus increasing the roughness length. The roughness lengths, which correspond to certain surface irregularities, are given in table 2-2. Note that the roughness length z_0 is not the same as the length of the roughness elements.

The outer part of the planetary boundary layer, which exhibits transient behaviour, is called the Ekman layer. Although the constant flux layer and the Ekman layer are depicted as two distinct contiguous layers, in reality the one gradually merges into the other. At the top of the Ekman layer, the wind velocity is equal to the geostrophic wind. The thickness of the Ekman layer varies from about 100 m for stable conditions to more than 2500 m during unstable conditions. Solar heating of the Ekman layer will occur, but unless high concentrations of water vapor and carbon dioxide prevail, it will be negligible compared to the other transport processes. The governing equations for momentum transfer in the Ekman layer are

$$\frac{\partial v_x}{\partial t} = 2\Omega \sin\Psi\left(v_y - v_{gy}\right) - \frac{1}{\rho}\frac{\partial p}{\partial x} + \frac{\partial}{\partial z}\left(\Gamma_m \frac{\partial v_x}{\partial z}\right) \qquad \text{... (2.5-11)}$$

and

$$\frac{\partial v_y}{\partial t} = -2\Omega \sin\Psi\left(v_x - v_{gx}\right) - \frac{1}{\rho}\frac{\partial p}{\partial y} + \frac{\partial}{\partial z}\left(\Gamma_m \frac{\partial v_y}{\partial z}\right) \qquad \text{... (2.5-12)}$$

for the x- and y-directions respectively.

In the above equations, v_{gx} and v_{gy} are the components of the geostrophic wind. In the absence of solar heating of the atmosphere, the governing equation for heat transfer is

$$\frac{\partial \theta}{\partial t} = \frac{\partial}{\partial z}\left(\Gamma_h \frac{\partial \theta}{\partial z}\right) + \frac{q}{\rho c_p} \qquad \ldots (2.5\text{-}13)$$

Table 2-2. Roughness lengths associated with different surfaces.

Surface configuration	z_0, [m]
Urban areas	
Central business district	8.000000
High density residential	4.500000
Low density residential	2.000000
Rolling relief	
Coastal bush	1.000000
Open savannah	0.800000
Full grown root crops	0.250000
Shrubs	0.150000
Flat relief, vegetated	
Uncut grass	0.070000
Crop stubble	0.020000
Snow and short grass	0.002000
Flat relief, unvegetated	
Natural snow	0.001000
Bare sand	0.000400
Open sea	0.000200
Water	0.000100
Snow	0.000050
Mud flats and ice	0.000001

Estoque [63ES1] assumed a linear decrease in the eddy diffusion coefficient in the Ekman layer, but criticized this assumption as a serious weakness in his own model. O'Brien [70BR1] suggested a third order hermetic polynomial interpolation for the eddy diffusion coefficient in the Ekman layer. He achieved this by matching the eddy diffusion coefficient and its gradient for the constant flux layer and the Ekman layer at the interface between the two layers. Furthermore, he assumed that the gradient of the eddy diffusion coefficient vanishes at the top of the Ekman layer. This enabled him to eliminate the discontinuity in the gradient of the eddy diffusion coefficient at the top of the constant flux layer. Sasamori [71SA1] imposed an additional condition, namely that

the eddy exchange coefficient vanishes at the top of the Ekman layer to prevent heat or momentum exchange between the free atmosphere and the Ekman layer. With these assumptions, the eddy diffusion coefficent in the Ekman layer is given by

$$\Gamma(z) = \left(\frac{z - z_p}{z_p - z_c}\right)^2 \left\{\Gamma(z_c) + (z - z_c)\left[\left(\frac{\partial \Gamma}{\partial z}\right)\Big|_{z_c} - \frac{2\Gamma(z_c)}{z_p - z}\right]\right\} \qquad \ldots (2.5\text{-}14)$$

2.5.2 BOUNDARY LAYER HEIGHT

If the boundary layer dynamics are parameterized, the thickness of the planetary boundary layer for neutral stratification of the atmosphere is given by [70BR1]

$$z_p = \frac{\kappa v_*}{2\Omega \sin \Psi} \qquad \ldots (2.5\text{-}15)$$

with Ω the rotational velocity of the earth, and Ψ the latitude. Equation (2.5-15) may also be used for unstable conditions. Under adiabatic and unstable conditions, the constant flux layer thickness is approximately 10 % of that of the planetary boundary layer [72TE1]

$$z_c = 0.1 z_p \qquad \ldots (2.5\text{-}16)$$

For stable stratification, Zilitinkevic [72ZI1] derived the following expression for the planetary boundary layer thickness

$$z_p = \kappa \left\{\frac{v_* L}{2\Omega \sin \Psi}\right\}^{0.5} \qquad \ldots (2.5\text{-}17)$$

Due to the reduced scale of turbulence, the constant flux layer, where viscous shear still has an influence, becomes more significant, and Zeman [79ZE1] suggested the following relation

$$z_c = \frac{0.3\, z_p}{1 + \frac{L}{z_p}} \qquad \ldots (2.5\text{-}18)$$

2.5.3 BOUNDARY CONDITIONS

To solve the heat transfer equations {equations (2.5-1) and (2.5-3)}, the surface temperature is required. This task is easily performed by considering an energy balance for a thin layer at ground level, as shown in figure 2-7. All fluxes directed towards the surface are taken as negative. In the absence of evaporation or condensation at the surface, the energy balance yields

$$-q_{sens} + \sigma T^4 + q_{soil} - (1 - \alpha_r) I_s - I_{LW} = 0 \qquad \ldots (2.5\text{-}19)$$

with α_r the albedo of the earth's surface. Assuming that no moisture will enter the soil during condensation, and that all dew will evaporate again as if from an impervious surface, the latent heat of evaporation/condensation of the dew will enter equation (2.5-19) as an energy source. Evaporation from the vegetation is ignored.

Calculating the terrestrial radiation is rather tiresome [64LA1] and involves integration of the radiant energy over all wavelengths bands. Various empirical models exist to calculate the terrestrial radiation of the earth's surface under clear skies. One such model is attributed to Swinbank (in Preston-Whyte and Tyson [88PR1])

$$I_{LW}' = 1.2\sigma T^4 - 171 \qquad \ldots (2.5\text{-}20)$$

with T in Kelvin. Equation (2.5-20) is not valid for subzero Celsius temperatures.

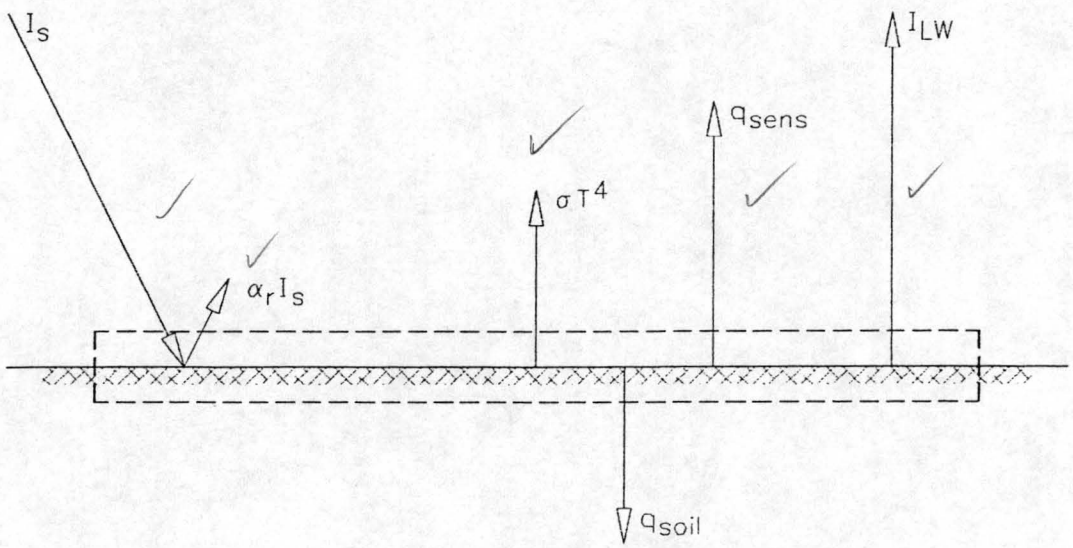

Figure 2-7. Control volume for energy balance at earth's surface.

Predominantly clear skies are experienced over the South African interior during the dry winter months, but cloud cover is easily incorporated into the energy balance. Preston-Whyte and Tyson [88PR1] suggested a non-linear cloud factor, that varies with cloud type and height, to account for the radiation intercepted and scattered by the clouds. Long-wave terrestrial radiation to the surface is modified, using the following relation

$$I_{LW} = I_{LW}' \left(1 + a N^2\right) \qquad \ldots (2.5\text{-}21)$$

with N the fraction of the sky covered by clouds. Furthermore, some of the radiant heat emitted by the surface is intercepted by the clouds, while some of it is reflected back to the surface. Hence, the Stefan-Boltzmann term in equation (2.5-19) should be multiplied by a correction factor

$$1 - b N^2 \qquad \ldots (2.5\text{-}22)$$

to account for this. Typical values for the coefficients a and b [88PR1] in equations (2.5-21) and (2.5-22) are listed in table 2-3.

Table 2-3. Radiation correction factors for clouds.

Cloud type	Height [m]	a	b
Cirrus	12 200	0.04	0.16
Cirrostratus	8 390	0.08	0.32
Altocumulus	3 660	0.17	0.66
Altostratus	2 140	0.20	0.80
Stratocumulus	1 220	0.22	0.88
Stratus	460	0.24	0.96
Fog	0	0.25	1.00

The usual assumptions [63ES1], [64LA1], [70SA1] on the other boundaries are accepted, namely the temperature in the soil does not vary over the span of a few days, the wind at the top of the Ekman layer is geostrophic and constant, the profiles for temperature and wind velocities are continuous at the top of the constant flux layer, and the temperature lapse rate in the free atmosphere is constant and conforms to the international standard atmosphere [78BA1].

2.5.4 DETERMINING THE PARAMETERS v_*, θ_* and L

The accuracy of the flux parameters depends on the number of available meteorological measurements. It is simply a case of the more measurements, the better the results. Measured profiles are preferred above point measurements. Unfortunately, this is hardly ever the case in meteorology. When wind and temperature profiles are available, the resulting parameters will invariably be better than those obtained when wind and temperature measurements are taken at only one height. Wind profiles are in general quite sensitive to the surface geometry, and due to its turbulent nature, data tends to be scattered.

When no wind or temperature profiles are available, two empirical methods may be used to determine the parameters v_*, θ_* and L, namely the energy balance method of De Bruin and Holtslag [82BR1], and Golder's [72GO1] method for calculating the other parameters from the scaling length, modified by Shir and Shieh [74SH1].

Golder used the mean wind speed 10 m above the ground level, v_{10}, (assuming it to fall within the constant flux layer) in combination with the incoming solar radiation to establish a stability class. Shir and Shieh correlated Golder's data to express the stability parameter s as a continuous function.

a) Daytime (1 hour after sunrise to 1 hour before sunset):

$$s = \begin{cases} 0.4167\,v_{10} - 3.5833; & 634\,W/m^2 < I_s \le 950\,W/m^2 \\ 0.3905\,v_{10} - 2.9952; & 318\,W/m^2 < I_s \le 634\,W/m^2 \\ 0.3357\,v_{10} - 2.3762; & 0\,W/m^2 \le I_s \le 318\,W/m^2 \end{cases} \quad \ldots (2.5\text{-}23)$$

b) Transient period 1 hour before sunset:

$$s = 0.1213\,v_{10} - 1.0532 \quad \ldots (2.5\text{-}24)$$

c) Night-time (Sunset to sunrise):

$$s = \begin{cases} -0.2167\,v_{10} + 1.5333; & \text{Cloud cover} \le 0.5 \\ -0.3595\,v_{10} + 2.6881; & \text{Cloud cover} > 0.5 \end{cases} \quad \ldots (2.5\text{-}25)$$

d) Transient period 1 hour after sunrise:

$$s = -0.1244\,v_{10} + 1.0347 \quad \ldots (2.5\text{-}26)$$

Other methods exist for classifying the atmosphere into different stability classes. Some of these are listed on pp. 37-39 in reference [87BU1]. Once the stability parameter s is known, the Monin-Obukhov length L is found from [74SH1]

$$\frac{1}{L} = \frac{s}{|s|}\left[0.216586 \ln\left(1.2 + \frac{10}{z_0}\right)\right] \times 10^{f(s)} \qquad \ldots (2.5\text{-}27)$$

where

$$f(s) = \frac{-4}{1 + 1.3|s|^{0.85}}$$

Substitute equation (2.5-5b) into equation (2.5-4) and integrate to find the scaling velocity v_*

$$\begin{aligned} \int_{z_0}^{z}\int \frac{d}{dz}\left(\Gamma_m \frac{dv}{dz}\right) dz\,dz &= \int_{z_0}^{z} \Gamma_m \frac{dv}{dz} dz \\ \therefore \quad \int_{v_0}^{v} dv &= \frac{v_*}{\kappa}\int_{z_0}^{z} \frac{\phi_m(z/L)}{z} dz \\ v - 0 &= \frac{v_*}{\kappa}\int_{\xi_0}^{\xi} \frac{\phi_m(\xi)}{\xi} d\xi \\ v &= \frac{v_*}{\kappa}\varphi_m(\xi) \end{aligned} \qquad \ldots (2.5\text{-}28)$$

Shir and Shieh [74SH1] assumed a linear wind profile in the first 10 m of the atmosphere, but this practice will introduce large errors, since the actual profile is almost logarithmic [64LA1]. Using equation (2.5-8) for the scaling length, a new value for the scaling velocity is calculated from

$$v_* = \frac{\kappa v_{10}}{\varphi(\xi_{10})} \qquad \ldots (2.5\text{-}29)$$

with $\varphi(\xi_{10})$ given by

$$\varphi(\xi_{10}) = \int_{\xi_0}^{\xi_{10}} \frac{\phi(\xi)}{\xi} d\xi \qquad \ldots (2.5\text{-}30)$$

The values of $\varphi(\xi_{10})$ for the different universal functions $\phi_h(\xi)$ and $\phi_m(\xi)$ are given in appendix A. From Monin and Obukhov's definition of the scaling length (equation (2.5-8)), the scaling temperature θ_* is calculated next

$$\theta_* = \frac{T_{1.5} v_*^2}{g \kappa^2 L} \qquad \ldots (2.5\text{-}31)$$

Once v_* and θ_* are known, the shapes of the wind and temperature profiles in the constant flux layer are fixed.

De Bruin and Holtslag's [82BR1] method depends on an estimate of the sensible heat exchange between the atmosphere and the surface, q_{sens} and previously known wind and temperature profiles at time t to predict the new profiles at time t+Δt. Once the sensible heat flux is known, the shear velocity, v_* and the scaling length L can be calculated iteratively, using the universal functions for wind and temperature profiles, together with the definition of the Monin-Obukhov length. Without any knowledge about the old shape of the wind and temperature profiles, this method is of no use.

De Bruin and Holtslag [82BR1] suggested an empirical method for determining the sensible heat flux during daytime. At any time t, find the sensible heat flux from

$$q_{sens} = \frac{(1 - a_0) f(T) + g(T)}{f(T) + g(T)} \left\{ (1 - \alpha_r) I_s + I_{LW} - \sigma T^4 - q_{soil} \right\} - a_1 \qquad \ldots (2.5\text{-}32)$$

f(T) and g(T) are temperature dependent functions, while the constants a_0 and a_1 depend on the terrain. For conditions normally encountered in the temperate zones, $a_0 = 1$ and $a_1 = 20$ for $0.025 \text{ m} \leq z_0 \leq 0.5 \text{ m}$. When the roughness length exceeds 0.5 m, both

constants vanish. Under extremely dry conditions, $a_0 = 0.65$ while a_1 remains unaltered. The functions f(T) and g(T) are given by

$$f(T) = 0.646 + 6 \times 10^{-4}(T - 273.15) \quad \ldots (2.5\text{-}33)$$

and

$$g(T) = 4 \times 10^{3} \frac{\varepsilon(T)}{(T - 35.8)^2} \quad \ldots (2.5\text{-}34)$$

respectively, where

$$\varepsilon(T) = 10^{[7.5(T - 273.15)/(T - 35.8) + 0.786]} \quad \ldots (2.5\text{-}35)$$

with T in Kelvin. The surface temperature enters equation (2.5-32) through the radiation balance, since the radiation emitted at the surface, as well as the terrestrial radiation, I_{LW} depends on the surface temperature, thus contributing further to the iterative nature of the solution.

During night-time, equation (2.5-32) is no longer valid, and Holtslag and Van Ulden [87HO1] proposed

$$q_{sens} = -\frac{90}{1 + \frac{4}{(v_{10})^2}}(1 - 0.9N^2) \quad \ldots (2.5\text{-}36)$$

According to Van Dop et al [79DO1], the above equation is restricted to a positive net radiative heat flux. If the net radiative heat flux becomes negative, the sensible heat should be calculated from

$$q_{sens} = 0.4\{(1 - \alpha_r)I_s + I_{LW} - \sigma T^4\} \quad \ldots (2.5\text{-}37)$$

A first estimate of the shear velocity is made from the known velocity profile calculated at time t. At time t, the Monin-Obukhov length, and hence the universal functions ϕ are also known. Thus, using the proper integration of the universal function ϕ_m, find

$$v_* = \frac{\kappa v_{10}}{\varphi(\xi)} \qquad \ldots (2.5\text{-}38)$$

A new value of the scaling temperature, θ_* is calculated from equation (2.5-6), and using the new values for v_* and θ_*, Monin and Obukhov's scaling length, L, is calculated from equation (2.5-8). Using this value of L, the wind and temperature profiles in the constant flux layer are recalculated, and one has to repeat the process until sufficient convergence is achieved. These converged profiles are then adopted for time $t + \Delta t$.

Although these models were derived primarily to predict temperature and wind profiles, rather than analysing them, the reasoning behind them provides a valuable means for parameterizing atmospheric variables for later use in evaluating the influence of ambient conditions on cooling tower performance.

CHAPTER 3

DRY-COOLING TOWER PERFORMANCE

3.1 INTRODUCTION

A dry-cooling tower transfers heat from the process fluid, say water, to the atmosphere. The water is confined to the inside of the tubes, with air flowing across its outside. Since the air-side heat transfer coefficient is much lower than that on the water side, fins are required to increase the air-side heat transfer area for a more compact design. Bundles of finned tubes are indeed the heart of any air-cooled heat exchanger.

3.2 AIR-SIDE HEAT TRANSFER

The performance characteristics of heat exchanger bundles are normally determined under idealized conditions in laboratory wind tunnels designed for that purpose, and the results are presented in empirical form. It is usual practice to present the data so obtained in dimensionless form. From dimensional analysis, it follows that the convective heat transfer coefficient may be presented in terms of the Nusselt number, Nu, which is a function of the Reynolds number, Re. In order to evaluate the air-side Reynolds number, some form of an equivalent diameter, d_e is required. Thus, in general

$$Nu = \frac{h d_e}{k} = \phi(Re) \qquad \ldots (3.2\text{-}1)$$

In the literature, a myriad definitions for the air-side equivalent diameter for finned tubes are proposed, which only leads to confusion and often rules out any meaningful comparison between different types of finned surfaces. Kröger [86KR1] defined two dimensional parameters that bypass the use of an equivalent diameter. He suggested that a dimensional heat transfer parameter Ny, should be used instead of the Nusselt number.

This parameter is expressed in terms of a dimensional flow parameter, Ry that replaces the Reynolds number

$$Ry = \frac{1}{\mu}\left(\frac{\dot{m}}{A_{fr}}\right) \qquad \ldots (3.2\text{-}2)$$

The effective air-side heat transfer coefficient may be expressed in terms of Kröger's [86KR1] dimensional heat transfer parameter, Ny

$$Ny = \frac{h_f A_f}{k_a A_{fr} Pr^{1/3}} = a_{Ny} Ry^{b_{Ny}} \qquad \ldots (3.2\text{-}3)$$

Kröger [86KR1] found that an exponential expression like that on the right hand side of equation (3.2-3) fits his experimental data well.

The isothermal pressure drop over a heat exchanger bundle is expressed in the following form [86KR1]

$$(K_{he})_{iso} = \frac{\Delta p_a}{0.5\rho_a v_a^2} = a_{he} Ry^{b_{he}} \qquad \ldots (3.2\text{-}4)$$

In a heat exchanger, the air expands as it is heated up, and there is an additional pressure loss due to the acceleration of air through the bundle. For a non-isothermal bundle, isothermal pressure loss coefficient is modified to account for this additional pressure loss

$$K_{he} = (K_{he})_{iso} + \frac{2}{\sigma^2}\left(\frac{\rho_{ai} - \rho_{ao}}{\rho_{ai} + \rho_{ao}}\right) \qquad \ldots (3.2\text{-}5)$$

with the area ratio, σ, defined as

$$\sigma = \frac{\text{Open flow area}}{\text{Frontal bundle area}} \qquad \ldots (3.2\text{-}6)$$

3.3 WATER-SIDE HEAT TRANSFER

Dimensional analysis suggests that the heat transfer coefficient for a fluid flowing on the inside of a tube should be of the form

$$Nu = \phi(Re, Pr) \qquad \ldots (3.3\text{-}1)$$

For fully developed turbulent flow, the heat and momentum transfer are almost totally controlled by the boundary layer. Since the boundary layer is quite often extremely thin, the surface finish of the tube is expected to have some influence over it [82HO1], [95DO1]. Researchers were forced to resort to experimental methods to determine the functional relationship suggested by equation (3.3-1). Petukhov [70PE1] developed the following relationship for fully developed turbulent flow through smooth tubes

$$Nu = \frac{(f/8)\,Re\,Pr}{1.07 + 12.7(f/8)^{0.5}\left[Pr^{0.667} - 1\right]}\left(\frac{\mu_b}{\mu_t}\right)^{0.25} \qquad \ldots (3.3\text{-}2)$$

if heat is transferred from the fluid to the tube wall. In equation (3.3-2), f is the friction factor, that may either be determined from the Moody diagram, or for computational purposes, from the following relation for smooth tubes [54FI1]

$$f = \left[1.83\log(Re) - 1.64\right]^{-2} \qquad \ldots (3.3\text{-}3)$$

Haaland [83HA1] modified equation (3.3-3) to account for the effect of surface roughness

$$f = 0.3086\left[\log\left\{\frac{6.9}{Re} + \left(\frac{\varepsilon / d}{3.7}\right)^{1.11}\right\}\right]^{-2} \qquad \ldots (3.3\text{-}4)$$

for the relative roughness, $\varepsilon/d > 10^{-4}$.

If entrance effects are expected to be of importance, Gnielinski [75GN1] suggested the following modification of equation (3.3-2)

$$Nu = \frac{(f/8)(Re - 1000)Pr\left[1 + (d/L)^{0.667}\right]}{1 + 12.7(f/8)^{0.5}\left[Pr^{0.667} - 1\right]} \qquad \ldots (3.3\text{-}5)$$

Equation (3.3-5) is applicable in the range $2300 < Re < 10^6$, $0.5 < Pr < 10^4$ and $0 < (d/L) < 1$.

3.4 NATURAL DRAFT COOLING TOWERS

The function of the cooling tower shell is to induce, by means of buoyancy effects, atmospheric air to flow through the finned tube heat exchanger bundles arranged horizontally inside the tower structure, as shown in figure 3-1. The air inside the tower is heated up, and consequently, its density is lower than that of the atmospheric air outside the tower at the same elevation. Assuming a constant pressure everywhere in the plane of the tower exit, the hydrostatic pressure inside the tower is lower than the atmospheric pressure outside the tower at the same elevation due to the lower density of the air inside the tower. This pressure difference causes air to flow through the tower at a rate that is dependent on the tower dimensions, the heat exchanger characteristics and the other flow resistances encountered [61LO1], [77BU1].

The heat rejected by the water flowing through the finned tubes is picked up by the air flowing across it, and a simple energy balance yields

$$Q = \dot{m}_a c_{pa}(T_{ao} - T_{ai}) = \dot{m}_w c_{pw}(T_{wi} - T_{wo}) \qquad \ldots (3.4\text{-}1)$$

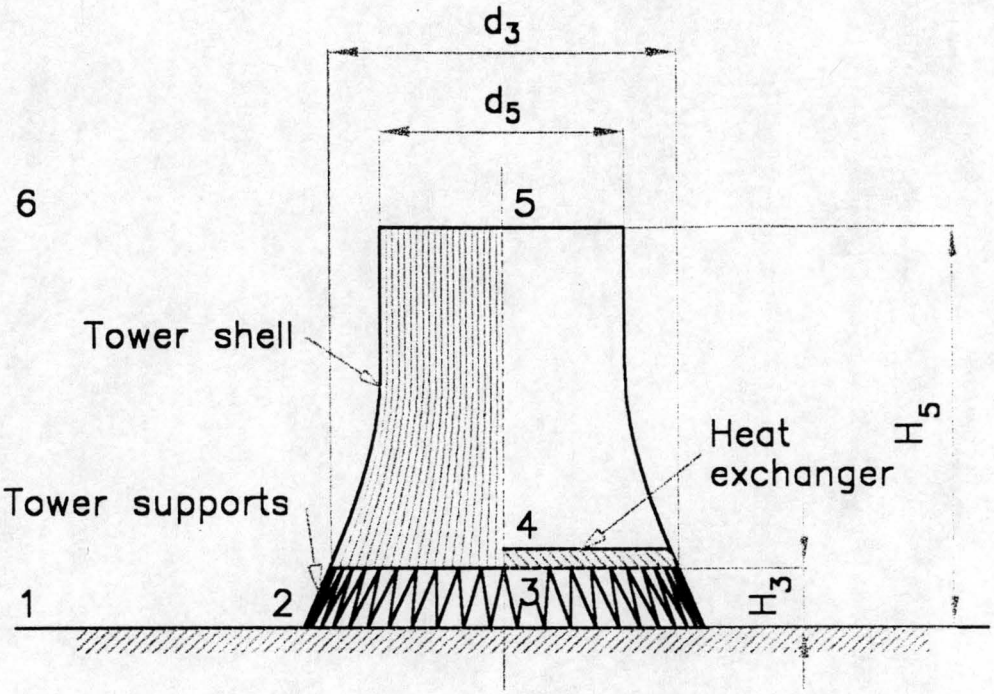

Figure 3-1. Definition sketch for a natural draft dry-cooling tower.

Using the heat exchanger characteristics, this heat transfer may also be expressed as

$$Q = \varepsilon\left(\dot{m} c_p\right)_{min} \left(T_{wi} - T_{ai}\right) \qquad \ldots (3.4\text{-}2)$$

with e the effectiveness of the heat exchanger. Expressions for the effectiveness for different heat exchanger configurations are given by Holman [82HO1]. The effectiveness is a function of the NTU, which in turn depends on the overall heat transfer coefficient, UA, that is given by

$$UA = \left[\frac{1}{h_f A_f} + \frac{1}{h_w A_w}\right]^{-1} \qquad \ldots (3.4\text{-}3)$$

The NTU-effectiveness method utilizes the known inlet air and water temperatures, and is preferred above the LMTD method in numerical work for its greater numerical stability during early iterations.

The hydrostatic pressure distribution is given by equation (2.3-1), and for a perfect gas, it becomes

$$dp = -\left(\frac{p}{RT}\right)dz \qquad \ldots (3.4\text{-}4)$$

With the pressure p_{a1} known at ground level, the pressure p_{a5} at the tower exit is found from integration of equation (3.4-4). This requires that the atmospheric temperature profile must be known.

Atmospheric air accelerates from stagnant conditions at 1 (see figure 3-1) and flows through the tower supports at 2, and changes direction before it enters the heat exchanger at 3. An additional pressure loss (Δp_{ct}) due to flow separation, contraction and distortion of the inlet flow pattern was first observed by Lowe and Christie [61LO1], and has since been refined by Geldenhuys and Kröger [86GE1], Du Preez and Kröger [88PR1] and Terblanche [93TE1]. A pressure balance between 1 and 4 yields

$$p_1 - \left(p_4 + 0.5\rho_{a4} v_{a4}^2\right) = \left(K_{ts} + K_{ct} + K_{ctc} + K_{he} + K_{cte}\right)_{he} \left(2\rho_{a34}\right)^{-1} \left(\frac{\dot{m}_a}{A_{fr}}\right)^2 + \rho_{a3} g H_3 \qquad \ldots (3.4\text{-}5)$$

All the pressure loss coefficients are based on the frontal area of the heat exchanger, A_{fr}, and the mean density through it, ρ_{a34}.

The density of the air entering the heat exchanger ρ_{a3} is found from the perfect gas law, and since the pressure drop across the heat exchanger in natural draft towers is small

(typically of the order of 100 Pa, mainly due to the low velocities encountered), the density of the air leaving the heat exchanger may be approximated by

$$\rho_{a4} \cong \frac{p_{a1}}{R\,T_{a4}} \qquad \ldots (3.4\text{-}6)$$

The reference density ρ_{a34} is simply based on the arithmetic mean of the temperatures T_{a3} and T_{a4}.

The loss coefficient associated with the tower supports, K_{ts}, is based on the drag coefficient for submerged two-dimensional bodies. Lists of the drag coefficients for such bodies are normally found in fluid mechanics textbooks. Hence

$$\Delta p_{ts} = \frac{N_{ts} F_{dts}}{\pi d_3 H_3} = \frac{0.5\rho_{a2} v_{a2}^2 C_{dts} (L_{ts} d_{ts}) N_{ts}}{\pi d_3 H_3} \qquad \ldots (3.4\text{-}7)$$

with N_{ts} the number of tower supports, L_{ts} the length of the tower supports and d_{ts} its effective diameter. Equation (3.4-7) may be rewritten in terms of the a pressure loss coefficient.

$$K'_{ts} = \frac{\Delta p_{ts}}{0.5\rho_{a2} v_{a2}^2} \qquad \ldots (3.4\text{-}8)$$

Since the air mass flow rate through a dry-cooling tower is constant, equation (3.4-8) may be written in terms of conditions at the heat exchanger. Hence, substituting equation (3.4-7) into (3.4-8), and applying the continuity equation between the tower supports and the heat exchanger, find

$$K_{ts} = \frac{C_{dts} L_{ts} d_{ts} N_{ts} A_{fr}^2}{(\pi d_3 H_3)^3} \left(\frac{\rho_{a34}}{\rho_{a2}}\right) \qquad \ldots (3.4\text{-}9)$$

Lowe and Christie [61LO1] observed an additional pressure loss in wet-cooling towers due to distorted inlet flow patterns and flow separation at the bottom edge of the tower shell, and this is taken into consideration through a cooling tower loss coefficient K_{ct}. Their model has subsequently been improved to allow for the higher flow resistance in dry-cooling towers, and Du Preez and Kröger [88PR1] proposed

$$K_{ct} = \left[-18.7 + 8.095\left(\frac{d_3}{H_3}\right) - 1.084\left(\frac{d_3}{H_3}\right)^2 + 0.0575\left(\frac{d_3}{H_3}\right)^3 \right] \times K_{he}^{[0.165 - 0.035(d_3/H_3)]} \quad \ldots (3.4\text{-}10)$$

for $19 \leq K_{he} \leq 50$ and $5 \leq (d_3/H_3) \leq 15$. Geldenhuys and Kröger [86GE1] suggested the following simplification of equation (3.4-10) for dry-cooling towers

$$K_{ct} = 0.72\left(\frac{d_3}{H_3}\right)^2 - 0.34\left(\frac{d_3}{H_3}\right) + 1.7 \quad \ldots (3.4\text{-}11)$$

If the heat exchanger bundles are arranged in V-arrays, the flow will enter the heat exchanger obliquely, resulting in further losses. Furthermore, on passing through the bundle, the streamlines will exit almost perpendicular to the downstream face of the bundle, and then converge into a jet parallel to the centerline of the tower. This jetting effect will result in flow separation at the downstream corners of the heat exchanger, which in turn gives rise to a distorted velocity profile through the exchanger. Kotze, Bellstedt and Kröger [86KO1] corrected equation (3.2-5) for oblique flow

$$K_{he\theta} = K_{he} + \left(\frac{1}{\sin\theta_m} - 1\right) \times \left[\left(\frac{1}{\sin\theta_m} - 1\right) + 2K_c^{0.5}\right] + K_d \quad \ldots (3.4\text{-}12)$$

with θ_m the mean flow incidence angle, and K_d the downstream pressure loss coefficient. K_c is an entrance contraction loss coefficient for the normal flow condition, and for most industrial finned tubes, a value of $K_c = 0.5$ may be adopted. Kotze, Bellstedt and Kröger [86KO1] suggested an expression for K_d based on half the apex angle θ of the V-array

$$K_d = \exp\left\{5.488405 - 0.2131209\left(\frac{\theta}{2}\right) + 3.533265\times10^{-3}\left(\frac{\theta}{2}\right)^2 - 2.901016\times10^{-4}\left(\frac{\theta}{2}\right)^3\right\}$$

... (3.4-13)

Due to the flow distortion downstream of the bundle, the flow incidence angle varies across the bundle, and its mean is slightly smaller than half the apex angle. The mean flow incidence angle may be approximated by

$$\theta_m = 0.0019\left(\frac{\theta}{2}\right)^2 + 0.9133\left(\frac{\theta}{2}\right) - 3.1558 \qquad \text{... (3.4-14)}$$

Since the heat exchanger bundles are normally of rectangular shape, it is impossible to cover the entire cross-sectional area of the tower inlet with it. This reduction in flow area will result in a contraction of the flow as it enters the heat exchangers, and a subsequent expansion upon its exit. These contraction and expansion losses are approximated by

$$K_{cte3} = 1 - \frac{2}{\sigma_c} + \frac{1}{\sigma_c^2} \qquad \text{... (3.4-15)}$$

and

$$K_{cte4} = (1 - \sigma_c)^2 \qquad \text{... (3.4-16)}$$

respectively. Weisbach [00WE1] determined the contraction ratio experimentally, and his data is presented in the following empirical form

$$\sigma_c = 0.6144517 + 0.04566493\left(\frac{A_{e3}}{A_3}\right) - 0.336651\left(\frac{A_{e3}}{A_3}\right)^2 + 0.4082743\left(\frac{A_{e3}}{A_3}\right)^3 + 2.672041\left(\frac{A_{e3}}{A_3}\right)^4 - 5.963169\left(\frac{A_{e3}}{A_3}\right)^5 + 3.558944\left(\frac{A_{e3}}{A_3}\right)^6$$

... (3.4-17)

In equation (3.4-16), σ_e is the porosity of the tower cross section, i.e.

$$\sigma_e = \frac{A_{e3}}{0.25\pi d_3^2} \qquad \ldots (3.4\text{-}18)$$

The effective area A_{e3} corresponds to the horizontally projected frontal area of the heat exchanger bundles. For use in equation (3.4-5), equations (3.4-15) and (3.4-16) must be referred to the mean flow conditions through the heat exchanger:

$$K_{ctc} = K_{ctc3}\left(\frac{\rho_{a34}}{\rho_{a3}}\right)\left(\frac{A_{fr}}{A_{e3}}\right)^2 \qquad \ldots (3.4\text{-}19)$$

and

$$K_{cte} = K_{cte3}\left(\frac{\rho_{a34}}{\rho_{a4}}\right)\left(\frac{A_{fr}}{A_{e3}}\right)^2 \qquad \ldots (3.4\text{-}20)$$

respectively. Downstream of the heat exchanger, the flow is essentially isentropic, and from the first law of thermodynamics, find

$$c_{pa4}\,T_{a4} + 0.5v_{a4}^2 + gH_4 = c_{pa5}\,T_{a5} + 0.5v_{a5}^2 + gH_5 \qquad \ldots (3.4\text{-}21)$$

Noting that the heat exchanger is thin relative to the height of the tower, and invoking some of the relations for low speed isentropic flow [76ZU1], equation (3.4-21) may be approximated by

$$\left(p_{a4} + 0.5\rho_{a4}\,v_{a4}^2\right) - \left(p_{a5} + 0.5\rho_{a5}\,v_{a5}^2\right) \approx \rho_{a45}\,g\left(H_5 - H_4\right) \qquad \ldots (3.4\text{-}22)$$

with the mean density in the tower between 4 and 5

$$\rho_{a45} = \frac{\rho_{a4} + \rho_{a5}}{2} \qquad \ldots (3.4\text{-}23)$$

Due to adiabatic expansion of the air as it rises, it follows from the energy equation that the temperature at the tower outlet, T_{a5}, will be slightly lower than that of the air at the exit of the heat exchanger:

$$T_{a5} = T_{a4} - \left[\frac{\left(v_{a5}^2 - v_{a4}^2\right) + 2g\left(H_5 - H_4\right)}{2c_{pa}}\right] \qquad \ldots (3.4\text{-}24)$$

Structural considerations dictates that natural draft towers have a hyperbolic shape, with the diameter at the top smaller than at the bottom. Hence, both terms in brackets in equation (3.4-24) will be positive, confirming that T_{a5} will indeed be lower than T_{a4}. The kinetic energy term in equation (3.4-24) is insignificant, and may be omitted from the equation.

The density of the warm air leaving the tower is found from the perfect gas law, assuming that the pressure is constant everywhere in the plane of the tower outlet. Far away from the tower, at 6, the pressure is found from the proper integration of equation (3.4-4), using the atmospheric temperature profile.

Add equations (3.4-9), (3.4-11), (3.4-12), (3.4-19) and (3.4-20) to find the pressure drop through the tower:

$$p_{a1} - p_{a5} = \left\{\sum_j K_j\right\}_{he} \frac{1}{2\rho_{a34}}\left(\frac{\dot{m}_a}{A_{fr}}\right)^2 - \int_{H_1}^{H_3} \frac{g\,p(z)}{R\,T(z)}dz + \rho_{a45}\,g\left(H_5 - H_4\right) + \frac{\rho_{a5}\,v_{a5}^2}{2}$$

$$\ldots (3.4\text{-}25)$$

The pressure drop through the tower must equal the hydrostatic pressure drop outside the tower. Hence, if v_{a5} is expressed in terms of the air mass flow through the tower, equation (3.4-25) may be written as

$$-\int_{H_1}^{H_5}\frac{g\,p(z)}{R\,T(z)}dz = \left\{\sum_j K_j\right\}_{he}\frac{1}{2\rho_{a34}}\left(\frac{\dot{m}_a}{A_{fr}}\right)^2 - \int_{H_1}^{H_3}\frac{g\,p(z)}{R\,T(z)}dz + \rho_{a45}\,g(H_5 - H_4) + \frac{\rho_{a5}}{2}\left(\frac{\dot{m}_a}{A_5}\right)^2 \quad \ldots (3.4\text{-}26)$$

The integrals are deliberately left untreated in equations (3.4-25) and (3.4-26), since they depend on the atmospheric temperature profiles. Equation (3.4-26) is known as the draft equation for a natural draft dry-cooling tower.

If the atmosphere is adiabatic, equation (3.4-26) simplifies to a more familiar form [77BU1]

$$(\rho_{a1} - \rho_{a4})g(H_5 - H_3) = \left(\sum_j K_j\right)_{he}\frac{1}{2\rho_{a34}}\left(\frac{\dot{m}_a}{A_{fr}}\right)^2 + \frac{1}{2\rho_{a5}}\left(\frac{\dot{m}_a}{A_5}\right)^2 \quad \ldots (3.4\text{-}27)$$

CHAPTER 4

FULL SCALE TESTS

4.1 INTRODUCTION

Extensive field tests were performed during July and August 1990 on cooling tower 1 at the Kendal power station. The purpose of these tests was to determine the effect of ambient temperature stratification on the performance of the cooling tower.

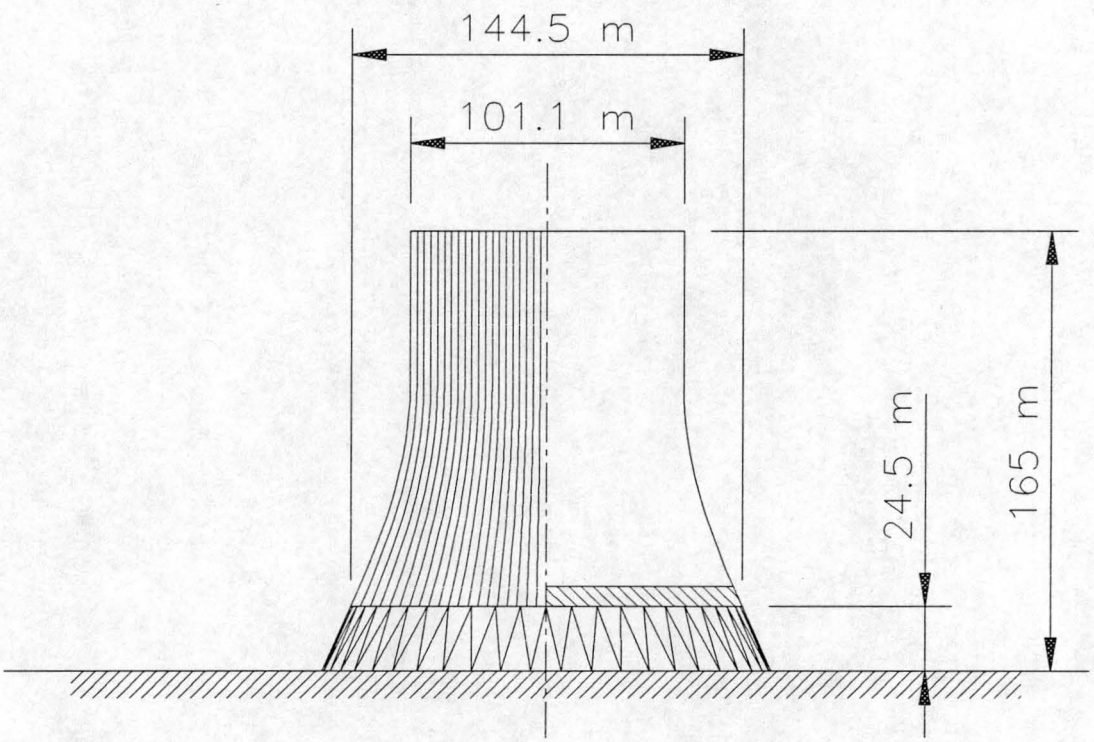

Figure 4-1. Schematic lay-out of one of the Kendal dry-cooling towers.

At full load, the six turbines of the Kendal power station generate 4 000 MW, making it the largest natural draft dry-cooled power station in the world. The waste heat is rejected by six hyperbolic natural draft dry-cooling towers, each measuring 165 m in height with a base diameter of 144.5 m. The towers have an inlet height of 24.5 m, while the diameter at the throat is 101.1 m. From the throat to the tower exit, the shell is

almost cylindrical. A sketch of the tower is given in figure 4-1. The heat exchanger bundles comprise of horizontal V-arrays arranged radially in the tower inlet cross-sectional area.

Cooling water is circulated via two 3.1 m diameter ducts between the tower and the surface condenser by three pumps connected in parallel. It takes approximately nine minutes for the water to pass through the entire cooling system. Given a constant heat rejection rate at the condenser, the water inlet temperature at the cooling tower will take nine minutes to respond to changes in atmospheric conditions. In contrast to the cooling cycle, only 90 seconds elapse from the time the water enters the tower, until its exit.

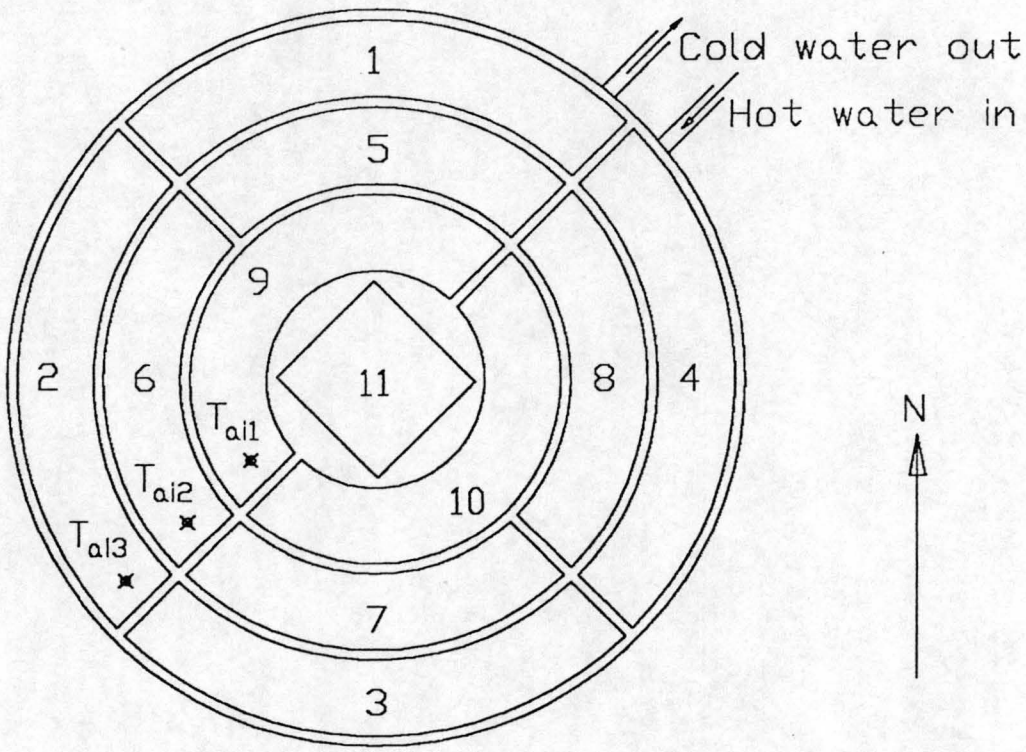

Figure 4-2. Plan view, showing the arrangement of the heat exchanger bundles in 11 sectors.

The heat exchanger bundles are arranged in eleven sectors as shown in figure 4-2, that are individually controlled from the control room. Upon shut-down of a sector, the cooling water is drained immediately and the sector is filled with nitrogen gas to prevent corrosion. A maximum of four sectors may be shut off at any given time.

An added benefit at the time was that the Kendal power station was still under construction, with only one unit in operation. This allowed the author the unique opportunity to study the interaction between a single cooling tower and one turbine and condenser, without interference from other towers nearby.

The ground plan of the site, showing the major buildings of the power station, is depicted in figure 4-3. Wind and temperature measurements were recorded on a 96 m tall weather mast, 700 m north of tower 1. This mast proved invaluable to the investigation, since the usual meteorological measurements are inadequate when one is interested not only in the variables themselves, but in their profiles as well.

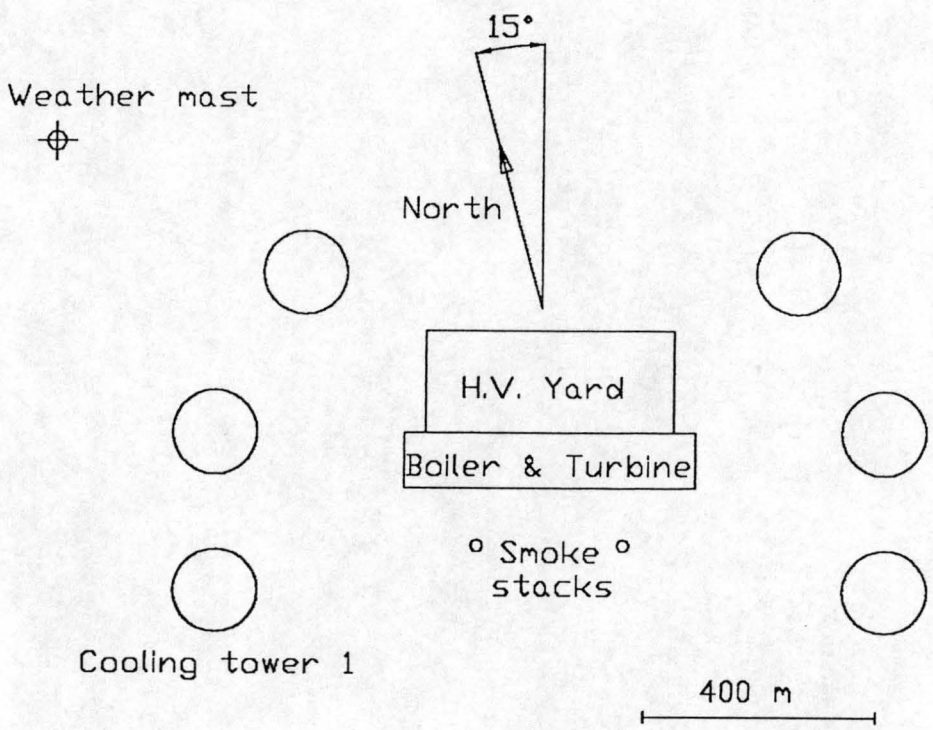

Figure 4-3. Ground plan of Kendal Power Station.

Kendal Power Station is situated in Mpumalanga, 90 km east of Johannesburg on the Eastern Transvaal Highveld, and approximately on the 26 ° South latitude. The station is situated in a vast open grassland of low, rolling hills, that is almost devoid of trees. It is in a rural area with agriculture the major economic activity. There are no tall obstacles, except the structures of the power station itself, in the proximity of the weather mast.

The Eastern Transvaal Highveld is in a summer rainfall area, as is most of the South African interior. During winter, low wind speeds, clear skies and very dry conditions normally prevail.

4.2 INSTRUMENTATION

Meteorological measurements, consisting of dry-bulb temperature, wind speed and wind direction were taken at the weather mast, while the barometric pressure was measured at ground level. These readings were logged continuously, and averaged values were stored on tape every six minutes.

The wind speed and direction were derived from the readings of a cluster of three anemometers, mounted perpendicular to each other along a Cartesian grid with the x-axis facing east, the y-axis north and the z-axis upwards. These anemometer clusters were mounted at 10 m, 20 m, 40 m, 65 m and 96 m above ground level respectively. At each of these elevations, a thermocouple measured the ambient air temperature. Additional thermocouples were mounted at 1.2 m, 2.5 m and 5.0 m above ground level to measure the sharp changes in the air temperature close to the ground.

In addition to the meteorological data, measurements were taken at the cooling tower to reflect the response of the cooling system to variations in the meteorological conditions. The air inlet temperature was measured by three unshielded chromel-alumel thermocouples, 1.5 m below the bundles in the positions shown in figure 4-2. Although radiation exchange between the tip of the thermocouple and the heat exchanger will raise the temperature recorded by the thermocouple, it can be shown that this increase in temperature is of the same order as the accuracy of the thermocouple itself. Furthermore, eight evenly spaced thermocouples were strung vertically across the tower inlet height, between the tower supports.

The water inlet temperature was measured at the hot water duct by two thermocouples attached to its outer wall. By insulating the thermocouples with a 250 mm diameter cone

filled with poly-urethane foam, it was ensured that the temperature of the wall was essentially the same as the water temperature. Furthermore, by placing the thermocouples just past a 90 ° elbow in the pipe, the corresponding mixing ensured that the temperature measured was representative of the bulk water temperature. The water outlet temperature was measured individually for each sector in an attempt to determine the uneven temperature distribution resulting from the influence of cross-winds on the tower. This problem was addressed in detail by Du Preez [92DU1].

An hourly log of the water mass flow rate through the tower was obtained from the control room (courtesy of ESKOM). ESKOM also supplied hourly logs of the generator output. For further details on especially wind and air mass flow rate measurements, the reader is referred to Du Preez [92DU1].

All the thermocouple readings were collected by a DIGILINK III datalogger, using its internal ice point as a reference. The internal ice point was calibrated against the melting point of crushed ice for each individual thermocouple, and the resultant maximum deviation never exceeded 0.2 °C. A calibration constant was calculated for each thermocouple to compensate for this deviation. The datalogger's standard correlation for chromal-alumel thermocouples was used to convert the thermocouple's millivolt readings into degrees Celsius.

Four thermocouples, suspended from cables strung across the tower exit, were used to measure the air outlet temperature. These thermocouples were approximately 110 m above the heat exchanger. Each thermocouple was protected from solar radiation by a reflective radiation shield.

Twelve calibrated vane-anemometers, mounted at the same elevation, measured the air speed through the tower. The anemometers were positioned along north-east and north-west axes, in the positions shown in figure 4-4. Radially, they were spaced such that they represent equal flow areas. All the anemometer and thermocouple readings were also collected on the DIGILINK III.

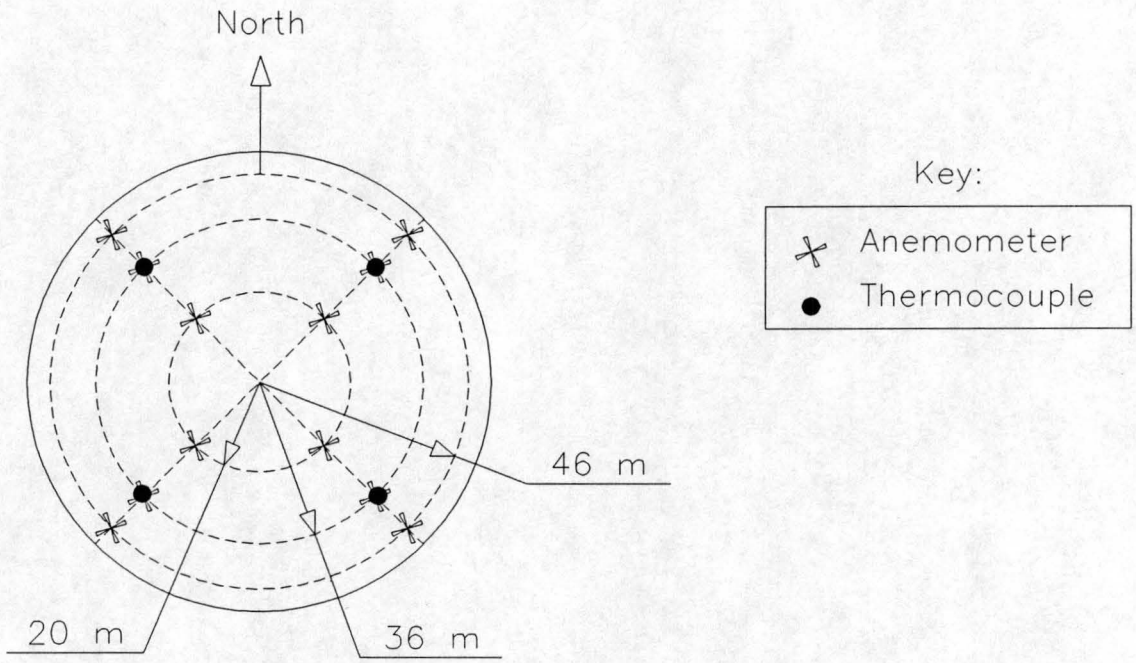

Figure 4-4. Positioning of anemometers and thermocouples to measure air flow through the tower and the air outlet temperature.

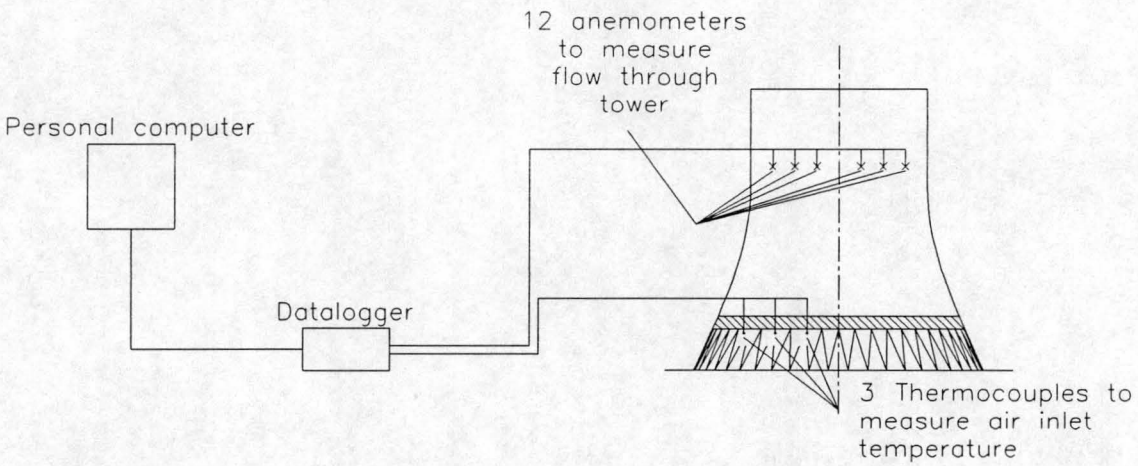

Figure 4-5. Schematic lay-out of test equipment.

Every ten seconds, a complete set of recorded data was transmitted to an Olivetti M21 personal computer, programmed to receive the data. Anemometer readings were converted to wind speeds, and temperature readings were corrected by the program, whereupon the five minute integrated averages were stored on disk. A schematic representation of the data acquisitioning system is shown in figure 4-5.

4.3 DISCUSSION OF THE DATA

Visual observation proved to be a valuable tool for detecting general trends in the data, as shown in figures 4-6 through 4-12. Although the tests were run continuously for almost two months, only 9 August 1990 could be considered to be a windless day. For most of that day, the wind speed rarely exceeded 2 m/s, but around 20:00, the wind speed increased to approximately 4 m/s. Du Preez [92DU1] found that the influence of cross-winds on the tower is negligible if the average wind speed drops below 2 m/s. Hence, secondary effects on the tower's performance on that day, may be attributed to the sole effect of temperature inversions. The ambient temperature and the heat rejection rate are the primary variables.

During the test period, the generator output was kept constant at 500 MW, but was occasionally raised to 660 MW, a situation that is reflected clearly in the water temperatures.

These generator loads convert to heat rejection rates of 800 MW and 1000 MW at the tower, as depicted in figure 4-10. Ideally, the turbine output should have been constant if one wants to determine the influence of diurnal variations in the atmospheric parameters on the tower's performance. Discarding data measured during periods of full-load (660 MW), the resulting gaps in the data will restrict the calculations severely, thus this data was retained, while special attention was given to potential transitional phenomena. The water mass flow rate was kept constant throughout the test period.

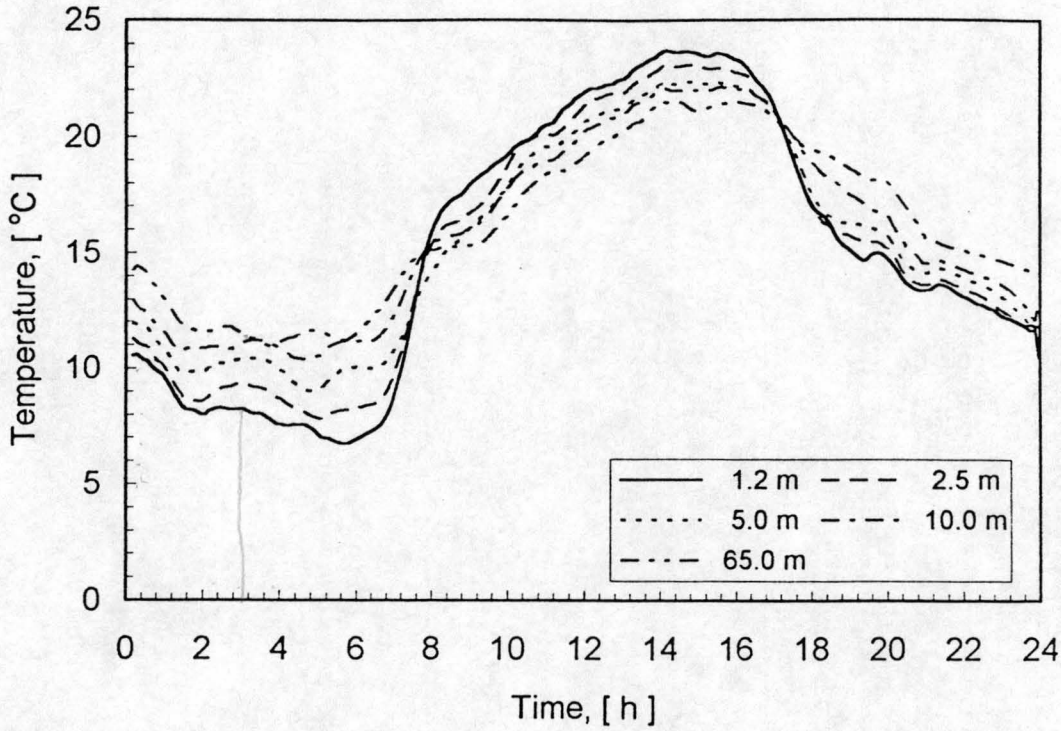

Figure 4-6. Ambient air temperatures measured at weather mast (9 August 1990).

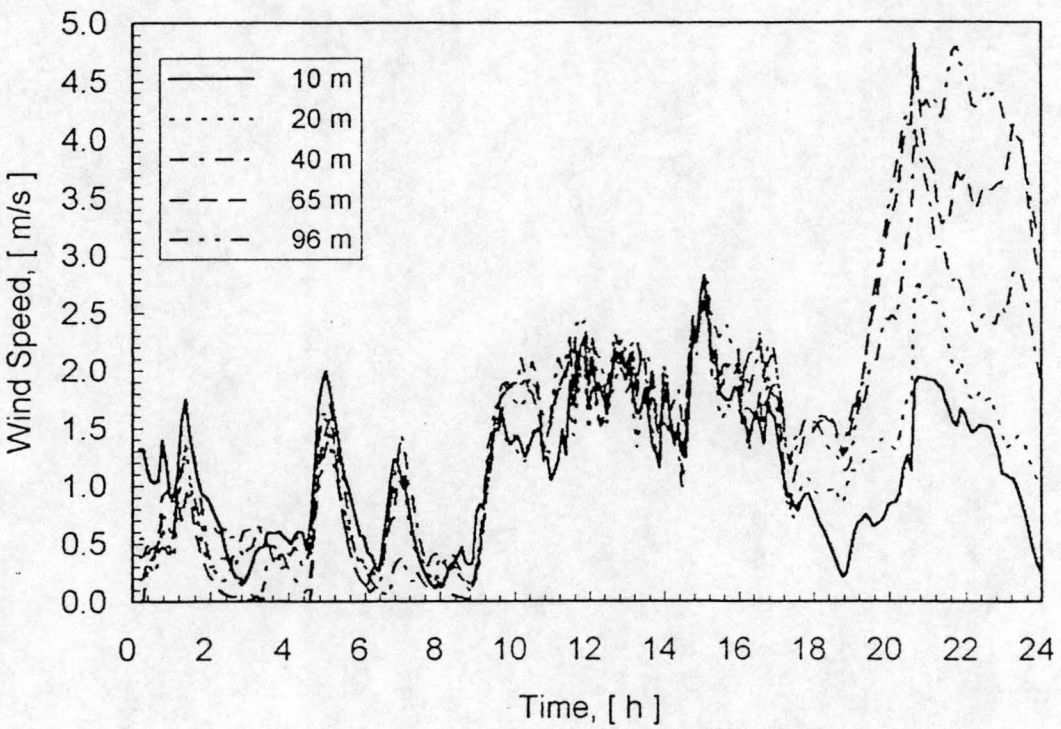

Figure 4-7. Wind speeds measured at the mast (9 August 1990).

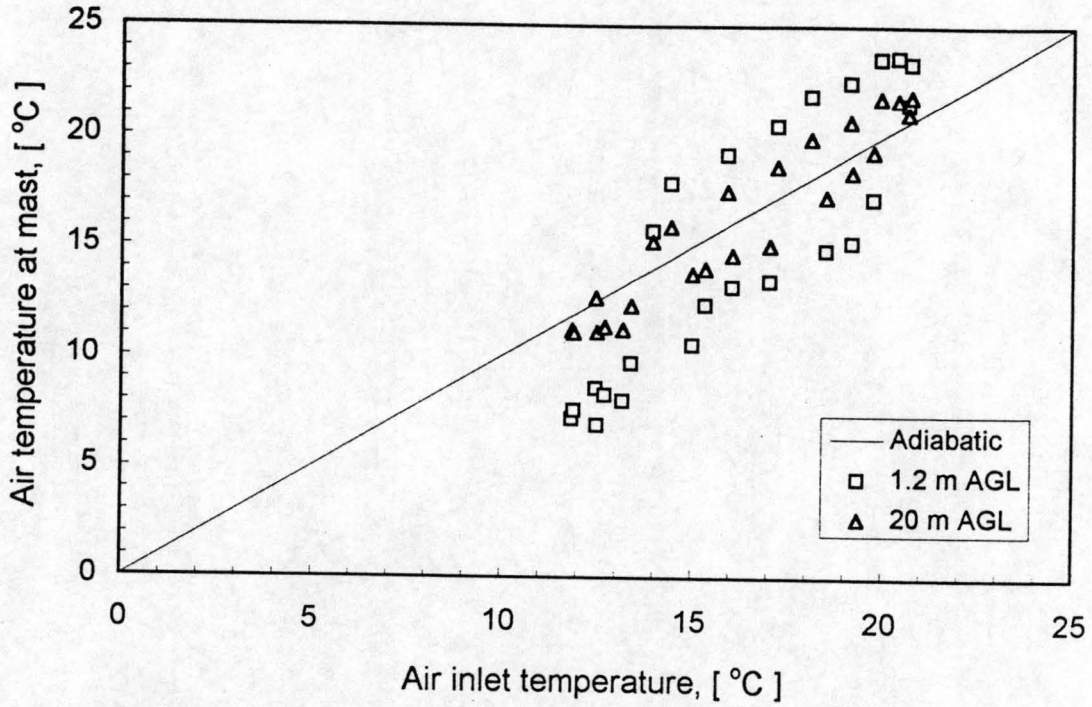

Figure 4-8. Comparison of the air temperatures measured at the heat exchanger and at the weather mast (9 August 1990).

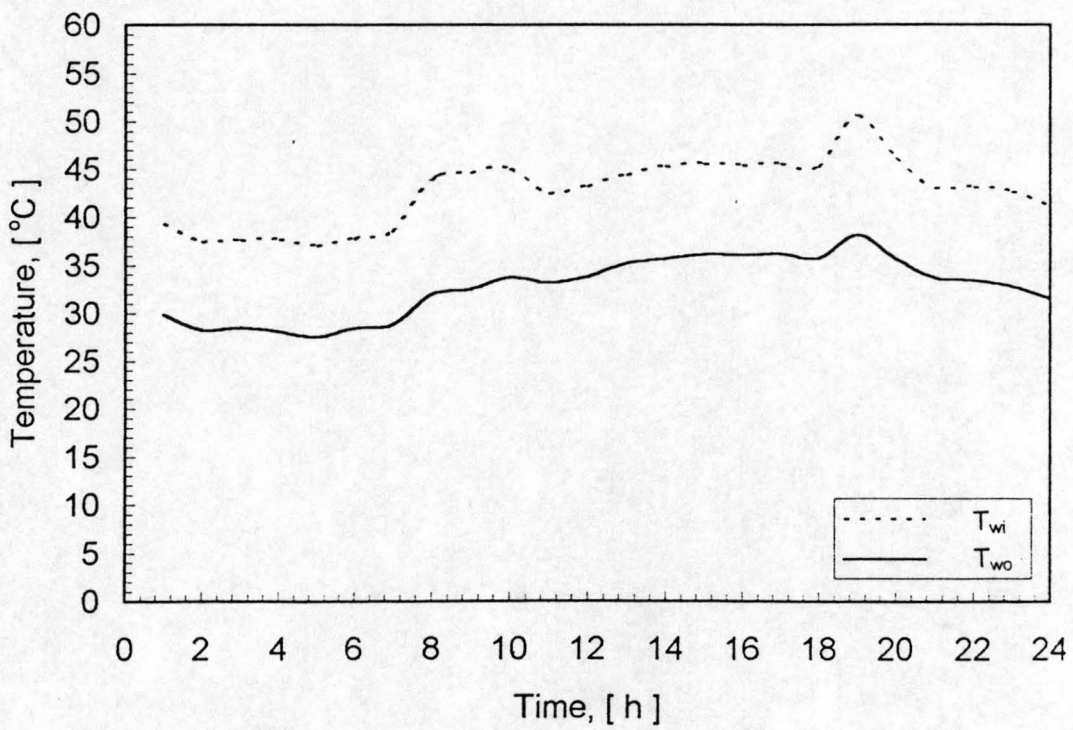

Figure 4-9. Water temperatures measured at the tower (9 August 1990).

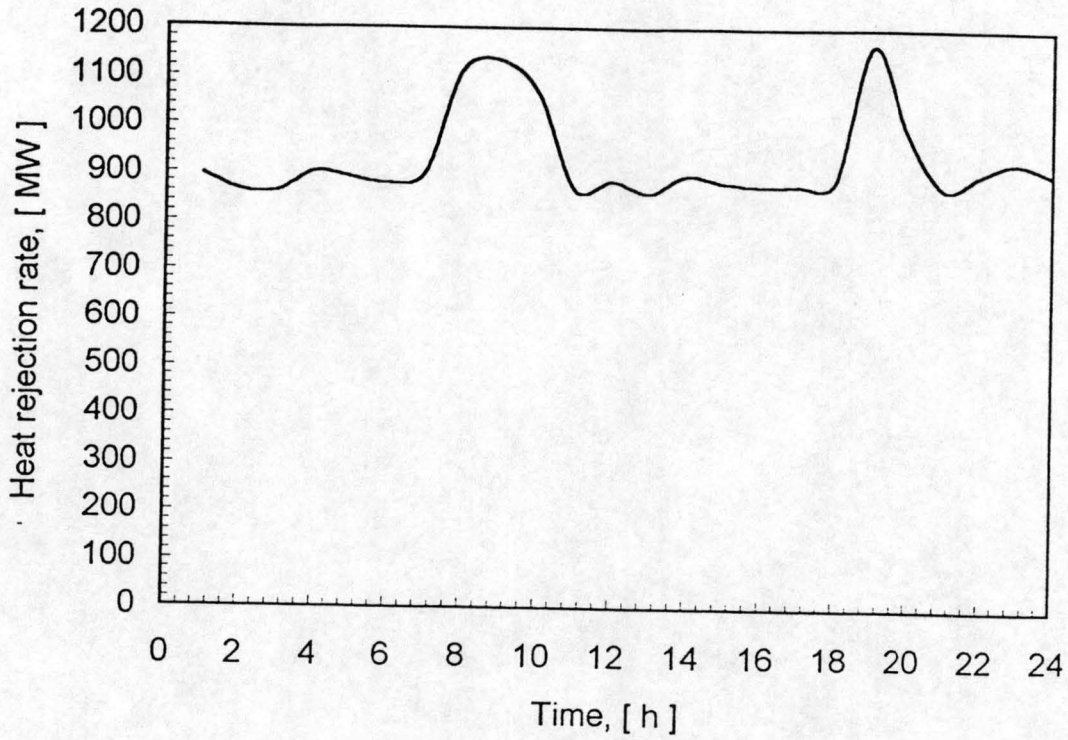

Figure 4-10. Heat rejected by the tower (9 August 1990).

The variation in wind speed with height is presented in figure 4-7. For most of the day, the average wind speed was below 2 m/s. At such low wind speeds, considerable scatter occurs in both the wind speed and direction. Furthermore, the scatter in the wind speed is of the same order of magnitude as the average wind speed, and the wind speed measurements become unreliable. Thus, for determining the atmospheric stability parameters, preference will be given to the temperature profiles, which are more consistent.

Large differences between the air inlet temperature measured underneath the heat exchanger at the tower, and the ambient air temperature measured at 1.2 m at the weather mast were observed. Most significantly, the air inlet temperature measured at the tower is higher than the ambient temperature during the night, but this situation is reversed during the day. The larger differences observed early in the morning (00:00 to 08:00) may be attributed to the continuous development of the temperature inversion during the night. One would have expected the same trend in the early evening (sunset to 24:00), but on this particular day, the wind speed picked up significantly at 20:00.

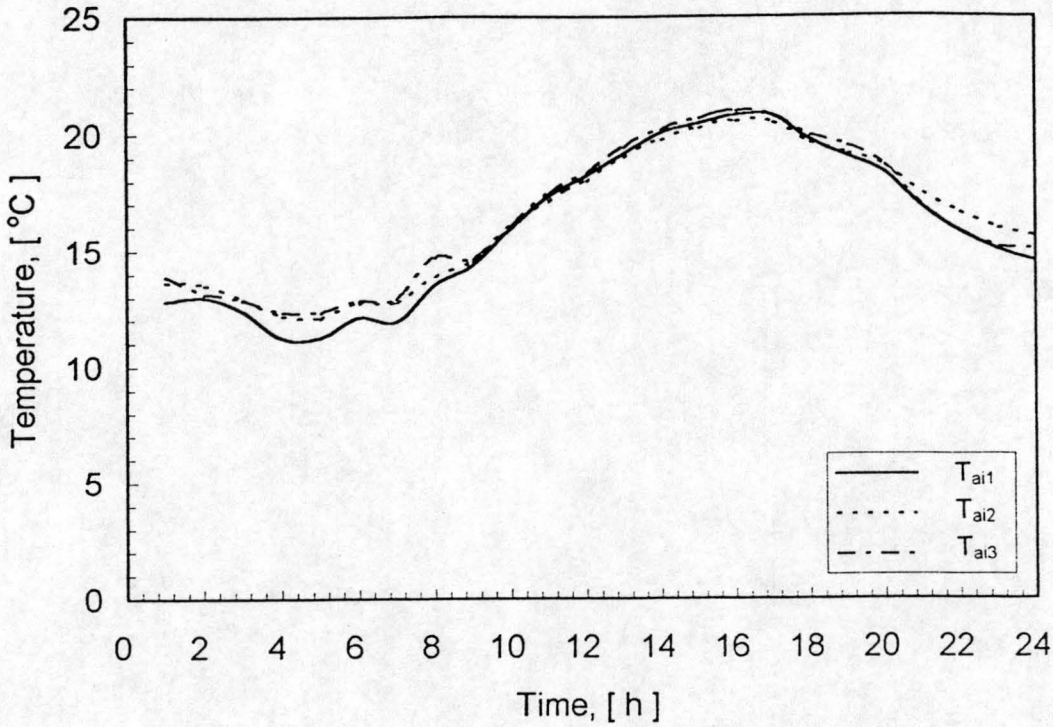

Figure 4-11. Air temperatures measured at the heat exchanger inlet.

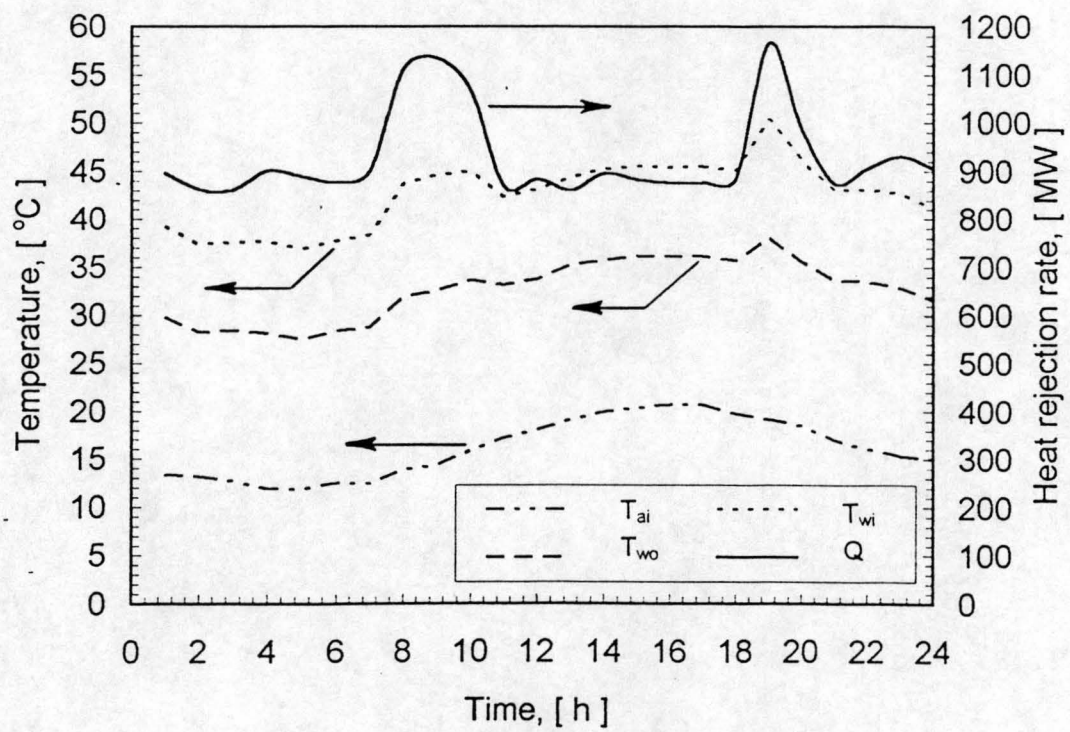

Figure 4-12. Variation of the water inlet- and outlet temperatures, air inlet temperature and heat rejection rate during the day (9 August 1990).

The increased turbulence associated with the higher wind speeds probably somewhat suppressed the development of the early evening inversion layer on this day.

The magnitude of the difference in air temperature measured at the weather mast (at 1.2 m) and underneath the heat exchanger at the tower inlet is significantly lower than the strength of the temperature stratification. Furthermore, the air inlet temperature relates to the temperature of the higher layers, as measured at the weather mast. These layers are also subjected to smaller diurnal temperature fluctuations than the lower layers, as shown in figure 4-6.

The air inlet temperature, as measured on three different radii underneath the heat exchanger bundles as shown in figure 4-2, showed little variation (see figure 4-11). This may be interpreted in one of two ways. Either a fair amount of mixing of air occurs prior to its entry to the heat exchanger bundles, or the tower draws in air mainly from higher elevations.

Abrupt changes in wind velocity and air temperature did not occur, and the tower operated in a presumably stable equilibrium with its environment throughout that day.

As expected, the water inlet and outlet temperature followed the air inlet temperature, measured directly under the heat exchanger bundles, closely, as shown in figure 4-12. This proves that the problem is not so much linked to the cooling tower itself, as specifying the correct air inlet temperature to the tower.

4.4 QUANTIFYING THE EFFECT OF TEMPERATURE STRATIFICATIONS ON TOWER PERFORMANCE

Hourly spot values of the data presented in figures 4-6 and 4-7 are presented in tables B-1 and B-2 respectively. The ambient air temperature at 1.2 m AGL and 20 m AGL is plotted against the air inlet temperature in figure 4-8. It is clear that the air inlet temperature (measured at a height of 23 m AGL) follows an ambient temperature

measured in its own plane more closely than the ambient temperature measured closer to the ground. This suggests that the air that flows through the tower, comes predominantly from the higher layers. Unfortunately, temperature measurements in these layers are seldom available.

If one considers the shape of a temperature inversion, for instance, it can roughly be quantified by the inversion strength (i.e. the maximum temperature difference in the layer, normally referenced against the ground level temperature) and the height at which the maximum inversion strength occurs. If the tower draws in air from different heights, not only the strength of the inversion, but also the inversion height will influence the air inlet temperature at the tower. If no temperature measurements are available in, say the first 100 m above ground level, it will be impossible to quantify the inversion height.

On the other hand, the unstable afternoon profile will exhibit a continuous temperature decrease with altitude, which makes defining an equivalent for the "inversion height" impossible for an unstable temperature profile. Obviously, no equivalent exists for the "inversion strength" as well.

In view of the limitations of the above definitions, the scaling temperature θ_*, as defined by equation (2.5-6), and the Monin-Obukhov scaling length, defined by equation (2.5-8). was used to characterise the temperature profiles. The scaling temperature has the advantage that it contains the sensible heat flux (or potential temperature gradient), and it is the sensible heat flux that is responsible for the inversion in the first place. Hence, it is an inherently good parameter to describe thermal transport processes in the atmosphere. Furthermore, the scaling temperature will change sign as the atmospheric conditions change from unstable during the day, to stable night-time conditions.

The Monin-Obukhov length represents the height at which the rates of mechanical and thermal production of turbulence in the atmosphere are equal. Above that height, mechanical production of turbulence, i.e. the effect of the wind, dominates. Due to the increased mixing above that height, the atmosphere will be almost adiabatic higher up, resulting in little further change of potential temperature with height. The Monin-

Obukhov length and the inversion height (when defined) should be related, and both will give an indication of the range within which the strongest wind and temperature gradients will occur.

Normally, the Monin-Obukhov length is used in its reciprocal form to avoid discontinuities when $L \rightarrow \infty$, and a parameter of the form

$$X = \frac{\theta_*}{|L|} \qquad \ldots (4.4\text{-}1)$$

should serve correlation purposes well. In equation (4.4-1), the absolute value of the Monin-Obukhov length is used, since it also changes sign if the ambient conditions change from stable to unstable or vice versa. Otherwise, the desirable property of θ_* to change sign when the atmosphere changes from stable to unstable or back, will be lost.

4.5 DETERMINING θ_*, v_* AND L

Equation (4.4-1) and the reasoning behind it are based on the assumption that the meteorological parameters v_*, θ_* and L can be derived from the available measurements. In this section, a method is proposed to derive these parameters from the measurements taken at the weather mast.

As an example, the averaged wind and temperature profiles measured at 03:00 on 9 August 1990 were used (see tables B-1 and B-2). First, the temperatures should be converted into potential temperatures, using equation (2.5-2). Since atmospheric pressure is hydrostatically compounded, the pressure at any elevation z is found from numerical integration of equation (2.3-1).

$$p(z+\Delta z) = p(z) - \frac{2gp(z)}{R\left[T(z)+T(z+\Delta z)\right]}\Delta z \qquad \ldots (4.5\text{-}1)$$

with T in Kelvin. Using the pressure and temperature measured at 1.2 m, find the pressure at 2.5 m:

$$p(2.5\text{ m}) = 84600\text{ Pa} - \frac{2\times 9.8\text{ m/s}^2\times 84600\text{ Pa}}{287.08\text{ J/kgK}\times[281.403\text{K}+282.494\text{K}]}\times(2.5\text{ m}-1.2\text{ m})$$

$$= 84587\text{ Pa}$$

The pressure at 2.5 m is then used to calculate the pressure at 5.0 m, and so forth.

1.2 m is used as a reference height, since it is the height at which the pressure was measured. Hence, at 1.2 m, the potential temperature will be exactly the same as the actual temperature. From equation (2.5-2), the potential temperature at 2.5 m is

$$\theta(2.5\text{ m}) = 282.494\text{ K}\times\left(\frac{84600\text{ Pa}}{84587\text{ Pa}}\right)^{(1.4-1)/1.4} = 282.507\text{ K}\ (9.357\ ^\circ\text{C})$$

The potential temperatures corresponding to the temperatures measured at 03:00 (table B-1) are given in table 4-1.

Table 4-1. Conversion of temperatures to potential temperatures.

z [m]	T(z) [°C]	p(z) [Pa]	θ(z) [°C]
1.2	8.253	84600	8.253
2.5	9.344	84587	9.357
5.0	10.365	84561	10.402
10.0	10.978	84510	11.064
20.0	11.324	84409	11.508
40.0	11.732	84206	12.112
65.0	11.551	83954	12.175
96.0	12.482	83643	13.412

The fact that the ambient potential temperature increased with height, as seen from table 4-1, means that the atmosphere is stable. Although ξ is still unknown, since L is

unknown, the fact that the atmosphere is stably stratified means that the appropriate form of the functions ϕ_m and ϕ_h from table 2-1 is

$$\phi_m = \phi_h = \left[1 + 22.8\xi\right]^{1/2}$$

The potential temperature at any elevation within the constant flux layer is found by integrating equation (2.5-3) twice.

$$\int_{z_0}^{z}\int \frac{d}{d\theta}\left(\Gamma_h \frac{d\theta}{dz}\right) = \int_{z_0}^{z} \Gamma_h \frac{d\theta}{dz} \qquad \ldots (4.5\text{-}2)$$

Substitute Γ_h from equation (2.5-5a) into equation (4.5-2) to find

$$\begin{aligned}
\int_{z_0}^{z} \Gamma_h \frac{d\theta}{dz} &= \int_{z_0}^{z} \frac{\kappa z}{\theta_* \phi_h(z/L)} \frac{d\theta}{dz} \\
\therefore \quad \int_{\theta_0}^{\theta} d\theta &= \frac{\theta_*}{\kappa}\int_{z_0}^{z} \frac{\phi_h(z/L)}{z} dz \\
\theta - \theta_0 &= \frac{\theta_*}{\kappa}\int_{z_0}^{z} \frac{\phi_h(z/L)}{z/L} d\left(\frac{z}{L}\right) \qquad \ldots (4.5\text{-}3) \\
\therefore \quad \theta &= \theta_0 + \frac{\theta_*}{\kappa}\int_{\xi_0}^{\xi} \frac{\phi_h(\xi)}{\xi} d\xi \\
&= \theta_0 + \frac{\theta_*}{\kappa}\varphi_h(\xi)
\end{aligned}$$

If $\varphi_h(\xi)$ is treated as a variable, equation (4.5-3) suggests a linear relationship between the potential temperature θ and φ_h. The integration for the wind speed was done earlier in chapter 2, and the wind speed is given by equation (2.5-28).

The scaling temperature θ_*, and the surface potential temperature θ_0 (corresponding to the roughness length z_0) and the scaling velocity v_* must be derived from the data given in tables B-1 and B-2. For a flat relief vegetated by tall grass, as is the case for the Kendal area, the roughness length is $z_0 = 0.07$ m according to table 2-2. Lacking further

information, an initial guess of L = 10 m is assumed. This value is corrected through an iterative process until final values of L = 2.474 m, θ_0 = 6.582 °C, θ_* = 0.118 °C and v_* = 0.040 m/s are obtained. Proof: With these values of θ_* and v_*, the Monin-Obukhov length is calculated from equation (2.5-8)

$$L = \frac{286.093\ \text{K} \times (0.040\ \text{m/s})^2}{9.8\ \text{m/s}^2 \times (0.4)^2 \times 0.118\ \text{K}} = 2.474\ \text{m}$$

Substitute these values of v_* and L into equation (2.5-17) to find the planetary boundary layer thickness z_p

$$z_p = 0.4 \times \left\{ \frac{0.040\ \text{m/s} \times 2.474\ \text{m}}{2 \times 7.2722 \times 10^{-5}\ \text{r/s} \times \sin(26°)} \right\}^{0.5} = 15.819\ \text{m}$$

Finally, the thickness of the constant flux layer is given by equation (2.5-18)

$$z_c = \frac{0.3 \times 15.819\ \text{m}}{1 + \dfrac{2.474\ \text{m}}{15.819\ \text{m}}} = 4.104\ \text{m}$$

Strictly speaking, only the temperatures measured at 1.2 m and 2.5 m above ground level fall inside the constant flux layer. However, it is undesirable to fit a line between two points, when it is known that both data points are subject to some variation. Thus, the temperature at 5 m was added to the analysis, since it is sufficiently close to this layer.

With the above determined value of L, ξ at 1.2 m is

$$\xi = \frac{1.2\ \text{m}}{2.474\ \text{m}} = 0.485$$

and

$$\xi_0 = \frac{0.07\ \text{m}}{2.474\ \text{m}} = 0.0283$$

Since $0.3 < \xi < 10$, it follows that the appropriate form of $\varphi_h(\xi)$ is given by equation (A.3-6). Hence

$$\begin{aligned}\varphi_h(0.485) &= 2\times\left(\sqrt{1+22.8\times0.485}-\sqrt{1+22.8\times0.0283}\right)\\ &\quad +2\times\ln\left[\left(\frac{\sqrt{1+22.8\times0.485}-1}{\sqrt{1+22.8\times0.485}+1}\right)\times\left(\frac{\sqrt{1+22.8\times0.0283}+1}{\sqrt{1+22.8\times0.0283}-1}\right)\right]\\ &= 7.3726\end{aligned}$$

A summary of $\varphi_h(\xi)$ and θ is given in table 4-2.

Table 4-2. ξ, θ and $\varphi_h(\xi)$ for the data points inside the constant flux layer.

z m	ξ	θ °C	$\varphi_h(\xi)$
1.2	0.4850	8.253	7.37255
2.5	1.0105	9.357	10.59134
5.0	2.0210	10.402	14.74844

Linear regression, using the method of least squares, is well documented [72DO1], [78WA1], [82WY1]. Using Microsoft Excell's built-in statistical functions to do a linear regression on the data given in table 4-2, with $\varphi_h(\xi)$ the independent variable and θ the dependent one, find

$$\theta = 6.582 + 0.295\varphi_h(\xi) \qquad \ldots (4.5\text{-}5)$$

with a correlation coefficient of 0.996. Comparing equation (4.5-5) with equation (4.5-3), it is clear that $\theta_0 = 6.582$ °C and $\theta_*/\kappa = 0.295$. Therefore, $\theta_* = 0.118$ °C.

The wind speed measurement at 10 m above ground level falls completely outside the constant flux layer. Since no wind speeds were measured below this height, it will be used. Due to the uncertainty in the wind measurement (large fluctuations in wind speed data and a mean wind speed quite close to the lower threshold of the anemometers), the simplest wind profile was adopted. The error introduced by this practice will be quite small ($\pm$ 20 %) in comparison with the uncertainty in the data (errors up to 100 % are possible). Hence, the scaling velocity is found from equations (4.5-4) and (A.1-1)

$$v_* = \frac{0.4 \times 0.434 \text{ m/s}}{\ln(4.042 / 0.0283)} = 0.040 \text{ m/s}$$

During the day, when unstable conditions prevail, the constant flux layer and the planetary boundary layer will be much thicker than at night. Most of the measuring points will then fall inside the constant flux layer. A procedure similar to that used to determine θ_0 and θ_* for the temperature profile, should be applied to extract the scaling velocity v_* from the wind speed measurements.

Hourly values of the meteorological parameters are given in table B-3. The correlation of temperature data with equation (4.5-3) was usually good, with a correlation coefficient of 0.9 and higher. Correlation of the wind data was hardly possible at times, and even under the most favourable conditions, the correlation coefficient rarely exceeded 0.7. Burger [87BU1] reported similar correlation coefficients for his wind data.

In conclusion, it can be said that it was possible to determine the parameters θ_* and L from the measured temperatures and wind speeds. This would enable one to determine the meteorological parameter X, defined in equation (4.4-1). In the next section, it will be shown that the effect of any ambient temperature distribution on the cooling tower performance can be described with the aid of the parameter X.

4.6 CORRELATING THE AIR INLET TEMPERATURE AGAINST THE METEOROLOGICAL PARAMETER X

In figure 4-8, the air inlet temperature immediately upstream of the heat exchanger at the tower was plotted against the ambient temperature measured at 1.2 m on the weather mast. It is clear from figure 4-8 that there is a non-linear relationship between the two temperatures. When these temperatures were converted to potential temperatures, the difference between them, $\Delta\theta_{ai}$, shows a strong diurnal variation, changing sign from positive during the night, i.e. the tower inlet temperature is higher than the temperature measured at 1.2 m, to negative during the day, as shown in figure 4-13.

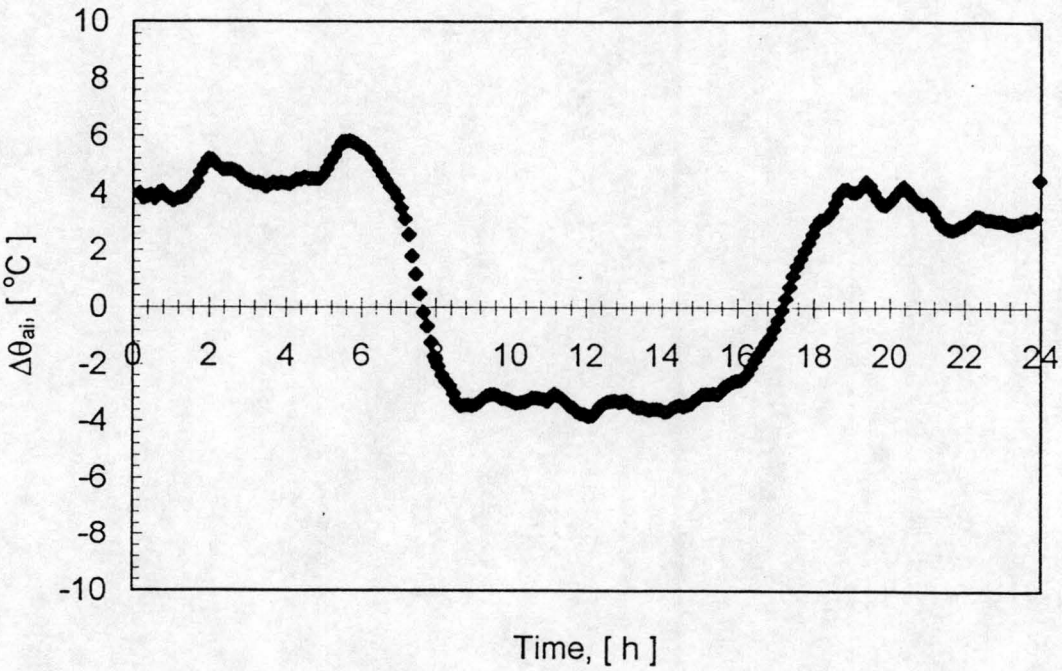

Figure 4-13. Deviation of the air inlet temperature at the tower from ambient temperature far away from the tower.

The parameter X defined by equation (4.5-1) takes these diurnal variances into account, since it inherently contains the meteorological parameters θ_* and v_* that characterise the temperature and wind profiles in the atmospheric boundary layer.

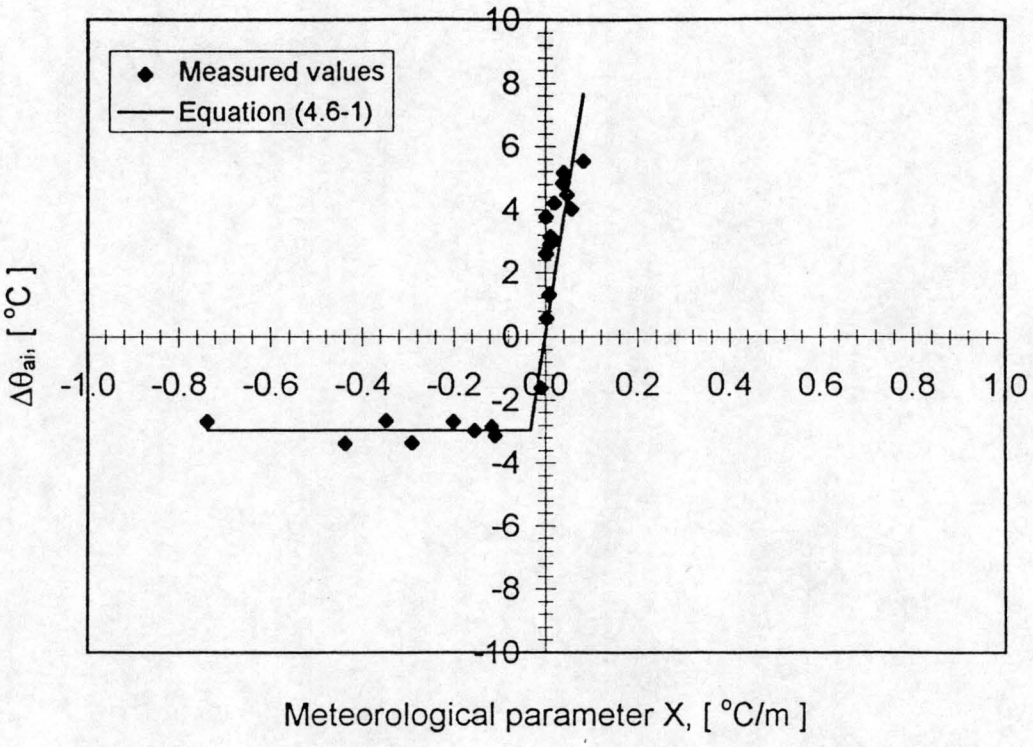

Figure 4-14. $\Delta\theta_{ai}$ as a function of the meteorological parameter X.

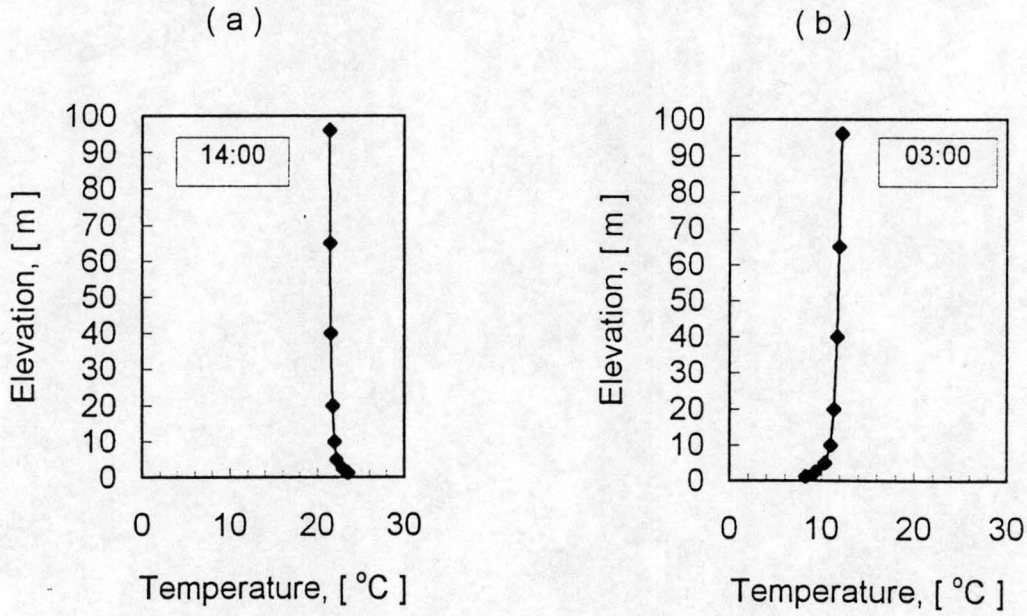

Figure 4-15. Examples of an unstable daytime temperature profile (a), and an early morning temperature inversion (b).

$\Delta\theta_{ai}$ is plotted against the parameter X in figure 4-14. For negative values of X, i.e. unstable daytime conditions, $\Delta\theta_{ai}$ is almost constant, whereas it increases sharply for positive X. Theoretically, $\Delta\theta_{ai}$ should be zero when X is zero, but during the tests, no adiabatic conditions were observed.

Figure 4-14 is easily explained in terms of the two potential temperature profiles depicted in figure 4-15. During the day, a sharp decrease in potential temperature is observed in the lowest few metres of the atmospheric boundary layer, whereafter the potential temperature remains almost constant with height. Wind induced turbulent eddies (vertical motion) will be enhanced thermally, and mixing is sufficiently strong to eliminate any potential temperature differences except in the lowest few metres, where the strongest fluxes occur and mixing is impaired by the close proximity of the surface. Hence, the tower will draw in air from heights that are almost at the same potential temperature, except for a relatively thin layer close to the surface.

In contrast, during the night, the atmosphere is thermally stable, and any mixing of different air layers due to wind induced turbulence will be suppressed. In view of the low wind speeds, mixing will be poor, and the resulting temperature profile will be able to penetrate fairly deep into the constant flux layer, and perhaps spill over into the Ekman layer. Typically, the inversion height will be of the same order of magnitude as the tower exit height. Consequently, the tower draws in air from layers with different potential temperatures, and hence the air inlet temperature is expected to be more sensitive to the stability parameters.

No single curve seems to fit the data depicted in figure 4-14 well, but an envelope of two lines gives satisfactory results

$$\Delta\theta_{ai} = \begin{cases} 92.4565\,X & ; \quad -0.03211 \leq X \\ -2.9688 & ; \quad X < -0.03211 \end{cases} \qquad \ldots (4.6\text{-}1)$$

Equation (4.6-1) is plotted as a continuous line in figure 4-14. Equation (4.6-1) was forced through the origin, to take adiabatic conditions into account. This equation

should be used to calculate the air inlet temperature to the heat exchanger in cooling tower performance calculations. Equation (4.6-1) does not address the effect of ambient air temperature stratification on the draft equation (see equation (3.4-26)). This effect will be addressed in chapter 6.

CHAPTER 5

NUMERICAL ANALYSIS

5.1 INTRODUCTION

The performance of a dry-cooling tower under adiabatic atmospheric conditions is adopted as a reference against which tower performance under generalized atmospheric conditions may be measured. It is impossible to isolate the effect of atmospheric temperature stratification on such a cooling tower experimentally, since the strongest inversions or unstable temperature profiles will occur at low wind speeds ($v_w < 2$ m/s [92DU1]), whereas adiabatic conditions are normally associated with higher wind speeds ($v_w > 8$ m/s [72GO1]). Computational fluid dynamics (CFD) has the flexibility to address any atmospheric condition of interest, as well as the tower's response to it.

The air inlet temperature at the tower is selected as the datum variable between an actual case study and its adiabatic counterpart. This temperature can either be measured on an operational cooling tower, or in the absence of field data, it can be calculated from equation (4.6-1). In both cases, the temperatures should be converted into potential temperatures. The potential temperature is then prescribed on the whole domain to form the adiabatic counterpart. In doing this, the effect of the in air inlet temperature on tower performance is effectively removed. Thus, the influence of the temperature profile on the air flow rate through the tower via the buoyancy term can be studied in isolation.

5.2 NUMERICAL ANALYSIS

Numerical methods forfeit continuous information on the dependent variable ϕ, as obtained from the exact solution of the transport equation in favour of discrete values at pre-specified nodes. Hence, the generic name "discretization methods" for this family of numerical methods. Some approximations on the variance of the dependent variable ϕ

between node points are required prior to determining the algebraic expression involving f at each node point. It is common practice to use piece-wise linear profiles to describe the variance of ϕ between successive nodes. At least in theory, it is possible to use enough nodes to simulate small scale detail of the flow field. The main benefits of numerical modelling is the high speed and low cost involved in simulating a real situation. It has one severe limitation though - a numerical model is only as good as the physical model of the real situation from which it is derived. This limitation often crops up when dealing with turbulent flows.

5.2.1 MATHEMATICAL DESCRIPTION

Before it becomes possible to predict the performance of a cooling tower via computational fluid dynamics (CFD), it is necessary to transpose the physical transport processes occurring in the tower into a mathematical model. This model may in turn be discretisized in a way that conforms to the numerical method used. In the present study the general CFD code PHOENICS [87SP1] will be used.

CFD generally entails the solution of convective-diffusive transport of mass, momentum and energy on a discretisized domain. The differential form of the steady state convective-diffusive transport of a general dependent variable ϕ per unit volume is given by the following vector equation [80PA1]

$$\mathrm{div}\left(\rho \vec{v} \phi - \Gamma_\phi \, \mathrm{grad}\, \phi\right) = S_\phi \qquad \ldots (5.2\text{-}1)$$

with $\rho \vec{v}$ representing the convection and Γ_ϕ is a diffusion coefficient unique to the dependent variable ϕ. S_ϕ is a source term, that may include effects such as gravity or wall friction. In general, the dependent variable ϕ is a function of the space co-ordinates. The solution of the transport equation is closed by prescribing the appropriate boundary conditions.

5.2.2 DISCRETIZATION METHODS

The discretisized equation should contain essentially the same physical information as the differential equation from which it is derived. Different discretization methods may be obtained by employing different grids, assumptions on the variation of the variable between successive nodes and derivation methods, but, as expected, they all yield the same solution in the limiting case of a very large number of grid points.

Probably the best known of all the derivation methods is the finite-difference method, derived from the truncated Taylor-series expansion of the differential equation itself. The Taylor-series formulation is fairly straightforward, but is susceptible to mass flow inconsistencies due to the truncation error. This limits the maximum interval between grid points, leading to an unnecessary fine grid, and consequently high computational time and cost.

The above limitation of the finite-difference formulation has led Patankar [80PA1] to develop the control-volume formulation, which was adopted by Spalding [87SP1] for PHOENICS. The calculation domain is divided into a number of regular, non-overlapping control volumes surrounding each node. He then integrated the differential equation over each control volume, assuming piece-wise (linear) profiles for the variation of the dependent variable ϕ between successive nodes. This method implicitly satisfies the integral form of the conservation equations at each control volume, and hence over the entire calculation domain as well. Since this formulation contains no assumptions on the size of the control volumes, mass consistency automatically occurs, even for coarse grids, at least as long as the assumption of piece-wize profiles is within reason.

The foregoing discussion may be illustrated by a simple example of steady one dimensional heat conduction. The governing equation is

$$\frac{d}{dx}\left(k\frac{dT}{dx}\right) + S = 0 \qquad \ldots (5.2\text{-}2)$$

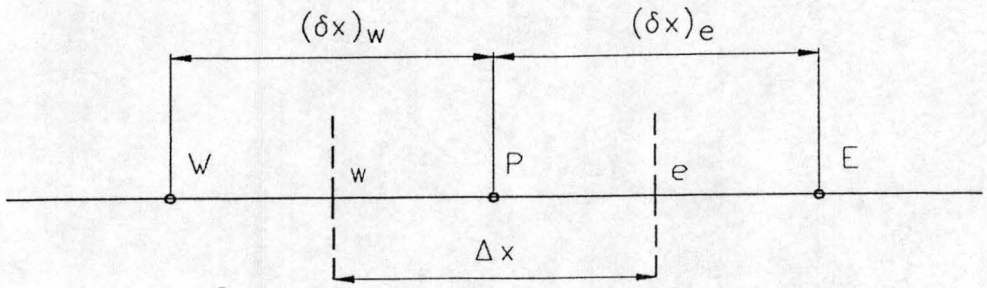

Figure 5-1. Grid point cluster for illustrative example.

with reference to the grid shown in figure 5-1. Upon integration, equation (5.2-2) becomes

$$\left(k\frac{dT}{dx}\right)\Bigg|_e - \left(k\frac{dT}{dx}\right)\Bigg|_w + \int_w^e S\,dx = 0 \qquad \ldots (5.2\text{-}3)$$

Assuming piece-wize linear temperature profiles between adjacent grid points, the resulting discretization equation is given by

$$\left(\frac{k_e}{\delta x_e} + \frac{k_w}{\delta x_w}\right)T_P = \frac{k_e}{\delta x_e}T_E + \frac{k_w}{\delta x_w}T_W + \overline{S}\,\Delta x \qquad \ldots (5.2\text{-}4)$$

Equation (5.2-4) assumes that the source term S remains constant over the entire cell during an iteration. Although this is often the case, it is not unusual for the source term to be a non-linear function of either the dependent variable ϕ or one of the space co-ordinates. The source term may be linearized to yield an even better approximation of the real physical situation at the grid point. Furthermore, proper linearization of the source term will speed up convergence, since full advantage is taken of the change in source term S_ϕ with ϕ. Patankar [80PA1] advocates a differential approach to source term linearization.

5.2.3 BODY-FITTED GRIDS

The hyperbolical shell section of a cooling tower gives rise to a domain boundary that is not parallel to any of the cartesian co-ordinate axes. However, the silhouette of the tower shell is a hyperbola of rotation, suggesting the use of cylindrical polar co-ordinates. Above the throat, the tower shell is cylindrical. To accomodate the hyperbolical section of the shell, a body fitted grid is used. The grid is constructed in such a way that individual cell boundaries coincide with the tower shell. These grid points have to be specified individually. In figure 5-2, the silhouette of the tower shell is shown.

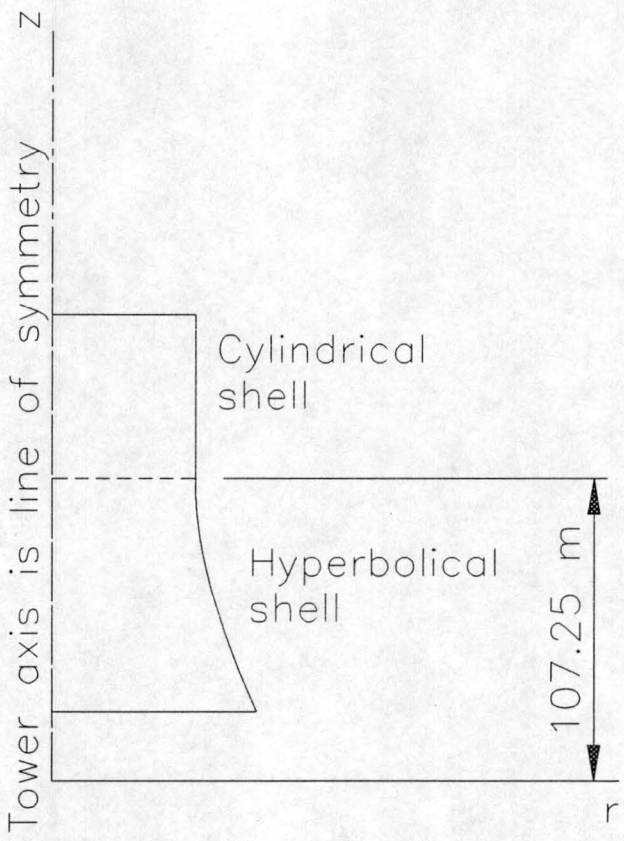

Figure 5-2. Sketch to describe tower silhouette in cylindrical co-ordinates.

Choosing the origin of the hyperbola as the point on the tower axis at the same height as the throat for convenience, as shown in figure 5-2, the shell profile beneath the throat is described by

$$\frac{r^2}{r_t^2} - \frac{z^2\left(r_i^2 - r_t^2\right)}{r_t^2\left(z_t - z_i\right)^2} = 1 \qquad \ldots (5.2\text{-}6)$$

where the subscript t refers to the throat. The rest of the grid points are obtained via algebraic interpolation over the calculation domain.

5.2.4 BOUNDARY CONDITIONS AND SPECIAL SOURCES

Unless otherwise specified, the PHOENICS code treats flow as if it is surrounded by a frictionless container. This is exactly the same condition that would apply for a plane of symmetry. From this it is evident that additional information is required to simulate solid boundaries and other external sources.

A number of routines are provided in the code to calculate wall friction at solid boundaries for both laminar and turbulent flows. The user may supplement this with coding of his/her own.

Resistances to air flow posed by the heat exchanger bundles and tower supports are represented as "sinks of momentum", and are expressed by

$$S_\phi = 0.5 K_j \rho v^2 \qquad \ldots (5.2\text{-}7)$$

in a form that is consistent with equations (3.2-4) and (3.4-8). The pressure loss coefficient K_j is unique for each component, and will normally be a function of the air flow rate.

The pressure drops due to non-uniform velocity profiles (equation 3.4-10)), flow contraction (equation 3.4-15), and expansion (equation 3.4-16)) are accounted for by the diffusion term in the momentum equation, and need no special treatment.

Buoyancy of the plume is a direct result of gravity acting on fluids of different densities, and may be expressed by

$$S_\phi = (\rho_\infty - \rho) g \Delta V \qquad \ldots (5.2\text{-}8)$$

with ΔV the volume of the control element. The density ρ, and the reference density ρ_∞ must be evaluated at the same elevation z. Furthermore, ρ_∞ must be evaluated far enough from the tower to exclude any possible influence of the tower on its immediate surroundings. Equation (5.2-8) applies equally to the warm air flowing through the tower shell, plume rise above the tower, entrainment of ambient air by the plume and the inflow of ambient air at the tower inlet. In essence, it represents the "chimney effect" normally associated with natural draft cooling towers.

Heat transfer in the heat exchanger bundles effectively raises the air temperature at a rate that depends on the air flow through the bundles and the temperature difference between the incoming water and air respectively. The water flow rate was kept constant. Invoking the well known ε-NTU method of heat exchanger design (equation 3.4-2), the temperature of the exhaust air for the k^{th} element is estimated

$$T_{a4,k} = T_{a3,k} + \frac{\varepsilon_k \times \min\left[\Delta \dot{m}_{a,k}\, c_{pa} \,;\, \Delta \dot{m}_{w,k}\, c_{pw}\right] \times \left(T_{wi,k} - T_{a3,k}\right)}{\Delta \dot{m}_{a,k}\, c_{pa}} \qquad \ldots (5.2\text{-}9)$$

with $\Delta \dot{m}_{a,k}$ and $\Delta \dot{m}_{w,k}$ the air and water mass flows through the k^{th} element, and ε_k the local effectiveness of the heat exchanger.

The model assumes a horizontal heat transfer area that covers the entire inlet cross-sectional area of the tower. In practice, this area will differ from the frontal area of the heat exchanger. The area of each cell was corrected to account for the difference between the geometric plan area of the element, ΔA_{geo} and the area actually available for heat transfer, ΔA_{ht}.

$$\Delta A_{ht} = \Delta A_{geo}\left(\frac{4A_{fr}}{\pi d_3^2}\right) \qquad \ldots (5.2\text{-}10)$$

A constant water inlet temperature was assumed for each cell. The ambient temperature was specified at the free inflow boundary, while windless conditions were assumed. A constant pressure boundary condition was specified at the outflow boundary where the plume leaves the domain. In order to prevent unrealistic conditions during the early iterations, any inflow crossing this boundary carries the same thermophysical properties as the in-cell values.

If the inflow boundary is specified far from the tower, the velocities at this boundary will be very small and of the same order as round-off errors. On the other hand, if the boundary is too close to the tower, the interaction between the inflow of ambient air at the tower inlet and entrainment by the plume will be lost. In appendix C, the potential flow pattern in the vicinity of the cooling tower is calculated analytically. As seen from figure C-3, there is no outflow of air at the vertical domain boundaries, even quite close to the tower. Furthermore, the streamlines have only a gentle curvature that smoothes out and becomes almost straight further away from the tower. Hence, positioning the vertical domain boundary ten tower radii away from the tower and enforcing straight streamlines at this boundary results in representative boundary conditions without sacrificing accuracy.

5.3 GENERAL DISCUSSION OF PHOENICS

Although the mathematical foundation of the PHOENICS computer code was discussed in section 5.2, it should be supplemented by some general remarks. PHOENICS is an acronym for Parabolic, Hyperbolic or Elliptic Numerical Integration Computational System. PHOENICS consists of four independent modules, namely a pre-processor, called SATELLITE, the main program, called EARTH, a post-processor, called PHOTON, and the self-instruction program called GUIDE (replaced by POLIS in later

versions). Only the first two modules are essential to run PHOENICS, with PHOTON a useful tool for presenting results.

User instructions are written in the Phoenics Instruction Language (PIL) and are usually entered group by group via an instruction file, called Q1. SATELLITE interprets the PIL instructions and translates them into standard FORTRAN for use by the main processor, called EARTH. Furthermore, SATELLITE looks for conflicting statements and computes all grid co-ordinates.

The main processor, EARTH, performs the actual flow-simulating calculations according to the instructions received via SATELLITE. EARTH can handle up to 50 dependent variables, which may be expanded as the need arises, provided that enough in-core memory is available. The user may influence EARTH via a FORTRAN subroutine called GROUND, of which the main function is to prescribe complex boundary conditions and supply property relations. An example file, GREX(GROUND example), contains coding for a number of simple boundary conditions. GROUND and GREX have the same groupwise structure as the instruction file Q1, which greatly simplifies the users' task to add coding of his/her own.

EARTH creates two output files, RESULT and PHIDA. While the user can enter and read RESULT, PHIDA is normally entered via the post-processor PHOTON, and contains all the necessary information to create a graphical presentation of the flow field.

SATELLITE and GROUND will normally suffice for the specialised needs of most users, but in the unlikely event that additional information is needed, the user may add his/her own FORTRAN coding to the main processor.

The Q1 file and a truncated GROUND subroutine for the Kendal cooling towers are listed in Appendix D.

The numerical simulations were done on a VAX 6000-410 computer, and typically 19 seconds central processor unit (CPU) time was required to complete a run. The results,

written to the file PHIDA, were processed by PHOTON and the graphical output was relayed to a TECHTRONIX 4107 video display unit (VDU), and when necessary, printed on a HP Laserjet III graphics printer.

5.4 THE KENDAL TOWERS

The grid for the Kendal tower is shown in figure 5-3. A 51 × 50 body-fitted grid in cylindrical co-ordinates was employed for the tower and its environment. The grid shown in figure 5-3 was truncated at 35 r-direction cells and 34 z-direction cells to give a better resolution.

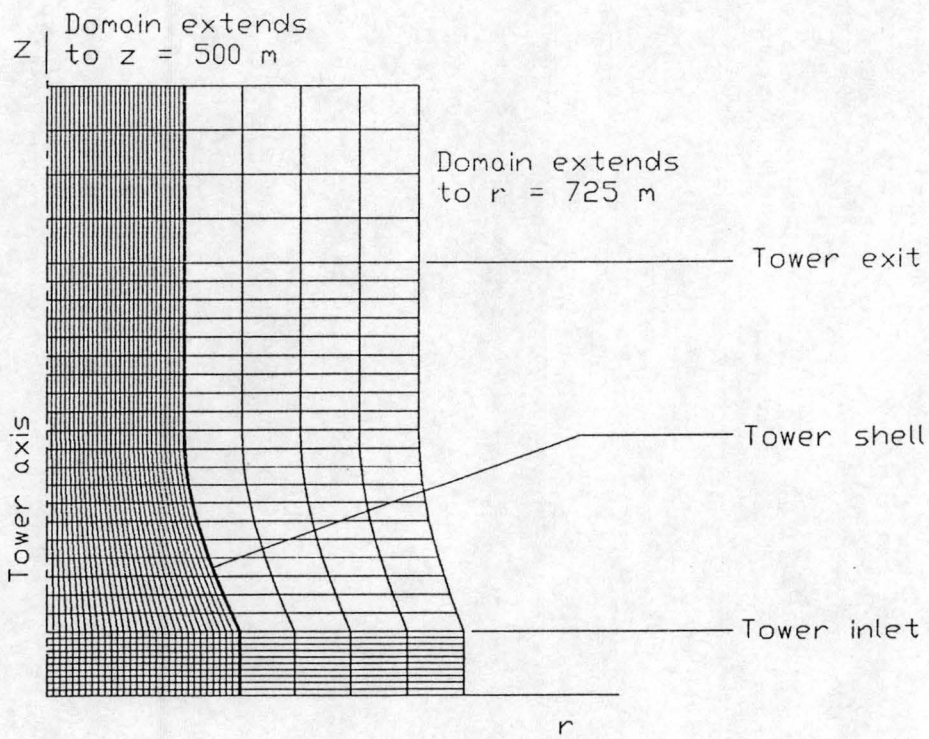

Figure 5-3. CFD grid for Kendal tower.

Symmetry was assumed in the longitudinal direction. The grid was selectively refined at the tower inlet for better resolution. 30 r-direction cells were used for the tower, one for the shell and a further 20 cells for the environment. In the z direction, ten cells were used in the tower inlet, 20 for the shell, and another 20 were used for the plume. The

co-ordinates of discrete grid points on the shell were calculated from equation (5.2-6). PHOENICS has a built-in facility to interpolate cell co-ordinates between the shell and domain boundaries, which gives a smooth transition from the hyperbolical shell to the cylindrical domain boundaries further out in the domain.

Vertical tower supports were assumed in the sense that they only act upon the radial component of the air velocity vector at the tower inlet opening, but the pressure loss coefficient was calculated using the actual length of the supports. The heat exchanger supports were not simulated, since the pressure drop through them will be negligible.

The flow calculations were restricted to the air side, and the corresponding water properties were derived from an energy balance at the end of each sweep. Apart from its flow resistance, the heat exchanger will raise the air temperature at a rate that depends on the local air and water mass flow rates, as well as the temperature difference between the air and water streams entering the heat exchanger. For each sweep, the temperature of the air is calculated from the ε-NTU-equation, equation (5.2-9). This temperature is then prescribed on the cell as an internal condition. From this temperature, the density of the warm air in the plume is calculated. When this density is subtracted from the density of the ambient air at the same height, the buoyancy force on the plume is determined. The temperature is corrected as the heat exchanger is visited upon subsequent iterations, until the convergence criteria is met.

All other boundary and internal conditions were handled in the usual way. PHOENICS' built-in wall functions are stored in GREX, from where it may be accessed via Q1. Atmospheric temperature profiles were stored in an indexed file, from where they were retrieved at the onset of each sweep.

After some preliminary work, aimed at obtaining a grid independent solution, simulations were performed for each temperature profile in table B-1. These results, as well as those for its adiabatic counterpart defined in section 5.1, are given in appendix E. Convergence was reached after approximately 75 iterations, as shown in figure 5-4.

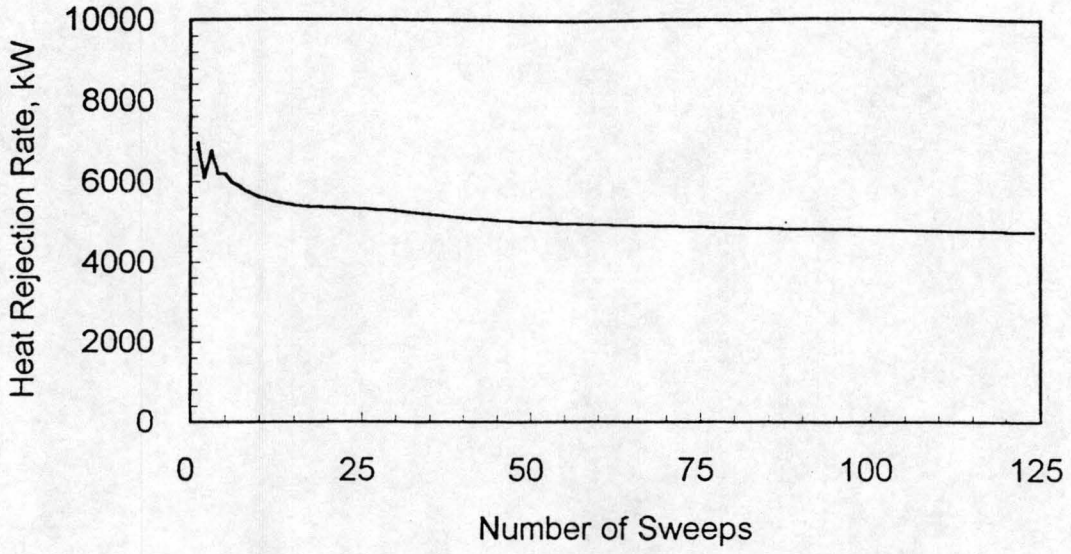

Figure 5-4. Numerical convergence of air mass flow rate.

Different turbulence models are supplied in subroutine GREX of PHOENICS. A few runs were executed using the high Reynolds number k-ε model in conjunction with PHOENICS built-in wall functions. An isotropic turbulent wind speed fluctuation of 0.5 m/s was imposed as an inlet condition for k. No data on the dissipation rate of atmospheric turbulence could be found, and ε was derived from assumed values of the effective viscosity. The k-ε model introduces two more equations to be solved, thus increasing the computational demands. However, no discernible differences were found between the flow fields obtained with the k-ε model in comparison with a laminar flow field, admittedly with a much higher viscosity. Also, choosing an effective viscosity of 1, 10, 100 and 1000 times the dynamic viscosity of air, had a negligible influence on the tower performance. Without clear benefits to be derived from the use of one of the more advanced turbulence models, the (laminar) viscosity was increased by three orders of magnitude to account for turbulence, and in doing this, the computation time is greatly reduced.

A relaxation factor of 20 % to 25 % was often required for the pressure and momentum equations for the first few iterations to improve numeric stability, whereafter it was removed for subsequent sweeps.

5.5 DISCUSSION OF RESULTS

As a first trial, the tower was simulated operating in an adiabatic atmosphere and the results were compared to a point model by Bellstedt [85BE1]. This point model was extensively tested against the Grootvlei 6 natural draft dry-cooling tower [85HO1]. Good agreement was found between the numerical prediction and point model, but PHOENICS underpredicted the air mass flow rate through the tower by approximately 200 kg/s, compared to Bellstedt's point model, that gives $\dot{m}_a = 31954\ kg/s$. For a fixed water inlet temperature, the water outlet temperature predicted by PHOENICS was 0.65 °C higher than that of the point model. The air flow pattern in the immediate environment of the tower is depicted in figure 5-5. From the figure, it can be seen that the tower draws in air over its full height, and the air inlet temperature will be a weighted average of the temperatures in this layer.

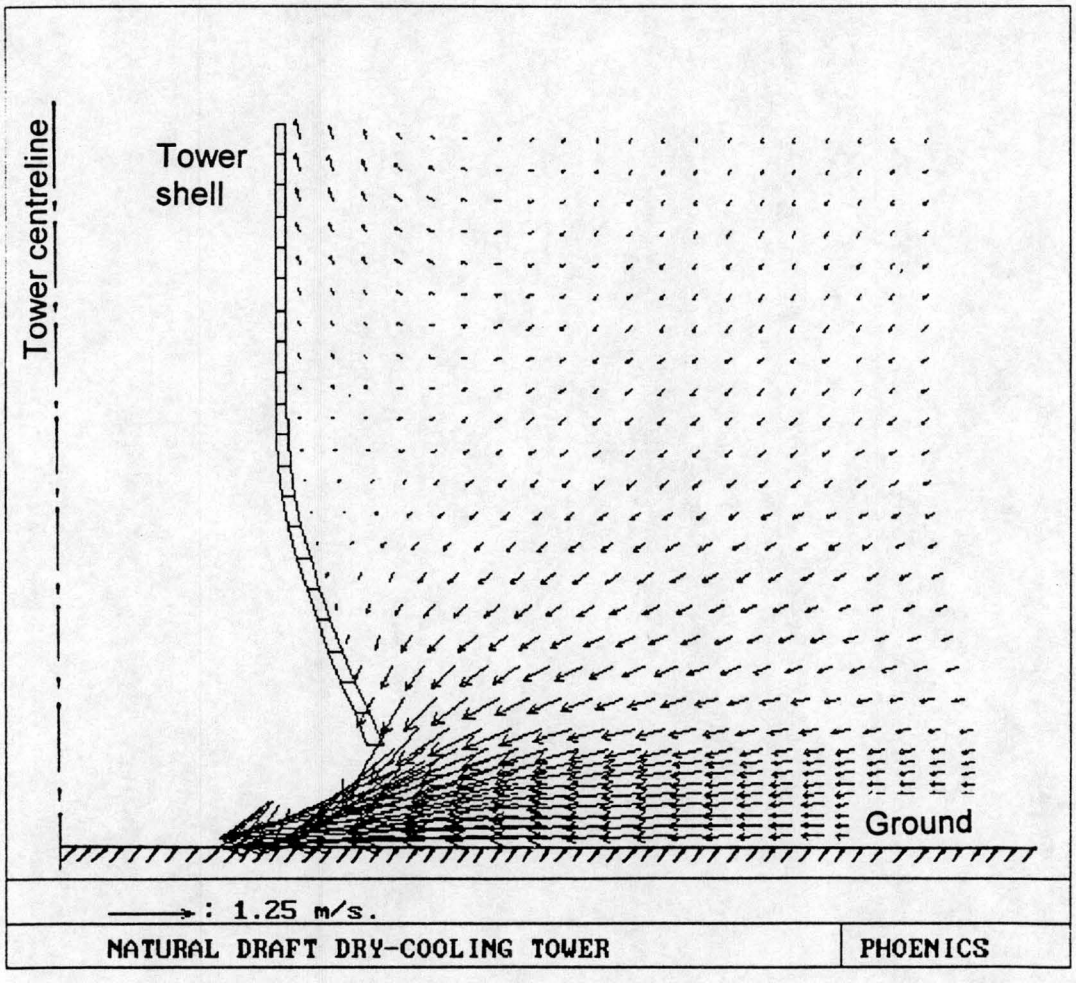

Figure 5-5. Velocity vector diagram for Kendal tower, adiabatic atmosphere.

A comparison between the numerical results and field data measured at 03:00 at Kendal on 9 August 1990 is given in table 5-1. The small difference in ambient air temperature is due to a regression done on the data prior to entering it into the computer program. Also shown in the table, are the predicted parameters if the tower is subjected to an adiabatic atmosphere, with the temperature as measured at 1.2 m above the ground. The predicted values for the air and water temperatures, the air mass flow rate and the heat rejected by the tower generally follows the experimentally observed trends at Kendal closely. Furthermore, the averaged air inlet temperature predicted by the model corresponds to the measured values. The model did however show a slight radial temperature profile directly underneath the fill, that was not observed during the field tests (see figure 4-10). This is probably due to the inadequacy of the turbulence model (constant viscosity) to predict mixing of the air in the wake of the tower supports upstream of the heat exchanger.

Table 5-1. Comparison of measured and predicted data at 03:00 on 9 August 1990.

	Measured	**Predicted with PHOENICS**	
		Actual	**Adiabatic**
Ambient temperature, 1.2 m AGL	8.25 °C	8.26 °C	8.26 °C
Air inlet temperature	12.72 °C	13.32 °C	8.26 °C
Air outlet temperature	Not measured		
Air mass flow rate	Not measured	32 077 kg/s	31 727 kg/s
Water inlet temperature	37.60 °C	38.27 °C	32.86 °C
Water outlet temperature	28.50 °C	29.53 °C	24.12 °C

Differences between the air mass flow rates predicted by the two numerical models are small, confirming that the influence of a temperature inversion is felt through its effect on the air inlet temperature, rather than on the air mass flow through the tower.

Kendal power station, including its cooling towers, are built on an embankment that is approximately 25 m (author's estimate) higher than the base of the weather mast. This

may be the reason why the temperatures measured at the tower inlet corresponds to higher than expected elevations, something also observed by Du Preez [92DU1].

CHAPTER 6

ILLUSTRATIVE EXAMPLES

6.1 INTRODUCTION

The present study will now be concluded with two numerical examples to illustrate the effect of ambient temperature stratification on the performance of a natural draft dry-cooling tower. First, a cooling tower operating under the influence of a temperature inversion will be considered. Thereafter, the same tower operating under the influence of an unstable afternoon temperature profile will be addressed. The theory presented in chapter 2 will be used to characterize the temperature profiles, while the necessary heat and momentum transfer are covered in chapter 3. The use of equation (4.6-1) in extracting the air inlet temperature from the available meteorological data will be demonstrated.

6.2 NUMERICAL EXAMPLE

At the time of this study, the Kendal Power Station was still under construction, and acceptance tests on the cooling towers were still to be done. Due to the sensitivity of the issue, permission to publish the heat exchanger characteristics were withhold by ESKOM and the contractor. This data is essential if one wants to illustrate the effect of temperature stratification on the performance of a natural draft cooling tower, and thus, the much older Grootvlei 6 natural draft dry-cooling tower, that is well documented [86KR1], [87GE1], will be used in the following examples.

Grootvlei is a 6 × 200 MW power station, currently in long term storage, served by four wet- and two dry-cooling towers. The dry-cooling towers were designed to reject 330 MW waste heat to an (adiabatic) ambient at 15.6 °C. The design water mass flow rate is

4390 kg/s, and the water inlet temperature is 61.45 °C. Figure 6-1 shows the major dimensions of the tower.

The heat exchanger consists of bundles of finned tubes, arranged in V-arrays, and the total frontal bundle area is 4 818.06 m^2. Grootvlei 6's finned tubes were extensively tested by Kotze [86KO1], who determined its heat transfer and pressure drop characteristics. The dimensionless heat transfer number, as defined by equation (3.2-3) is

$$Ny = 383.617\,Ry^{0.52376}$$

while the isothermal pressure loss coefficient for the heat exchanger, defined in equation (3.2-4) is

$$K_{he} = 1383.93\,Ry^{-0.33246}$$

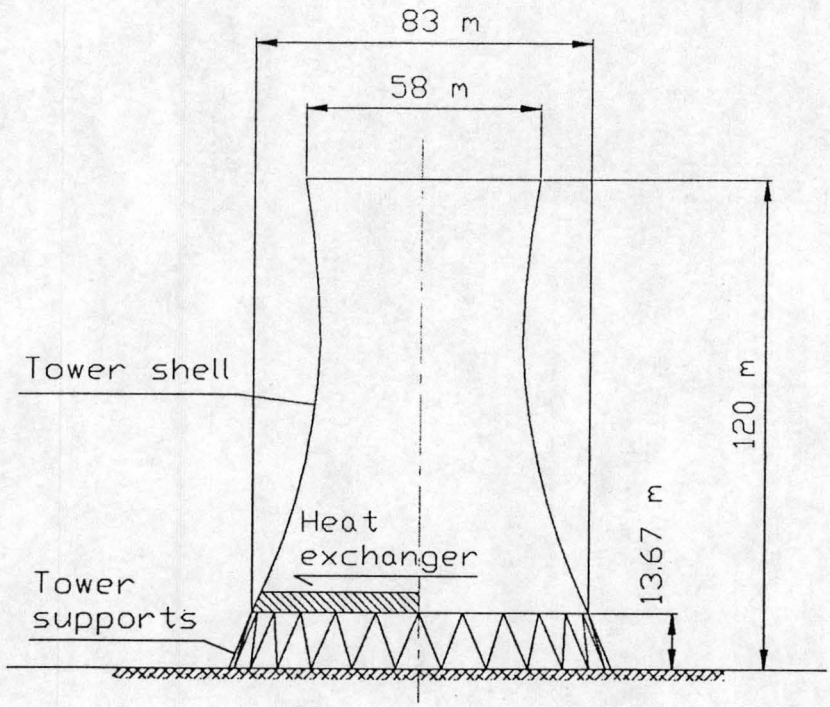

Figure 6-1. Schematic view of Grootvlei 6 natural draft dry-cooling tower.

Suppose that Grootvlei's number 6 cooling tower is required to serve a single condenser at the atmospheric conditions listed in table B-1. Assume a process that will keep the water mass flow and the heat rejection rate constant at 4390 kg/s and 330 MW respectively. A good example of a temperature inversion is the temperature profile measured at 03:00 on 9 August 1990 at Kendal. The air temperature at 1.2 m above ground level was 8.253 °C, and the wind speed 10 m above ground level 0.434 m/s. At such a low wind speed, measurements become difficult, and the meteorological parameters extracted from the wind profile would be unreliable. Under these conditions, it would make more sense to use Golder's stability class approach to determine v_*. The topography at Grootvlei is similar to that at Kendal, and a roughness length of $z_0 = 0.07$ m (see table 2-2) would apply to both sites. From equation (2.5-25), find for cloudless skies

$$s = -0.2167 \times 0.434\,\mathrm{m/s} + 1.5333 = 1.4393$$

With this value of s, find

$$f(s) = \frac{-4}{1 + 1.3|1.4393|^{0.85}} = -1.4432$$

and the Monin-Obukhov length, according to equation (2.5-27) is

$$\frac{1}{L} = +\left[0.216586 \ln\left(1.2 + \frac{10\,\mathrm{m}}{0.07\,\mathrm{m}}\right)\right] \times 10^{-1.4432} = 0.0388\,\mathrm{m}^{-1}$$

$$\therefore L = 25.776\,\mathrm{m}$$

The scaling velocity is found from equation (2.5-29)

$$v_* = \frac{0.4 \times 0.434\,\mathrm{m/s}}{\varphi(\xi_{10})} = 0.02387\,\mathrm{m/s}$$

Equation (2.5-4) is strictly applicable to the constant flux layer only. With the constant flux layer thickness z_c still unknown, the proper choice of ϕ_m is postponed until after the constant flux layer thickness has been determined. This requires an iterative process. First, one has to estimate z_c, and then determine the corresponding form of ϕ_m. This would enable one to calculate a new value of z_c, that has to be corrected in subsequent iterations. After convergence, a value of z_c = 7.713 m is obtained, which gives z_c/L = 0.299. Hence, $0 < z_c/L < 0.3$, which means that the appropriate form of $\varphi(\xi_{10})$ is given by equation (A.2-1)

$$\varphi(\xi_{10}) = \ln\left(\frac{10\,\text{m}/25.776\,\text{m}}{0.07\,\text{m}/25.776\,\text{m}}\right) + 6\left(\frac{10\,\text{m}}{25.776\,\text{m}} - \frac{0.07\text{m}}{25.776\,\text{m}}\right) = 7.273$$

The planetary boundary layer thickness is given by equation (2.5-17)

$$z_p = 0.4 \times \left\{\frac{0.02387\,\text{m/s} \times 25.776\,\text{m}}{2 \times 7.27 \times 10^{-5} \sin 26^\circ}\right\}^{0.5} = 39.294\,\text{m}$$

and the thickness of the constant flux layer from equation (2.5-18)

$$z_c = \frac{0.3 \times 39.294\ \text{m}}{1 + \dfrac{25.776\ \text{m}}{39.294\ \text{m}}} = 7.119\ \text{m}$$

θ_0 and θ_* is obtained in the way described in chapter 4, but using the value of L obtained above. Their respective values are θ_0 = 6.493 °C and θ_* = 0.243 °C. Employing these values for θ_* and L, the potential temperature at any elevation in the constant flux layer is given by equation (4.5-3)

$$\theta(z) = 6.493\,^\circ\text{C} + \frac{0.243\,^\circ\text{C}}{0.4}\left\{\ln\left(\frac{z}{0.07\ \text{m}}\right) + \frac{6 \times (z - 0.07\,\text{m})}{25.776\ \text{m}}\right\} \qquad \ldots (6.2\text{-}1)$$

In table 6-1, the potential temperatures, actual temperatures and pressures arising from equation (6.2-1) are tabulated at various heights within the constant flux layer. Other points of interest also tabulated include the tower inlet height, the top of the Ekman layer and the tower exit height of the Grootvlei 6 tower. Also shown in table 6-1, are the ambient temperatures measured within the constant flux layer at Kendal. Comparing the predicted and measured temperatures, it is clear that the predicted temperatures are somewhat lower than the measured ones. The meteorological parameter defined by equation (4.4-1) is

$$X = \frac{0.243\,^{\circ}C}{|25.776\ m|} = 0.00943\ ^{\circ}C/m$$

The potential temperature difference between the air entering the cooling tower and the temperature measured at 1.2 m above ground level is, according to equation (4.6-1)

$$\Delta\theta_{ai} = 92.4565\,m \times 0.00943\,^{\circ}C/m = 0.87\ ^{\circ}C$$

Table 6-1. Potential temperature profile in planetary boundary layer.

Elevation [m]	**Potential Temperature** [°C]	**Predicted Temperature** [°C]	**Measured Temperature** [°C]	**Pressure** [Pa]
1.20	8.379	8.379	8.253	84 600
1.79	8.705	8.700		84 594
2.38	8.961	8.950		84 588
2.50	9.006	8.993	9.344	
2.97	9.180	9.163		84 582
3.56	9.373	9.350		84 576
4.15	9.550	9.521		84 570
4.74	9.714	9.680		84 564
5.00	9.782	9.746	10.365	
5.33	9.869	9.829		84 558
5.92	10.016	9.970		84 552
6.51	10.157	10.105		84 546
7.10	10.293	10.236		84 540
13.67	10.293	10.172		84 473
39.29	10.293			
120.00	10.293			

If 1.2 m is adopted as the reference height from which the potential temperature is calculated, the potential temperature and the actual temperature will coincide at that height. Using the measured temperatures as a reference, the potential temperature of the air entering the tower is 8.253 °C + 0.87 °C = 9.123 °C. From the definition of the potential temperature, equation (2.5-2) find

$$T_{ai} = (273.15 + 9.123)\left(\frac{84\,472}{84\,600}\right)^{(1.4-1)/1.4} = 9.01\,°C$$

The pressure at the tower inlet is calculated from equation (4.5-1). Starting at 1.2 m with a pressure of 84600 Pa, and dividing the constant flux layer into ten elements, the pressure at the next layer is

$$p_{1.2+\Delta z} = 84\,600\,Pa - \frac{2 \times 84\,600\ Pa}{287.08 \times (281.53 + 281.85)} = 84\,594\ Pa$$

The pressure calculations involve iterations for the temperature, since only the potential temperature is initially known. The converged values for the pressure are also shown in table 6-1.

Initially, only the air inlet temperature is known, and the water inlet temperature and the air mass flow rate must be guessed and repeatedly updated, until the operating point of the tower is found. After convergence, the iterations yield a water inlet temperature, T_{wi} = 54.69 °C, and a water outlet temperature of 36.70 °C. The air mass flow rate is 10507 kg/s, and the temperature of the air leaving the heat exchanger is T_{a4} = 40.20 °C.

The mean air temperature through the heat exchanger is

$$T_{a34} = 0.5 \times (9.01\,°C + 40.20\,°C) = 24.61\ °C$$

The properties of dry air at this temperature may be calculated from equations (F.1-1) to (F.1-4), i.e.

Density	ρ_{a34}	=	0.9897 kg/m^3
Specific heat	c_{pa34}	=	1006.87 J/kg K
Dynamic viscosity	μ_{a34}	=	1.8365×10^{-5} kg/m s
Thermal conductivity	k_{a34}	=	0.02605 W/m K
Prandtl number	Pr_{a34}	=	0.7099

The characteristic air flow number, defined by equation (3.2-2) is

$$Ry = \frac{1}{1.8365 \times 10^{-5}\ kg/m\,s}\left(\frac{10507\ kg/s}{4818.06\ m^2}\right) = 118743\ m^{-1}$$

and the heat transfer number [equation (3.2-3)] is

$$Ny = 383.61731 \times \left(118743\ m^{-1}\right)^{0.523761} = 174494$$

The effective air-side heat transfer coefficient is also given by equation (3.2-3)

$$\begin{aligned} h_{ae} A_e &= 0.02605\ W/mK \times (0.7099)^{0.333} \times 4818.06\ m^2 \times 174494 \\ &= 19535351\ W/K \end{aligned}$$

In the laboratory tests [86KO1], half tubes were inserted at the ends of the bundle to utilise the full flow area. In practice, this is not the case, and the air-side heat transfer coefficient is corrected for the reduction in heat transfer area

$$h_{a34} = 19535351\ W/K \times (154/156) = 19284898\ W/^\circ C$$

The mean water temperature is

$$T_{wm} = 0.5 \times (54.69 + 36.70)\,^\circ C = 45.70\ ^\circ C$$

The properties of water at this temperature are calculated from equations (F.2-2) to (F.2-4)

Specific heat	c_{pw}	=	4 177.54 J/kg K
Dynamic viscosity	μ_w	=	5.8653×10^{-4} kg/m s
Thermal conductivity	k_w	=	0.6380 W/m K
Prandtl number	Pr_w	=	3.8407

The water side Reynolds number is

$$Re_w = \frac{\rho_w v_w d_t}{\mu_w}$$

The water flows through 142 bundles in parallel, and each bundle has a total of 154 tubes, but the water passes twice through the bundle, hence there are only 77 tube entrances. The total cross-sectional area of all the tubes is

$$A_{tts} = 142 \times 77 \times \pi (0.0216)^2 / 4 = 4.0066 \text{ m}^2$$

and the water velocity through the tubes is

$$v_w = \frac{\dot{m}_w}{\rho_w A_{tts}} = \frac{4390}{\rho_w \times 4.0066}$$

Substitute this velocity into the expression for the Reynolds number to find

$$Re_w = \frac{\rho_w \times 4390 \times 0.0216}{\rho_w \times 4.0066 \times 5.8653 \times 10^{-4}} = 40355$$

According to the Reynolds-Colburn analogy, the heat transfer coefficient is related to the skin friction factor. From equation (3.3-4), the latter is

$$f = 0.3086\left[\log\left\{\left(\frac{6.9}{40355}\right) + \frac{5.24\times 10^{-4}}{3.7}\right\}^{1.11}\right]^{-2} = 0.02318$$

The heat transfer coefficient on the inside of the tube is expressed in terms of the Nusselt number, and from equation (3.3-5), find

$$Nu = \frac{(0.02318/8)\times(40355 - 1000)\times 3.8407\times\left[1 + (0.0216/15)^{0.667}\right]}{1 + 12.7\times(0.02318/8)^{0.5}\left[(3.8407)^{0.667} - 1\right]} = 222.534$$

Derive the heat transfer coefficient from the definition of the Nusselt number:

$$h_w = \left(\frac{0.6380}{0.0216}\right)\times 222.534 = 6572.632\ W/m^2K$$

The total surface area available for heat transfer on the water side is

$$A_w = \pi d_t L_t n_{tb} n_b = \pi \times 0.0216 \times 15 \times 154 \times 142 = 22272.558\ m^2$$

With $h_{ae}A_e$, h_w and A_w known, the overall heat transfer coefficient for the heat exchanger is given by equation (3.4-3)

$$UA = \left[\frac{1}{6572.632\times 22272.558} + \frac{1}{19284898}\right]^{-1}$$

$$= 17040087\ W/K$$

Contrary to the computational fluid mechanics model, as described in chapter 5, no problems were experienced with the logarithmic mean temperature difference, ΔT_{lm}. With the temperature correction factors known, the logarithmic temperature difference is expected to give superior results to the NTU-effectiveness model, where counterflow

was assumed. For crossflow, and using the notation of figure 3-1, the logarithmic temperature difference is given by

$$\Delta T_{lm} = \frac{(T_{wi} - T_{a4}) - (T_{wo} - T_{a3})}{\ln\{(T_{wi} - T_{a4})/(T_{wo} - T_{a3})\}}$$

$$= \frac{(54.69\ °C - 40.20\ °C) - (36.70\ °C - 9.01\ °C)}{\ln\{(54.69\ °C - 40.20\ °C)/(36.70\ °C - 9.01\ °C)\}}$$

$$= 20.38\ °C$$

The logarithmic temperature difference for a crossflow heat exchanger must be corrected by a correction factor F that depends on the heat exchanger configuration, and the heat transfer between the air and the water stream then becomes

$$Q = UAF\Delta T_{lm} \qquad \ldots (6.2\text{-}2)$$

F is normally determined graphically, but for computational purposes, Roetzel's [84RO1] correlations may be used. Using Roetzel's calculation scheme for a crossflow heat exchanger with four tube rows and two water passes, the correction factor F = 0.95017. Substitute the appropriate values into equation (6.2-2) to find the heat rejected by the tower to the atmosphere

$$Q = 17040087\ W/K \times 0.95017 \times 20.38\ K = 330\ MW$$

Compare this value with the heat picked up by the air (equation (3.4-1)):

$$Q_a = 10507.02\ kg/s \times 1006.875\ J/kgK \times (40.20\ °C - 9.01\ °C) = 330\ MW$$

and the heat given up by the water [also equation (3.4-1)]

$$Q_w = 4390\ kg/s \times 4177.538\ J/kgK \times (54.69\ °C - 36.70\ °C) = 330\ MW$$

From the above, the tower is clearly in thermal equilibrium.

The draft equation, equation (3.4-26), must also be satisfied. The air densities upstream and downstream of the heat exchanger is found from the perfect gas law, using the appropriate temperature and pressure at the elevation of the heat exchanger, p_{a3}. Thus, find $\rho_{a3} = 1.0444$ kg/m^3 and $\rho_{a4} = 0.9404$ kg/m^3. The air density through the heat exchanger is based on the mean air temperature through it, thus giving $\rho_{a34} = 0.9897$ kg/m^3.

According to equation (3.2-4), the isothermal pressure loss coefficient for the heat exchanger is

$$\left(K_{he}\right)_{iso} = 1383.93 \times \left(118743\right)^{-0.33246} = 28.446$$

The air is heated up as it passes through the heat exchanger, expands, and will accelerate. This causes an additional pressure drop not addressed by the isothermal pressure loss coefficient. $(K_{he})_{iso}$ is corrected for non-isothermal flow by equation (3.2-5)

$$K_{he} = 28.446 + \frac{2}{\left(0.433\right)^2} \times \left[\frac{1.0444\ \text{kg/m}^3 - 0.9404\ \text{kg/m}^3}{1.0444\ \text{kg/m}^3 + 0.9404\ \text{kg/m}^3}\right] = 29.005$$

Furthermore, in a V-array, the flow is not normal to the heat exchanger, resulting in further pressure losses, based on the mean flow angle through it. This angle θ_m is given by equation (3.4-14)

$$\theta_m = 0.0019 \times \left(0.5 \times 61.5\ ^\circ\right)^2 + 0.9133 \times \left(0.5 \times 61.5\ ^\circ\right) - 3.1558\ ^\circ = 26.725\ ^\circ$$

The downstream pressure loss coefficient depends only on the apex angle of the heat exchanger, and is given by equation (3.4-13)

$$K_d = \exp\left[5.4884 - 0.2131\left(\frac{61.5^\circ}{2}\right) + 3.5333\times10^{-3}\left(\frac{61.5^\circ}{2}\right)^2 - 0.2901\times10^{-4}\left(\frac{61.5^\circ}{2}\right)^3\right]$$

$$= 4.1886$$

K_{he} is corrected for oblique flow by equation (3.4-12)

$$K_{he\theta} = 29.005 + \left(\frac{2\times 0.9404\ \text{kg/m}^3}{1.0444\ \text{kg/m}^3 + 0.9404\ \text{kg/m}^3}\right)\times\frac{1}{\sin(26.725^\circ) - 1}$$
$$\times\left[\left(\frac{1}{\sin(26.725^\circ)} - 1\right) + 2\times(0.05)^{0.5}\right] + \frac{2\times 1.0444\ \text{kg/m}^3\times 4.1886}{1.0444\ \text{kg/m}^3 + 0.9404\ \text{kg/m}^3}$$

$$= 35.351$$

The pressure loss through the tower supports given by equation (3.4-9) is already based on the conditions at the heat exchanger

$$K_{ts} = \frac{2\times 15.78\ \text{m}\times 0.5\ \text{m}\times 60\times(4818.06\ \text{m}^2)^2\times 0.9897\ \text{kg/m}^3}{(\pi\times 82.958\,\text{m}\times 13.67\,\text{m})^3\times 1.0444\,\text{kg/m}^3} = 0.4606$$

and the cooling tower (inlet) loss coefficient is given by equation (3.4-11)

$$K_{ct3} = 0.72\times\left(\frac{82.958\ \text{m}}{13.67\ \text{m}}\right)^2 - 0.34\times\left(\frac{82.958\ \text{m}}{13.67\ \text{m}}\right) + 1.7 = 1.7911$$

Referred to the mean conditions at the heat exchanger, K_{ct3} becomes

$$K_{ct} = 1.7911\times\frac{0.9897\ \text{kg/m}^3}{1.0444\ \text{kg/m}^3}\times\left(\frac{4\times 4818.06\ \text{m}^2}{\pi\times(82.958\ \text{m})^2}\right)^2 = 1.7230$$

Projected onto a horizontal plane at the tower inlet height, the flow area through the heat exchanger is

$$A_{e3} = A_{fr} \sin(\theta/2) = 4818.06\ m^2 \times \sin(0.5 \times 61.5\ ^\circ) = 2463.44\ m^2$$

with θ the apex angle of the heat exchanger. The ratio of the open flow area to the total cross-sectional area is [see equation (3.4-18)]

$$\sigma_e = \frac{A_{e3}}{A_3} = \frac{2463.44\ m^2}{\pi \times (82.958\ m)^2} = 0.4558$$

From equation (3.4-17), find

$$\begin{aligned}\sigma_c &= 0.6145 + 0.04566 \times 0.4558 - 0.3367 \times (0.4558)^2 + 0.4083 \times (0.4558)^3 \\ &\quad + 2.6720 \times (0.4558)^4 - 5.9632 \times (0.4558)^5 + 3.5589 \times (0.4558)^6 \\ &= 0.6339\end{aligned}$$

and the contraction loss coefficient, K_{ctc3}, as defined by equation (3.4-15) is

$$K_{ctc3} = 1 - \frac{1}{0.6339} + \frac{1}{(0.6339)^2} = 0.3335$$

If K_{ctc3} is referred to the mean conditions at the heat exchanger, find

$$K_{ctc} = 0.3335 \times \left(\frac{0.9897\ kg/m^3}{1.0444\ kg/m^3}\right) \times \left(\frac{4818.06\ m^2}{2463.44\ m^2}\right)^2 = 1.2090$$

The expansion loss coefficient is simply based on $\sigma_e = A_{e3}/A_3$, and from equation (3.4-16), find

$$K_{cte4} = (1 - 0.4558)^2 = 0.2962$$

Referred to the mean conditions at the heat exchanger, it becomes

$$K_{cte} = 0.2962 \times \left(\frac{0.9897 \text{ kg/m}^3}{0.9404 \text{ kg/m}^3} \right) \times \left(\frac{4818.06 \text{ m}^2}{2463.44 \text{ m}^2} \right)^2 = 1.1924$$

The pressure at the tower inlet, as well as at the top of the tower, is found through integration of equation (3.4-4). The result of this integration was already given in table 6-1. Flow through the tower shell after the heat exchanger is essentially isentropic, and the air temperature gradient is found from equation (2.3-5)

$$\frac{dT}{dz} = \frac{9.8 \text{ m/s}^2 \times (1 - 1.4)}{1.4 \times 287.08 \text{ J/kgK}} = -0.00975 \text{ K/m}$$

and thus the temperature at the tower exit is

$$T_{a5} = 40.20 \text{ °C} - 0.00975 \text{ K/m} \times (120.00 - 13.67) \text{ m} = 39.17 \text{ °C}$$

The air density at the tower exit is found from the perfect gas law, $\rho_{a5} = 0.9301$ kg/m^3, giving an arithmetic mean air density in the shell of $\rho_{a45} = 0.9353$ kg/m^3. With all the pressure loss coefficients, pressures and densities known, the draft equation [equation (3.4-26)] may be evaluated. The left hand side of equation (3.4-26) is simply the pressure difference between the top of the tower and the measured barometric pressure at the reference height

$$LH = p_{a1} - p_{a6} = 84600 \text{ Pa} - 83396 \text{ Pa} = 1204 \text{ Pa}$$

The right hand side yields

$$RH = (0.4606 + 1.7230 + 1.2090 + 35.3505 + 1.1924) \times \frac{1}{2 \times 0.9897\ \text{kg/m}^3} \times \left(\frac{10507.02\ \text{kg/s}}{4818.06\ \text{m}^2} \right)^2$$

$$+ (84600 - 84473)\ \text{Pa} + 9.8\ \text{m/s}^2 \times 0.9353\ \text{kg/m}^3 \times (120.00 - 13.67)\ \text{m}$$

$$+ \frac{1}{2 \times 0.9301\ \text{kg/m}^3} \times \left(\frac{4 \times 10507.02\ \text{kg/s}}{\pi \times (58.00\ \text{m})^2} \right)^2$$

$$= 1204\ \text{Pa}$$

which confirms that the draft equation is also satisfied.

Table 6-2. Comparison of tower performance under adiabatic conditions and when subjected to a temperature inversion

	Adiabatic	**Inversion**
Ambient temperature, T_{a1}, °C	8.25	8.25
Air inlet temperature, T_{a3}, °C	8.25	9.01
Air outlet temperature, T_{a4}, °C	38.84	40.20
Air mass flow rate, kg/s	10715.21	10507.02
Characteristic air flow parameter, Ry, m^{-1}	121419	118743
Characteristic heat transfer number, Ny, m^{-1}	176543	174494
Effective air-side heat transfer coefficient, $h_{ae}A_e$, W/°C	19452721	19284898
Isothermal pressure loss coefficient, $(K_{he})_{iso}$	28.236	28.446
Heat exchanger pressure loss coefficient, $K_{he\theta}$	35.130	35.351
Support struts pressure loss coefficient, K_{ts}	0.461	0.461
Cooling tower pressure loss coefficient, K_{ct}	1.725	1.723
Cooling tower contraction loss coefficient, K_{ctc}	1.210	1.209
Cooling tower expansion loss coefficient, K_{cte}	1.191	1.192
Water inlet temperature, T_{wi}, °C	53.45	54.69
Water outlet temperature, T_{wo}, °C	35.45	36.70
Water side heat transfer coefficient, h_w, W/m^2 °C	6497.97	6572.63
Overall heat transfer coefficient, UA, W/°C	17147871	17040087
Logarithmic temperature difference, ΔT_{lm}, °C	20.25	20.38
Heat rejection rate, Q, MW	330	330
Atmospheric pressure at ground level, p_{a1}, Pa	84600	84600
Pressure at heat exchanger level, p_{a3}, Pa	84460	84473
Pressure at tower exit, p_{a6}, Pa	83375	83396
Pressure drop due to flow resistances, Δp_{res}, Pa	107.60	104.36
Total available draft, Δp_{draft}, Pa	107.60	104.36

If the atmosphere was adiabatic, and the same air temperature was measured at ground level, the air inlet temperature would have been the same as the ambient temperature, i.e. T_{a3} = 8.25 °C. The same calculation scheme yields a somewhat lower water outlet temperature (T_{wo} = 35.45 °C) and a somewhat higher air mass flow rate ($\dot{m}_a$ = 10715.21 kg/s) if the heat rejection rate stays unaltered. The calculations will not be repeated, but the results are presented in table 6-2, with the corresponding results for the tower operating under a temperature inversion also shown for comparison.

6.3 UNSTABLE AFTERNOON PROFILE

Consider the temperature profile measured at 14:00 on 9 August 1990. A wind speed of 1.322 m/s was measured at 10 m AGL, as shown in table B-2. Although the expected constant flux layer height would be in the order of 100 m, Golder's calculation scheme for the Monin-Obukhov scaling length will be followed to conform to the discussion above. Since the measurement was taken during daytime, an estimate of the incoming solar radiation is required. At 14:00, the time angle A, given by equation (2.2-5) is

$$A = (14 - 12) \times 15\,^\circ = 30\,^\circ$$

The number of days since the summer solstice, n_s = 229 days. From equation (2.2-3), the solar declination angle Φ is

$$\sin\Phi = -\cos\left\{(229 - 1)\,\text{days} \times \frac{180\,^\circ}{182.6\,\text{days}}\right\} \times \sin(23.5\,^\circ) = 0.2832$$

$$\therefore \Phi = 16.45\,^\circ$$

and the solar altitude angle Θ is found from equation (2.2-4)

$$\begin{aligned}\cos(90^\circ - \Theta) &= \sin(16.45^\circ)\times\sin(26^\circ) + \cos(16.45^\circ)\times\cos(26^\circ)\times\cos(30^\circ)\\ &= 0.8707\\ \therefore \quad \Theta &= 60.53^\circ\end{aligned}$$

The thickness of the air layer through which the incoming solar radiation has to pass, relative to the thickness of the atmosphere δ_0 (δ_0 = 1 atmosphere), is according to equation (2.2-1)

$$\delta = 1\,\text{atmosphere}\times\text{cosec}(60.53^\circ) = 1.1486\ \text{atmospheres}$$

Substitute this value of δ into equation (2.2-2) to find

$$I_s = 1377\ \text{W/m}^2 \times \exp(-0.431\times 1.1486) = 839.35\ \text{W/m}^2$$

Since this value falls within the range 630 W/m^2 < I_s < 950 W/m^2, the stability class from equation (2.5-23) is given by

$$s = 0.4167\times 1.322\ \text{m/s} - 3.5833 = -3.0324$$

This gives

$$f(s) = \frac{-4}{1 + 1.3\times|-0.0324|^{0.85}} = -0.9221$$

The Monin-Obukhov scaling length according to equation (2.5-27) is

$$\begin{aligned}L^{-1} &= \frac{-3.0324}{|-3.0324|}\times\left[0.216586\ln\left(1.2 + \frac{10\ \text{m}}{0.07\ \text{m}}\right)\right]\times 10^{-0.9221}\\ &= -0.1288\ \text{m}^{-1}\\ \therefore \quad L &= -7.765\ \text{m}\end{aligned}$$

With the Monin-Obukhov length known, the scaling velocity v_* can be found from equation (2.5-28).

$$v_* = \frac{0.4 \times 1.322 \text{ m/s}}{\varphi_m\{10\text{m}/(-7.765\text{m})\}} = 0.153 \text{ m/s}$$

with φ_m given by equation (A.4-7). For a slightly unstable atmosphere, i.e. $0 < z/L < -10$, the planetary boundary layer thickness is given by equation (2.5-15)

$$z_p = \frac{0.4 \times 0.153 \text{ m/s}}{2 \times 7.27 \times 10^{-5} \text{ s}^{-1} \times \sin(26°)} = 962.42 \text{ m}$$

and that of the constant flux layer by equation (2.5-16)

$$z_c = 0.1 \times 962.42 \text{ m} = 96.24 \text{ m}$$

Hence, the constant flux layer extends to just above the top of the weather mast, and all the temperature measurements will be used to determine θ_*. First, temperatures are converted to potential temperatures, using equation (2.5-2). A least squares fit on the potential temperatures, similar to that described in chapter 4, yields $\theta_0 = 28.577$ °C and $\theta_* = -0.905$ °C with a correlation coefficient of 0.9192. Employing the experimentally determined values of θ_* and L, the potential temperature profile in the constant flux layer is given by equations (4.5-3) and (A.4-6)

$$\theta(z) = 28.577\,°\text{C} - \frac{0.905\,°\text{C}}{0.4} \times \left[\ln\left\{ \frac{(1 + 16z/7.765\text{ m})^{0.5} - 1}{(1 + 16z/7.765\text{ m})^{0.5} + 1} \right\} + 3.3910 \right]$$

The most important temperatures and pressures required in the example are given in table 6-3. From the table, it is clear that the predicted temperatures are within 0.5 °C of the measured ones. The pressures were calculated in the same way as outlined in section 6.2 above.

Table 6-3. Temperature and pressure distributions in the atmosphere up to the height of the cooling tower.

Elevation	Temperature (Measured)	Temperature (Predicted)	Pressure
[m]	[°C]	[°C]	[Pa]
1.20	23.535	23.617	84600
2.50	22.911		
5.00	22.205		
10.00	21.984		
13.67		21.631	84478
20.00	21.770		
40.00	21.549		
65.00	21.461		
96.00	20.608		
96.24		20.300	83672
120.00		20.068	83441

According to equation (4-6-1), the difference between the potential temperature of the air entering the tower, and that measured at 1.2 m above ground level, is -2.969 °C. With 1.2 m the reference height at which the pressure is measured, the potential temperature at 1.2 m will be the same as the actual temperature at that height, i.e. 23.535 °C. Hence, the potential temperature of the air entering the tower will be 23.535 °C - 2.969 °C = 20.566 °C. With the pressure already known at the tower inlet height, the corresponding air temperature is calculated from equation (2.5-2)

$$T_{a3} = (273.15 + 20.566)\text{K} \times \left[\frac{84478\ \text{Pa}}{84600\ \text{Pa}}\right]^{0.4/1.4} = 293.605\ \text{K}\ (20.455\ ^\circ\text{C})$$

The operating point of the tower is calculated in exactly the same way as outlined in section 6.2 above, and the results are given in table 6-4. From the table, it is clear that the tower performs better under an unstable atmosphere, compared to an adiabatic one. This can be seen from the decrease in the water outlet temperature, from 54.00 °C for the adiabatic atmosphere, to 48.74 °C for the unstable atmosphere. Part of this reduction is simply due to the lower air inlet temperature (20.45 °C for the unstable atmosphere, compared to 23.54 °C for the adiabatic atmospere).

Table 6-4 Comparison of tower performance under adiabatic conditions and when subjected to a super-adiabatic temperature profile.

	Adiabatic	Super-adiabatic
Ambient temperature, T_{a1}, °C	23.54	23.54
Air inlet temperature, T_{a3}, °C	23.54	20.45
Air outlet temperature, T_{a4}, °C	58.38	52.88
Air mass flow rate, kg/s	9970	10099
Characteristic air flow parameter, Ry, m^{-1}	108011	110797
Characteristic heat transfer number, Ny, m^{-1}	166048	168277
Effective air-side heat transfer coefficient, $h_{ae}A_e$, W/°C	19247420	19230104
Isothermal pressure loss coefficient, $(K_{he})_{iso}$	29.356	29.109
Heat exchanger pressure loss coefficient, $K_{he\theta}$	36.257	36.013
Support struts pressure loss coefficient, K_{ts}	0.461	0.461
Cooling tower pressure loss coefficient, K_{ct}	1.7233	1.723
Cooling tower contraction loss coefficient, K_{ctc}	1.209	1.209
Cooling tower expansion loss coefficient, K_{cte}	1.192	1.192
Water inlet temperature, T_{wi}, °C	71.96	66.71
Water outlet temperature, T_{wo}, °C	54.00	48.74
Water side heat transfer coefficient, h_w, W/m^2 °C	7550	7265
Overall heat transfer coefficient, UA, W/°C	17270686	17187391
Logarithmic temperature difference, ΔT_{lm}, °C	20.11	20.21
Heat rejection rate, Q, MW	330	330
Atmospheric pressure at ground level, p_{a1}, Pa	84600	84600
Pressure at heat exchanger level, p_{a3}, Pa	84467	84478
Pressure at tower exit, p_{a6}, Pa	83446	83441
Pressure drop due to flow resistances, Δp_{res}, Pa	101.52	101.84
Total available draft, Δp_{draft}, Pa	101.52	101.84

6.4 PERFORMANCE OF THE KENDAL TOWER

The performance of the Kendal 1 dry-cooling tower was also calculated as outlined in section 6.2. These values were compared with the actual measurements at Kendal, as well as the results obtained from PHOENICS. In table 6-5, the results for the tower operating in the presence of an early morning inversion (03:00) is presented, while the results for the unstable afternoon (14:00) is presented in table 6-6. Further results are presented in appendix E. Agreement between the point model and the measured values is excellent, with only small differences between the measured and predicted water outlet

temperatures. The PHOENICS model tends to overpredict the air flow through the tower, but underpredict the water outlet temperature. Quite significant though, PHOENICS predicts air inlet temperatures quite close to the measured values.

Table 6-5. Comparison of measured and predicted results for Kendal tower operating under the influence of a temperature inversion.

	Measured	Point Model	PHOENICS
Ambient temperature, T_{a1}, °C	8.25	8.25	8.25
Air inlet temperature, T_{a3}, °C	12.72	12.72	13.32
Air outlet temperature, T_{a4}, °C	33.96	33.91	32.66
Air mass flow rate, $\dot{m}_a$ kg/s	29200	29253	32077
Water inlet temperature, T_{wi}, °C	37.60	37.60	37.60
Water outlet temperature, T_{wo}, °C	28.50	28.72	28.86
Heat rejection rate, Q, MW	624	624	624
Atmospheric pressure, p_{a1}, Pa	846000	84600	846000
Pressure at heat exchanger, p_{a3}, Pa	not measured	84357	N/A
Pressure at tower exit, p_{a6}, Pa	not measured	82971	N/A
Δp due to flow resistances, Δp_{res}, Pa	not measured	97.675	N/A
Total available draft, Δp_{draft}, Pa	not measured	97.675	N/A

Table 6-6. Same as table 6-5 above, but for unstable afternoon profile.

	Measured	Point Model	PHOENICS
Ambient temperature, T_{a1}, °C	23.35	23.35	23.35
Air inlet temperature, T_{a3}, °C	20.01	19.96	22.51
Air outlet temperature, T_{a4}, °C	40.70	40.53	42.24
Air mass flow rate, $\dot{m}_a$ kg/s	29500	29675	30935
Water inlet temperature, T_{wi}, °C	44.90	45.22	44.90
Water outlet temperature, T_{wo}, °C	35.60	35.74	36.16
Heat rejection rate, Q, MW	614	614	614
Atmospheric pressure, p_{a1}, Pa	84600	84600	84600
Pressure at heat exchanger, p_{a3}, Pa	not measured	84361	N/A
Pressure at tower exit, p_{a6}, Pa	not measured	82986	N/A
Δp due to flow resistances, Δp_{res}, Pa	not measured	101.77	N/A
Total available draft, Δp_{draft}, Pa	not measured	101.77	N/A

6.5 CONCLUSION

The examples clearly illustrate that the tower's performance does not only depend on the air temperature, usually measured at 1.5 m above ground level, but also on the ambient temperature profile. Furthermore, the tower's performance is impaired under a temperature inversion, while the opposite is true if the atmosphere is unstable.

CHAPTER 7

CLOSURE

In this thesis, the influence of ambient temperature stratification on a large natural draft dry-cooling tower has been investigated experimentally and analytically. It has been shown that the tower performance decreased in the presence of an ambient temperature inversion. This was already noted by Merkel [26ME1], Buxmann [77BU1], Tesche [81TE1] and Lauraine et al [88LA1]. However, the decrease in tower performance has been successfully correlated to the inversion[1] strength and depth, something that has not been done before. This success is contributed to the fact that it was possible to characterize atmospheric temperature profiles in terms of the meteorological parameters θ_* and L. These parameters are derived from the actual temperature profiles, and are related to the inversion strength and depth respectively. Furthermore, it was also pointed out that the tower's performance will actually increase if a superadiabatic temperature profile prevails in the atmospheric boundary layer. In the past, this fact has been overlooked, probably because it is not perceived as a problem by cooling tower operators and vendors alike. It is proposed that vendors should be taking advantage of this knowledge during the design phase.

Based on the knowledge gained through this work, the author recommends the following:

- The air inlet temperature should be measured at the heat exchanger for tower performance evaluation and efficiency tests.

- Unless both the cooling tower operator and vendor agree to use the proposed model, Lauraine et al's [88LA1] should be used for cooling tower acceptance test purposes.

---

1 More correctly, one should refer to temperature stratification strength and depth, since this method is by no means restricted to temperature inversions, but can handle a superadiabatic temperature profile in the atmosphere equally well.

- The annual average ambient temperature and adiabatic temperature lapse rate could still be used in the basic cooling tower design, but due consideration should be given to the influence of ambient temperature stratification on the performance of the cooling tower under adverse conditions, such as maximum power generation, and ambient temperature extremes. In these cases, equation (4.6-1) should be used to determine the air inlet temperature, and the air flow through the tower should be evaluated from the proper integration of the hydrodynamic term in the draft equation.

- Cooling tower designers should take full advantage of the advances in computer hardware and computational fluid dynamics (CFD) packages, and use this as a design tool. Du Preez [92DU1], and Radosavljevic ans Spalding [89RA1] achieved notable success in predicting cooling tower performance under the influence of cross winds for natural draft dry- and wet-cooling towers respectively. In this thesis, it was shown that CFD satisfactorily predicts tower performance under ambient temperature stratification.

It is recommended that this work is expanded to include the efforts of Du Preez [92DU1] and Radosavljevic and Spalding [89RA1] to predict the performance of both natural draft wet- and dry-cooling towers under any set of atmospheric conditions. Furthermore, field tests on a natural draft wet-cooling tower is strongly recommended, since the distribution of moisture in the atmospheric boundary layer will also enter the analysis. These towers also have a much larger inlet diameter to height height ratio, but the implication of that on tower performance was excluded from the present investigation.

REFERENCES

00WE1 Weisbach, J., Die Eksperimental-Hydraulik, J.S. Engelhardt, Freiburg, 1855.

26ME1 Merkel, F., Verdunstungskuhlung, VDI Zeitschrift, Vol. 70, pp. 123-128, January 1926.

41SC1 Schmidt, W., Turbulente Ausbreitung eines Stromes Erhitzter Luft, Zeitschrift fur Angewendte Mathematik und Mechanik, Vol. 21, No. 6, pp. 351-363, 1941.

52CH1 Chilton, W., Performance of Natural Draught Water Cooling Towers, Proceedings of the Institution of Electrical Engineers, London, Vol. 99, No. 77, pp. 440-456, 1952.

52RO1 Rouse, H., Yih, C.S. and Humphreys, H.W., Gravitational Convection from a Buoyancy Source, Tellus, Vol. 4, pp. 201-210, 1952.

54BA1 Batchelor, G.K., Heat Convection and Buoyancy Effects in Fluids, Quarterly Journal of the Royal Meteorological Society, Vol. 80, pp. 339-358, 1954.

54FI1 Filonenko, G.K., Teploenergetika, No. 4, 1954.

54MO1 Monin, A.S. and Obukhov, A.M., Basic Regularity in Turbulent Mixing in the Surface Layer of the Atmosphere, Frud. Geofig. Inst. Akad. Nauk., Vol. 24, pp. 151-163, 1954.

56MO1 Morton, B.R., Taylor, G.I. and Turner, J.S., Turbulent Gravitational Convection from Maintained and Instantaneous Sources, Proceedings of the Royal Society of London, Series A, Vol. 234, pp. 1-23, 1956.

57MO1 Morton, B.R., Buoyant Plumes in a Moist Atmosphere, Journal of Fluid Mechanics, Vol. 2, pp. 127-144, 1957.

58TA1 Taylor, G.I., Flow Induced by Jets, Journal of the Aero/Space Sciences, pp. 464-465, 1958.

59MO1 Morton, B.R., Forced Plumes, Journal of Fluid Mechanics, Vol. 5, pp. 151-163, 1959.

61LO1 Lowe, H.J. and Christie, D.G., Heat Transfer and Pressure Drop Data on Cooling Tower Packings and Model Studies of the Resistance of Natural Draught Towers to Airflow, Proceedings of the International Heat Transfer Conference, Colorado, 1961.

61RI1 Ricou, F.P. and Spalding, D.B., Measurement of Entrainment by Axial-Symmetrical Turbulent Jets, Journal of Fluid Mechanics, Vol. 11, pp. 21-32, 1961.

63ES1 Estoque, M., A Numerical Model of the Atmospheric Boundary Layer, Journal of Geophysic Research, Vol. 68, No. 4, pp. 1103-1113, 1963.

64LA1 Laikhtman, D.L., Physics of the Boundary Layer of the Atmosphere, Oldbourne Press, London, 1964.

66AR1 Arpaci, V.S., Conduction Heat Transfer, Addison-Wesley Publishing Co., Reading, Massachusetts, 1966.

68SC1 Schlichting, H., Boundary Layer Theory, McGraw-Hill Book Co., New York, 1968.

69AB1 Abraham, G. and Eysink, W.D., Jets Issuing into Fluid with a Density Gradient, Journal of Hydraulic Research, Vol. 7, No. 2, pp. 145-175, 1969.

70BR1 O'Brien, J.J., A Note on the Vertical Structure of the Eddy Exchange Coefficient in the Planetary Boundary Layer, Journal of Atmospheric Sciences, Vol. 27, pp. 1213-1215, 1970.

70FO1 Fox, D.G., Forced Plumes in a Stratified Fluid, Journal of Geophysic Research, Vol. 75, No. 33, pp. 6818-6835, 1970.

70PE1 Petukhov, B.S., Heat Transfer and Fluid Friction in Turbulent Pipe Flow with Variable Physical Properties, in Advanced Heat Transfer, Edited by Hartnett, J.P. and Irvine, T.F., Academic Press, New York, 1970.

70SA1 Sassamori, T., A Numerical Study of Atmospheric and Soil Boundary Layers, Journal of the Atmospheric Sciences, Vol. 27, pp. 1122-1137, 1970.

70TO1 Townsend, A.A., Entrainment and the Structure of Turbulent Flow, Journal of Fluid Mechanics, Vol. 41, No. 1, pp. 13-46, 1970.

71HI1 Hirst, E.A., Buoyant Jets Discharged into Quiescent Stratified Ambients, Journal of Geophysical Research, Vol. 76, No. 30, pp. 7375-7384, 1971.

72DO1 Dorn, W.S. and McCracken, D.D., Numerical Methods with Fortran IV Case Staudies, John Wiley and Sons, New York, 1972.

72GO1 Golder, D., Relations Among Stability Parameters in the Surface Layer, Boundary Layer Meteorology, Vol. 3, pp. 47-57, 1972.

72TE1 Tennekes, H. and Lumley, J.L., A Course in Turbulence, MIT Press, Cambridge, Massachusetts, 1972.

72ZI1 Zilitinkevic, S.S., On the Determination of the Height of the Ekman Boundary Layer, Boundary Layer Meteorology, Vol. 3, pp. 141-145, 1972.

73TU1 Turner, J.S., Buoyancy Effects in Fluids, Cambridge University Press, Cambridge, England, 1973.

74SH1 Shir, C.C. and Shieh, L.J., A Generalized Urban Air Pollution Model and its Application to the Study of SO_2 Distributions in the St. Louis Metropolitan Area, Journal of Applied Meteorology, Vol. 13, pp. 185-204, 1974.

74SN1 Sneck, H.J. and Brown, D.H., Plume Rise from Large Thermal Sources such as Dry Cooling Towers, Journal of Heat Transfer, Vol. 96, pp. 232-238, 1974.

74WH1 White, F.M., Viscous Fluid Flow, McGraw-Hill Book Co., New York, 1974.

75PR1 Pryputniwicz, R.J. and Bowley, W.W., An Experimental Study of Vertical Buoyant Jets Discharged into Water of Finite Depth, Journal of Heat Transfer, Vol. 97, pp. 274-281, 1975.

76RA1 Rajaratnam, N., Turbulent Jets, Elsevier Scientific Publishing Co., Amsterdam, 1976.

76ZU1 Zucrow, M.J. and Hoffman, J.D., Gas Dynamics, Vol. I, John Wiley and Sons, New York, 1976.

77BU1 Buxmann, J., Der Einfluss von Temperaturschichtungen auf die Wärmeleistung eines Trockenkühlturmes mit Naturzug, Brennstoff-Wärme Kraft, Vol. 29, pp. 90-94, 1977.

77DA1 Daugherty, R.L. and Franzini, J.B., Fluid Mechanics with Engineering Applications, McGraw-Hill Book Co., New York, 1977.

78BA1 Baer, E., Einfluss des Windes auf die Strömung im Kamin eines Naturzugkühlturms, Ph. D. Thesis, University of Karlsruhe, 1978.

78YU1 Yule, A.J., Large-Scale Structure in the Mixing Layer of a Round Jet, Journal of Fluid Mechanics, Vol. 89, No. 3, pp. 413-432, 1978.

79CH1 Chen, C.J. and Nikitopoulos, C.P., On the Near Field Characteristics of Axisymmetric Turbulent Buoyant Jets in a Uniform Environment, International Journal of Heat and Mass transfer, Vol. 22, pp. 245-255, 1979.

79DO1 Van Dop, H., Steenkist, R. and Nieuwstadt, E.T.M., Revised Estimates for Continuous Shoreline Fumigation, Journal of Applied Meteorology, Vol. 18, pp. 133-137, 1979.

79ZE1 Zeman, O., Parameterization of the Dynamics of Stable Boundary Layers and Nocturnal Jets, Journal of Applied Atmospheric Sciences, Vol. 36, pp. 792-804, 1979.

80PA1 Patankar, S.V., Numerical Heat Transfer and Fluid Flow, Hemisphere Publishing Co., New York, 1980.

81AF1 Afzal, N., Mixed Convection in a Two-Dimensional Buoyant Plume, Journal of Fluid Mechanics, Vol. 105, pp. 347-368, 1981.

81RA1 Rapp, D., Solar Energy, Prentice-Hall, Englewood Cliffs, 1981.

81TE1 Tesche, W., Inversions - Frequency and Influence on Natural Draught Cooling Towers, VGB-Kraftwerkstechnik, Vol. 7, pp. 535-542, 1981.

82BR1 De Bruin, H.A.R., and Holtslag, A.A.M., A Simple Parameterization of the Surface Fluxes of Sensible Heat and Latent Heat During Daytime Compared with the Penman-Monteith Concept, Journal of Applied Meteorology, Vol. 21, pp. 1610-1621, 1982.

82HO1 Holman, J.P., Heat Transfer, McGraw-Hill Inc., New York, 1982.

83HA1 Haaland, S.E., Simple and Explicit Formulas for the Friction Factor in Turbulent Pipe Flow, Journal of Fluids Engineering, Vol. 105, No. 3, pp. 89-90, 1983.

84DU1 Du Plessis, J.P., Axi-Symmetrical Potential Flow through a Cooling Tower, Department of Applied Mathematics Report TW 84-2, University of Stellenbosch, 1984.

84RO1 Roetzel, W., Berechnung von Wärmeübertragern, VDI-Wärmeatlas, pp. Ca1-Ca31, VDI-Verlag, Dusseldorf, 1984.

85BE1 Bellstedt, M.O., Performance Prediction of Dry-Cooling Towers, M.Eng. Thesis, University of Stellenbosch, 1985.

85HO1 Hoffmann, J.E., Bedryfspuntvoorspelling by Natuurlike Trek Droë Koeltorings, B. Eng. Project, University of Stellenbosch, 1985.

85RO1 Rohsenow, W.M., Hartnett, J.P. and Ganic, E.N., Handbook of Heat Transfer Applications, McGraw-Hill Inc., New York, 1985.

86GE1 Geldenhuys, J.D. and Kröger, D.G., Aerodynamic Inlet Losses in Natural Draft Cooling Towers, Proceedings of the 5th IAHR Cooling Tower Workshop, Monterey, 1986.

86KO1 Kondo, O. and Yamazawa, A., Aerodynamic Roughness over an Inhomogeneous Ground Surface, Boundary Layer Meteorology, Vol. 35, pp. 331-348, 1986.

86KO1 Kotze, J.C.B., Bellstedt, M.O. and Kröger, D.G., Pressure Drop and Heat Transfer Characteristics of Inclined Finned Tube Heat Exchanger Bundles, Proceedings of the 8th International Heat Transfer Conference, San Francisco, 1986.

86KR1 Kröger, D.G., Performance Characteristics of Industrial Finned Tubes Presented in Dimensional Form, International Journal of Heat and Mass Transfer, Vol. 29, 1986.

86SU1 Surridge, A.D., Extrapolation of the Nocturnal Temperature Inversion from Ground Based Measurements, Atmospheric Environment, Vol. 20, 1986.

86BU1 Burger, L.W., A High Resolution Model for Multiple Source Dispersion of Air Pollutants under Complex Atmospheric Structure, Ph. D. Thesis, University of Natal, Durban, 1986.

87HO1 Hoffmann, J.E., Bedryfspunt Voorspelling vir Nat Koeltorings (Performance Prediction on Wet-Cooling Towers), M.Eng. Thesis, University of Stellenbosch, 1987.

87SP1 Spalding, D.B. and Rosten, H.I., The PHOENICS Reference Manual, CHAM Report TR 200, Huntsville, Alabama, 1987.

87SP2 Spalding, D.B. and Rosten, H.I., The PHOENICS Beginner's Guide, CHAM Report TR 100, Huntsville, Alabama, 1987.

88GE1 Gebhart, B., Jaluria, Y., Mahajan, R.L. and Sammakia, B., Buoyancy Induced Flows and Transport, Hemisphere Publishing Co., Washington, 1988.

88LA1 Lauraine, H., Lemmens, P. and Manjoie, M., Experimental Data Coupling Atmospheric Temperature Inversions and Cooling Tower Performances, Proceedings of the 6th IAHR Cooling Tower Workshop, Pisa, 1988.

88PR1 Preston-Whyte, R.A. and Tyson, P.D., The Atmosphere and Weather of Southern Africa, Oxford University Press, Cape Town, 1988.

88PR2 Du Preez, A.F. and Kröger, D.G., Experimental Evaluation of Aerodynamic Inlet Losses in Natural Draft Dry-Cooling Towers, Proceedings of the 6th IAHR Cooling Tower Workshop, Pisa, 1988.

89JU1 Jury, M.R. and Tosen, G.R., Characteristics of the Winter Boundary Layer over the African Plateau: 26° South, Boundary Layer Meteorology, Vol. 49, pp. 53-76, 1989.

89RA1 Radosavljevic, D. and Spalding D.B., The use of PHOENICS to Simulate Three-Dimensional Effects in Natural-Draught Cooling Towers, The PHOENICS Journal of Computational Fluid Dynamics and its Applications, Vol. 1, No. 4, pp. 409-458, February 1989.

92PR1 Du Preez, A.F., The Influence of Cross-Winds on the Performance of Natural Draft Dry-Cooling Towers, Ph. D. Thesis, University of Stellenbosch, 1992.

93BE1 Benton, D.J. and Mirsky, G.R., Impact of Atmospheric Lapse Rate on Power Plant Performance, Proceedings of the American Power Conference, Vol. 55, No. 2, 1993.

93PR1 Du Preez, N., Department Industrial Engineering, University of Stellenbosch, (Private communication).

93TE1 Terblanche, J.E., Inlaatverliese by Koeltorings, M. Eng. Thesis, University of Stellenbosch, 1993.

93ZU1 Zunkel, M., Earth, Marine and Atmospheric Sciences, CSIR, Pretoria (Private communication).

95DO1 Douglas, J.F., Gasiorek, J.M. and Swaffield, J.A., Fluid Mechanics, Longmans, London, 1995.

APPENDIX A

INTEGRATION OF THE UNIVERSAL FUNCTIONS

A.1 Adiabatic atmosphere

If the atmosphere is adiabatic, the universal functions $\phi_m(\xi)$ and $\phi_h(\xi)$ are both equal to unity. Hence, in both cases, equation (2.5-29) integrates to

$$\varphi(\xi) = \int_{\xi_0}^{\xi} \frac{\phi(\xi)}{\xi} d\xi = \int_{\xi_0}^{\xi} \frac{d\xi}{\xi} = \ln\left(\frac{\xi}{\xi_0}\right) \qquad \text{... (A.1-1)}$$

A.2 Moderately stable atmosphere

From table 2-1, the form of the universal function for heat and momentum transfer are again the same, i.e.

$$\phi(\xi) = 1 + 6\xi$$

and upon integration, one has

$$\varphi(\xi) = \int_{\xi_0}^{\xi} \frac{\phi(\xi)}{\xi} d\xi = \int_{\xi_0}^{\xi} \frac{1 + 6\xi}{\xi} d\xi = \ln\left(\frac{\xi}{\xi_0}\right) + 6(\xi - \xi_0) \qquad \text{... (A.2-1)}$$

Equation (A.2-1) is the origin of the familiar log-linear profiles quoted for the wind and temperature profiles in the atmospheric boundary layer. Note that the log-linear profiles are strictly applicable to the moderately stable atmosphere, although it fits the experimental data reasonably well [64LA1].

A.3 Stable atmosphere, i.e. $0.3 < \xi < 10$

According to table 2-1, the appropriate form of the universal function for both heat and momentum transfer is

$$\phi(\xi) = \sqrt{1 + 22.8\xi}$$

and the integral become

$$\varphi(\xi) = \int_{\xi_0}^{\xi} \frac{\phi(\xi)}{\xi} d\xi = \int_{\xi_0}^{\xi} \frac{\sqrt{1 + 22.8\xi}}{\xi} d\xi \qquad \text{... (A.3-1)}$$

Let

$$\zeta^2 = 1 + 22.8\xi \qquad \text{... (A.3-2)}$$

or

$$\xi = \frac{\zeta^2 - 1}{22.8} \qquad \text{... (A.3-3)}$$

Differentiate equation (A.3-3) to find

$$d\xi = \frac{2\zeta}{22.8} d\zeta \qquad \text{... (A.3-4)}$$

Substitute equations (A.3-2) and (A.3-4) into equation (A.3-1) and solve the transformed integral

$$\begin{aligned}\varphi(\xi) &= 2\int_{\zeta_0}^{\zeta} d\zeta + 2\int_{\zeta_0}^{\zeta} \frac{d\zeta}{\zeta^2 - 1} \\ &= 2\zeta\Big|_{\zeta_0}^{\zeta} + 2\ln\left\{\frac{\zeta - 1}{\zeta + 1}\right\}\Bigg|_{\zeta_0}^{\zeta} \\ &= 2(\zeta - \zeta_0) + 2\ln\left\{\frac{\zeta - 1}{\zeta + 1} \times \frac{\zeta_0 + 1}{\zeta_0 - 1}\right\}\end{aligned} \quad \ldots (A.3\text{-}5)$$

Substitute equation (A.3-2) back into equation(A.3-5) to find

$$\begin{aligned}\varphi(\xi) &= 2\left(\sqrt{1 + 22.8\xi} - \sqrt{1 + 22.8\xi_0}\right) \\ &\quad + 2\ln\left[\left\{\frac{\sqrt{1 + 22.8\xi} - 1}{\sqrt{1 + 22.8\xi} + 1}\right\} \times \left\{\frac{\sqrt{1 + 22.8\xi_0} + 1}{\sqrt{1 + 22.8\xi_0} - 1}\right\}\right]\end{aligned} \quad \ldots (A.3\text{-}6)$$

A.4 Moderately unstable atmosphere, i.e. -10 < ξ < 0

The universal function for heat transfer is according to table 2-1

$$\phi_h(\xi) = [1 - 16\xi]^{-1/2}$$

Upon integration, find

$$\varphi_h(\xi) = \int_{\xi_0}^{\xi} \frac{\phi_h(\xi)}{\xi} d\xi = \int_{\xi_0}^{\xi} \frac{d\xi}{\xi\sqrt{1 - 16\xi}} \quad \ldots (A.4\text{-}1)$$

Let

$$x^2 = 1 - 16\xi \quad \ldots (A.4\text{-}2)$$

Thus

$$\xi = \frac{1 - x^2}{16}$$

and

$$d\xi = -\frac{x}{8} dx \qquad \text{... (A.4-3)}$$

Substitute equations (A.4-2) and (A.4-3) into equation (A.4-1) to find

$$\int_{\xi_0}^{\xi} \frac{d\xi}{\xi\sqrt{1 - 16\xi}} = \int_{x_0}^{x} \frac{2\,dx}{x^2 - 1} \qquad \text{... (A.4-4)}$$

Split the denominator on the right hand side of equation (A.4-4) into its partial fractions to find

$$\begin{aligned} \int_{x_0}^{x} \frac{2\,dx}{x^2 - 1} &= \int_{x_0}^{x} \frac{dx}{x - 1} - \int_{x_0}^{x} \frac{2\,dx}{x + 1} \\ &= \ln(x - 1)\Big|_{x_0}^{x} - \ln(x + 1)\Big|_{x_0}^{x} \qquad \text{... (A.4-5)} \\ &= \ln\left\{\frac{x - 1}{x + 1}\right\} - \ln\left\{\frac{x_0 - 1}{x_0 + 1}\right\} \end{aligned}$$

It is a simple matter of back-substitution to write the integral in term of the original variable ξ

$$\varphi_h(\xi) = \ln\left\{\frac{\sqrt{1 - 16\xi} - 1}{\sqrt{1 - 16\xi} + 1}\right\} - \ln\left\{\frac{\sqrt{1 - 16\xi_0} - 1}{\sqrt{1 - 16\xi_0} + 1}\right\} \qquad \text{... (A.4-6)}$$

The universal function for momentum transfer is

$$\phi_m(\xi) = [1 - 16\xi]^{-1/3}$$

Hence

$$\varphi_m(\xi) = \int_{\xi_0}^{\xi} \frac{d\xi}{\xi[1 - 16\xi]^{1/3}} \qquad \text{... (A.4-7)}$$

Now let

$$y^3 = 1 - 16\xi$$

or

$$\xi = \frac{1 - y^3}{16} \qquad \text{... (A.4-8)}$$

Differentiate equation (A.4-8) to get

$$d\xi = -\frac{3y^2}{16} dy \qquad \text{... (A.4-9)}$$

Substitute equations (A.4-8) and (A.4-9) into equation (A.4-7)

$$\varphi_m(\xi) = \int_{y_0}^{y} \frac{3y\,dy}{y^3 - 1} \qquad \text{... (A.4-10)}$$

If one split the denominator into partial fractions, equation (A.4-10) become

$$\varphi_m(\xi) = \int_{y_0}^{y} \frac{dy}{y - 1} - \int_{y_0}^{y} \frac{(y - 1)dy}{y^2 + y + 1} \qquad \text{... (A.4-11)}$$

The first integral in equation (A.4-11), say I_1, is simply

$$I_1 = \ln(y-1)\Big|_{y_0}^{y} = \ln\left\{\frac{y-1}{y_0-1}\right\} = \ln\left\{\frac{[1-16\xi]^{1/3}-1}{[1-16\xi_0]^{1/3}-1}\right\} \qquad \ldots (A.4\text{-}12)$$

The second integral, I_2, is further split by the rather clever re-arrangement of terms

$$I_2 = \frac{1}{2}\int_{y_0}^{y}\frac{\{(2y-1)+3\}}{y^2+y+1}dy = \frac{1}{2}\int_{y_0}^{y}\frac{(2y-1)}{y^2+y+1}dy = \frac{1}{2}\int_{y_0}^{y}\frac{3}{y^2+y+1}dy \qquad \ldots (A.4\text{-}13)$$

Note that the numerator of the first integral on the right hand side of equation (A.4-13) is exactly the derivative of the denominator. This integrates to

$$\begin{aligned} I_2 &= 0.5\ln(y^2+y+1)\Big|_{y_0}^{y} = 0.5\ln\left\{\frac{y^2+y+1}{y_0^2+y_0+1}\right\} \\ &= 0.5\ln\left\{\frac{[1-16\xi]^{2/3}+[1-16\xi]^{1/3}+1}{[1-16\xi_0]^{2/3}+[1-16\xi_0]^{1/3}+1}\right\} \end{aligned} \qquad \ldots (A.4\text{-}14)$$

while the second integral yields

$$\begin{aligned} I_4 &= \frac{3}{2}\times\left[\frac{2}{\sqrt{3}}\tan^{-1}\left\{\frac{2y+1}{\sqrt{3}}\right\}\right]\Bigg|_{y_0}^{y} \\ &= \sqrt{3}\times\left[\tan^{-1}\left\{\frac{2[1-16\xi]^{1/3}}{\sqrt{3}}\right\}-\tan^{-1}\left\{\frac{2[1-16\xi_0]^{1/3}}{\sqrt{3}}\right\}\right] \end{aligned} \qquad \ldots (A.4\text{-}15)$$

The final value of $\varphi_m(\xi)$ is given by a combination of equations (A.4-12), (A.4-14) and (A.4-15).

A.5 Very unstable (convective) atmosphere, i.e. $\xi < -10$

The universal function for heat transfer is exactly the same as for the moderately unstable atmosphere, and equation (A.4-6) applies. For momentum transfer, the universal function $\phi_m(\xi)$ is

$$\phi_m(\xi) = [1 - 16\xi]^{-1/4}$$

in which case equation (2.5-29) become

$$\varphi_m(\xi) = \int_{\xi_0}^{\xi} \frac{d\xi}{\xi[1 - 16\xi]^{1/4}} \qquad \text{... (A.5-1)}$$

Let

$$u = [1 - 16\xi]^{1/4}$$

or

$$\xi = \frac{1 - u^4}{16} \qquad \text{... (A.5-2)}$$

Upon differentiation, equation (A.5-2) yields

$$d\xi = -\frac{u^3}{4} du \qquad \text{... (A.5-3)}$$

Substitute equations (A.5-2) and (A.5-3) into equation (A.5-1)

$$\varphi_m(\xi) = \int_{u_0}^{u} \frac{4u^2}{u^4 - 1} du \qquad \text{... (A.5-4)}$$

Divide the denominator in equation (A.5-4) into its partial fractions and find

$$\begin{aligned}
\varphi_m(\xi) &= \int_{u_0}^{u} \frac{2\,du}{u^2+1} + \int_{u_0}^{u} \frac{du}{u-1} - \int_{u_0}^{u} \frac{du}{u+1} \\
&= 2\tan^{-1}(u)\Big|_{u_0}^{u} + \ln(u-1)\Big|_{u_0}^{u} - \ln(u+1)\Big|_{u_0}^{u} \\
&= 2\left\{\tan^{-1}(u) - \tan^{-1}(u_0)\right\} + \ln\left\{\frac{u-1}{u_0-1}\right\} - \ln\left\{\frac{u+1}{u_0+1}\right\} \\
&= 2\left\{\tan^{-1}(u) - \tan^{-1}(u_0)\right\} + \ln\left\{\frac{u-1}{u+1}\times\frac{u_0+1}{u_0-1}\right\}
\end{aligned} \qquad \text{... (A.5-5)}$$

Backsubstitute equation (A.5-2) into equation (A.5-5) to find the final form of equation (A.5-1)

$$\begin{aligned}
\varphi_m(\xi) &= 2\left\{\tan^{-1}\left(\left[1-16\xi\right]^{1/4}\right) - \tan^{-1}\left(\left[1-16\xi_0\right]^{1/4}\right)\right\} \\
&\quad + \ln\left\{\frac{\left[1-16\xi\right]^{1/4}-1}{\left[1-16\xi\right]^{1/4}+1}\times\frac{\left[1-16\xi_0\right]^{1/4}+1}{\left[1-16\xi_0\right]^{1/4}-1}\right\}
\end{aligned} \qquad \text{... (A.5-6)}$$

APPENDIX B

HOURLY SPOT VALUES OF AIR TEMPERATURES AND WIND SPEEDS MEASURED AT KENDAL ON 9 AUGUST 1990

Table B-1: Hourly spot values of air temperature measured on the weather mast, August 1990.

Time	01:00	02:00	03:00	04:00	05:00	06:00
z [m]	T(z) [°C]	T(z) [°C]	T(z) [°C]	T(z) [°C]	T(z) [°C]	T(z) [°C]
1.2	9.710	7.998	8.253	7.572	7.183	6.895
2.5	10.115	8.559	9.344	8.709	7.839	8.294
5.0	10.886	9.824	10.365	9.980	9.035	10.038
10.0	11.595	10.828	10.978	10.894	10.504	11.096
20.0	12.281	11.222	11.324	11.069	11.193	11.103
40.0	12.865	11.518	11.732	11.227	11.442	10.844
65.0	13.054	11.567	11.551	11.049	11.574	11.426
96.0	12.979	11.369	12.482	11.529	11.506	11.922

Time	07:00	08:00	09:00	10:00	11:00	12:00
z [m]	T(z) [°C]	T(z) [°C]	T(z) [°C]	T(z) [°C]	T(z) [°C]	T(z) [°C]
1.2	8.564	15.679	17.850	19.168	20.487	21.859
2.5	9.544	15.177	16.659	18.621	20.152	21.287
5.0	10.646	14.043	15.971	17.792	19.556	20.542
10.0	12.131	15.214	16.027	17.671	18.941	20.180
20.0	12.639	15.227	15.877	17.489	18.635	19.894
40.0	13.171	15.355	15.737	17.060	18.192	19.416
65.0	13.341	15.073	15.275	16.542	18.339	19.120
96.0	13.187	14.526	14.726	16.014	17.601	18.476

Table B-1: (continued)

Time	13:00	14:00	15:00	16:00	17:00	18:00
z [m]	T(z) [°C]	T(z) [°C]	T(z) [°C]	T(z) [°C]	T(z) [°C]	T(z) [°C]
1.2	22.462	23.535	23.590	23.332	21.461	17.180
2.5	21.883	22.911	23.077	22.776	21.394	17.051
5.0	21.205	22.205	22.338	22.177	21.166	17.644
10.0	20.874	21.984	21.976	22.057	21.181	18.945
20.0	20.682	21.770	21.683	21.855	21.053	19.310
40.0	20.340	21.549	21.276	21.544	20.987	19.548
65.0	20.159	21.461	21.092	21.467	20.888	19.457
96.0	19.396	20.608	20.363	20.776	20.285	18.992

Time	19:00	20:00	21:00	22:00	23:00	24:00
z [m]	T(z) [°C]	T(z) [°C]	T(z) [°C]	T(z) [°C]	T(z) [°C]	T(z) [°C]
1.2	15.192	14.834	13.426	13.184	12.360	10.540
2.5	15.781	15.250	13.646	13.533	12.630	11.300
5.0	16.275	15.785	14.162	14.022	13.215	11.920
10.0	17.578	16.652	14.582	14.365	13.719	12.990
20.0	18.358	17.251	15.048	14.589	14.003	13.750
40.0	18.656	17.717	15.637	14.854	14.363	14.300
65.0	18.687	18.067	15.753	15.191	14.707	14.230
96.0	18.462	18.013	15.627	15.249	14.647	14.190

Table B-2: Wind speeds measured on the weather mast, 9 August 1990.

Time	01:00	02:00	03:00	04:00	05:00	06:00
z [m]	$v_w(z)$ [m/s]	$v_w(z)$ [m/s]	$v_w(z)$ [m/s]	$v_w(z)$ [m/s]	$v_w(z)$ [m/s]	$v_w(z)$ [m/s]
10.0	1.3325	0.4375	0.4340	0.5545	1.6120	0.4120
20.0	0.9260	0.2220	0.1520	0.4360	1.2105	0.3165
40.0	1.0500	0.4875	0.5540	0.3840	1.4085	0.1875
65.0	0.8215	0.0000	0.0210	0.0000	1.2010	0.2635
96.0	1.0350	0.1985	0.5190	0.1505	1.1145	0.0300

Time	07:00	08:00	09:00	10:00	11:00	12:00
z [m]	$v_w(z)$ [m/s]	$v_w(z)$ [m/s]	$v_w(z)$ [m/s]	$v_w(z)$ [m/s]	$v_w(z)$ [m/s]	$v_w(z)$ [m/s]
10.0	0.7385	0.2710	1.1600	1.3940	1.1466	1.9010
20.0	0.6670	0.1970	1.0450	1.3820	1.3905	1.7160
40.0	0.9615	0.3055	1.1890	1.9505	1.8505	1.9445
65.0	0.6725	0.0355	1.0630	2.0215	1.7360	1.7540
96.0	0.2620	0.2535	1.0950	1.8080	1.9360	2.0585

Time	13:00	14:00	15:00	16:00	17:00	18:00
z [m]	$v_w(z)$ [m/s]	$v_w(z)$ [m/s]	$v_w(z)$ [m/s]	$v_w(z)$ [m/s]	$v_w(z)$ [m/s]	$v_w(z)$ [m/s]
10.0	1.9105	1.3220	2.3495	1.5910	1.0295	0.6020
20.0	1.8120	1.3940	2.2050	1.6150	1.0580	1.0355
40.0	2.1110	1.5345	2.2780	2.0890	1.5165	1.5905
65.0	2.0740	1.4290	2.4060	1.7330	1.2440	1.6135
96.0	2.1430	1.2350	2.6875	2.1375	1.4910	1.4290

Time	19:00	20:00	21:00	22:00	23:00	24:00
z [m]	$v_w(z)$ [m/s]	$v_w(z)$ [m/s]	$v_w(z)$ [m/s]	$v_w(z)$ [m/s]	$v_w(z)$ [m/s]	$v_w(z)$ [m/s]
10.0	0.5900	1.0465	1.9855	1.4875	0.9305	0.0000
20.0	1.1780	1.5955	2.6920	1.7135	1.3685	0.8300
40.0	1.7810	2.9040	3.3390	2.4410	2.7070	1.5800
65.0	1.9850	3.8700	3.5885	3.6540	3.8650	2.7000
96.0	1.9565	4.0610	4.4175	4.4685	4.0260	3.1200

Table B-3: Meteorological parameters extracted from the wind speeds and ambient temperatures measured at Kendal.

	Time					
Parameter	01:00	02:00	03:00	04:00	05:00	06:00
θ_0, °C	8.560	6.365	6.582	5.637	5.142	4.376
θ_*, °C	0.119	0.109	0.118	0.130	0.203	0.155
v_*, m/s	0.083	0.040	0.040	0.040	0.106	0.040
L, m	10.519	2.690	2.474	2.255	9.883	1.880
z_p, m	46.886	16.496	15.819	15.103	51.163	13.791
z_c, m	11.488	4.255	4.104	3.942	12.864	3.641

	Time					
Parameter	07:00	08:00	09:00	10:00	11:00	12:00
θ_0, °C	6.790	N/A	23.806	25.447	27.340	29.134
θ_*, °C	0.141	N/A	-1.555	-1.172	-1.377	-1.409
v_*, m/s	0.053	N/A	0.134	0.192	0.171	0.191
L, m	3.633	N/A	-2.110	-5.809	-3.962	-4.825
z_p, m	22.031	N/A	837.960	1204.207	1074.467	1197.131
z_c, m	5.673	N/A	83.796	120.421	107.447	119.713

	Time					
Parameter	13:00	14:00	15:00	16:00	17:00	18:00
θ_0, °C	28.213	29.770	29.459	27.864	22.391	15.668
θ_*, °C	-1.045	-1.374	-0.998	-0.825	-0.145	0.132
v_*, m/s	0.194	0.151	0.221	0.176	0.114	0.101
L, m	-6.767	-3.133	-9.155	-7.100	-16.955	14.384
z_p, m	1219.357	949.391	1383.399	1107.222	718.176	60.409
z_c, m	121.936	94.939	138.340	110.722	71.817	14.637

	Time					
Parameter	19:00	20:00	21:00	22:00	23:00	24:00
θ_0, °C	13.622	13.782	12.501	12.534	11.576	9.333
θ_*, °C	0.172	0.157	0.127	0.099	0.106	0.119
v_*, m/s	0.121	0.217	0.215	0.152	0.135	0.065
L, m	15.695	55.451	67.201	42.458	31.106	6.454
z_p, m	68.969	173.887	190.598	127.096	102.471	32.388
z_c, m	16.855	39.553	42.274	28.581	23.583	8.107

APPENDIX C

ENTRAINMENT OF ATMOSPHERIC AIR BY THE PLUME AND ITS INFLUENCE ON THE FLOW PATTERN IN THE VICINITY OF A NATURAL DRAFT COOLING TOWER

C.1 INTRODUCTION

Uncertainties arise when one calculates numerically the supply of ambient air to a natural draft cooling tower during windless conditions, since the boundary conditions at the free boundaries are indeterminate. Even if the free inflow boundary is removed sufficiently far away from the tower in order to diminish the influence of the free boundary on the tower, physically unrealistic solutions may result since the velocities on the boundaries are of the same order of magnitude as round off errors. Furthermore, due to the extensive calculation domain, such a solution procedure may prove very costly in computational time. One of the main concerns of this study is to obtain a sound model to predict the air flow pattern through and around a natural draft cooling tower for use in the evaluation of the tower performance under non-adiabatic atmospheric conditions. Naturally, no such problems arise in the presence of cross-winds, since the wind velocity will generally exceed the velocities induced by the suction of the tower by a few orders of magnitude far away from the tower.

At the inlet of a cooling tower, two opposing effects determine the air flow. On the one hand, the tower draws in air from various altitudes. This downward motion is opposed by the upward entrainment of atmospheric air by the plume. Considering the fact that the plume engulfs approximately 10 % of its own volume flow per unit length, it is evident that the entrainment accounts for a significant portion of the total air flow. The balance between these two effects will determine the actual flow pattern in the vicinity of the tower. In natural draft towers, the plume and the tower inlet is removed in the order 100 m - 150 m from each other by the tower shell, which tends to diminish the effect of the plume close to the tower inlet.

In this study, only round, fully developed turbulent plumes, discharging into a surrounding ambient of the same fluid, will be considered. The motion is taken positive if directed upwards. Boussinesq's approximation will be used throughout, i.e. density differences are neglected everywhere except in the buoyancy terms.

C.2 ENTRAINMENT IN JETS AND PLUMES

The entrainment of non-turbulent fluid into a turbulent jet or plume in a uniform atmosphere was studied by Morton, Taylor and Turner [56MO1], [57MO1], [58TA1], [59MO1], whilst experimental investigations were done by Schmidt [41SC1], Rouse, Yih and Humphereys [52RO1], and Ricou and Spalding [61RI1]. This work was extended by Abraham and Eysink [69AB1], Fox [70FO1], and Hirst [71HI1] to cover plumes in non-uniform environments, and plumes discharged into a cross-wind, whilst Turner [73TU1], Rajaratnam [76RA1] (jets only) and Gebhart et al. [88GE1] captured the results of the research efforts in textbooks.

Morton [56MO1] adopted a "top hat" velocity profile for the plume (i.e. the velocity inside the plume at any cross-section through it is equal to the average velocity at that section, while the air outside the plume is stagnant) showed that the entrainment rate is proportional to the mean jet or plume velocity, whilst Townsend [70TO1] arrived at the same conclusion, considering the nature of turbulence. Thus

$$v_e = a_e \overline{v}_z \qquad \ldots (C\text{-}1)$$

with a_e a characteristic constant. These observations were confirmed by the experimental results of Ricou and Spalding [61RI1], who also found that the entrainment coefficient for plumes is slightly higher than that for jets.

This lead Fox [70FO1] to the conclusion that the entrainment coefficient is in part dependent on buoyancy as well. Combining the integral forms of the conservation

equations for mass, momentum and mechanical energy, Fox found, after some processing, an expression for the entrainment rate in terms of the other parameters

$$v_e = \left[a_1 + \frac{a_2}{Fr} \right] v_{z0} \qquad \ldots (C\text{-}2)$$

The densimetric Froude number, Fr, is an indication of the ratio of inertia to buoyancy and is defined as

$$Fr = \frac{v_{z0}^2}{g\left[(\rho_\infty - \rho)/\rho\right] b} \qquad \ldots (C\text{-}3)$$

In equation (C-2), the entrainment increases for decreasing Froude numbers, which helps to reconcile the difference in entrainment coefficients for jets and plumes. If there is a temperature inversion in the surrounding atmosphere, the buoyancy of the plume is continuously decreasing, and may eventually become negative as the plume rises above a equilibrium height. In addition, the vertical mean velocity is also decreasing to zero, so that the magnitude of the Froude number is also decreasing. Eventually, the entrainment coefficient will change sign, resulting in a net horizontal velocity out of the plume, and the plume is trapped in the inversion layer. In a stably stratified atmosphere, Morton's [56MO1] model exhibits a singularity in the plume radius, that goes to infinity at the maximum penetration height. Physical observations supports Fox's model, that is able to predict the plume shape depicted in figure C-1.

Hirst [71HI1] studied the dispersion of buoyant plumes into an atmosphere subject to a cross-wind, and he concluded that the numerical values chosen for a_1 and a_2 cannot be obtained theoretically, and it must be derived from laboratory experiments. He suggested

$$a_e = 0.057 + \frac{0.097}{Fr} \qquad \ldots (C\text{-}4)$$

C.3 PLUME RISE IN A STABLY STRATIFIED ATMOSPHERE

The presence of an atmospheric inversion is known to have a particularly unfavourable influence on the plume's ability to rise for two reasons. First, an inverted atmosphere is a stable one that inhibits any vertical motion of itself, or anything injected into it. Secondly, ground based inversions usually occur in the absence of winds whose turbulence promotes the dispersion of the plume. Because cooling towers are usually large sources, the ratio of plume height to source radius for them are expected to be much smaller than those produced in laboratory experiments [74SN1]. For this reason, smoke stacks, that may emit harmful gases, are sufficiently tall (200 m and higher) to enable the plume to penetrate ground based inversions and disperse pollutants more evenly.

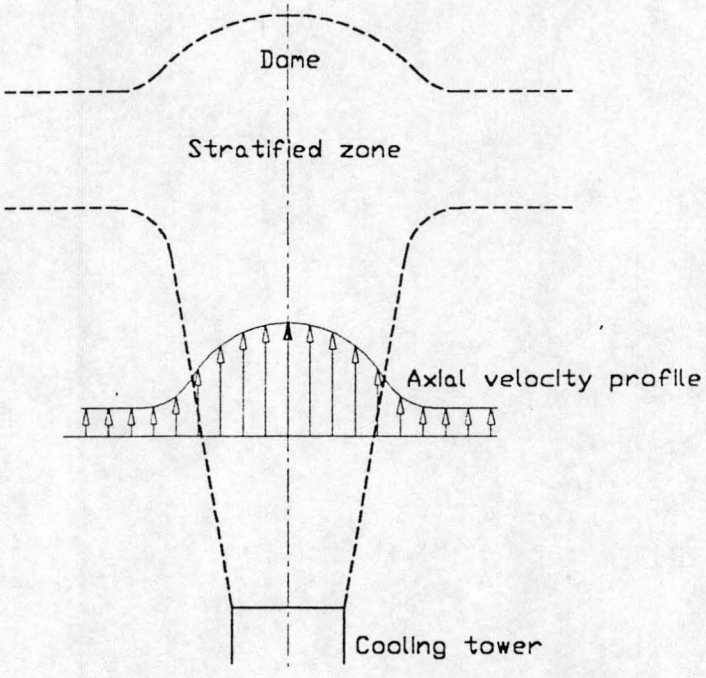

Figure C-1. Plume rise in a stably stratified ambient.

In the presence of a temperature inversion, the visible portion of a smoke filled plume has three clearly discernible heights [74SN1] that are indicated in figure C-1. Directly over the source there is a domelike region where the plume reaches its maximum height. The

plume gas that spills out of this dome is negatively buoyant and sinks to lower levels before reaching neutral buoyancy, and the plume will spread out indefinitely within the confines of this layer. As a result two other levels are observed, which are the upper and lower stratified boundaries of the sideways spreading plume. It is between these two levels that the effluent from the source is eventually stored in a stably stratified environment.

Initially, the jet is accelerated by buoyancy, causing the plume centreline velocity to increase. The net buoyancy force on the plume is decreased as the plume moves upwards due to entrainment of denser ambient fluid into the plume. In addition, for a stably stratified ambient, the ambient density also decreases with elevation. Thus, as the plume ascends, its density difference relative to its ambient steadily decreases, and is eventually reduced to zero. At this stage, there is no accelerating force, but the flow will continue upward by virtue of its upward momentum. However, it will now be subjected to a negative buoyancy force that will oppose, and eventually stop its upward motion. At this level of maximum penetration, the plume fluid is denser than the local surroundings, and will cascade downwards around the upward flow, and ultimately spread out laterally at a level of neutral buoyancy. This is often observed in the early morning in winter, when smoke from a fire or a short smoke-stack spreads out in a relatively thin horizontal layer.

As the buoyancy is decreasing, the Froude number also decreases, and may even become negative. The entrainment rate is affected in the process. Sneck and Brown [74SN1] investigated plume rise in a stably stratified environment experimentally. Based on their experimental evidence, it appears that the entrainment theory of Fox [70FO1] accurately predicts the maximum height of rise of a buoyant plume over a wide range of atmospheric conditions. Fox's model is also consistent with the dispersion of smoke plumes above a fire in a sugar cane field, as described by Morton [56MO1].

A plume will also rise indefinitely in an unstable atmosphere, but the buoyancy force acting on the plume air will exceed that acting on the same plume in an adiabatic

atmosphere. Hence, the plume will accelerate at a faster rate, and its centerline velocity will be higher than when the same plume is ejected into an adiabatic ambient.

C.4 SUPPLY OF FREE AIR TO COOLING TOWER

As far as the far field is concerned, the flow pattern induced by a cooling tower and its plume will behave like a potential flow, resulting in a considerable simplification of the mathematics involved in solving the flow field without losing accuracy. Since the governing equation for a potential flow is the La Place equation, the inherent linearity of the equation permits one to separate the tower inlet from the plume. The final solution of the air flow field in the vicinity of the tower is then obtained through superposition of the two individual solutions.

C.4.1 ENTRAINMENT OF AMBIENT AIR BY THE PLUME

Consider a buoyant plume with origin at point p(0,0,0) in a spherical polar co-ordinate set, as shown in figure C-2. The plume will spread out, but accelerate continuously under the influence of the buoyancy force, and Taylor [58TA1] has shown that the plume centreline velocity varies with $z^{1/3}$ in an adiabatic atmosphere.

Define a Stokes stream function $\psi(R,\theta,\phi)$ such that the components of the velocity vector are given by

$$v_R = \frac{1}{R^2 \sin\theta} \frac{\partial \psi}{\partial \theta}$$

and

$$v_\theta = \frac{1}{R \sin\theta} \frac{\partial \psi}{\partial R}$$

respectively. The flow is independent of the longitude angle ϕ, hence the third velocity component is disregarded. The continuity equation for steady, incompressible flow in terms of the stream function ψ in spherical co-ordinates is

$$\frac{1}{R^2}\frac{\partial}{\partial R}\left(R^2\frac{\partial \psi}{\partial R}\right)+\frac{1}{R^2\sin\theta}\frac{\partial}{\partial \theta}\left(\sin\theta\frac{\partial \psi}{\partial \theta}\right)=0 \qquad \ldots (C\text{-}5)$$

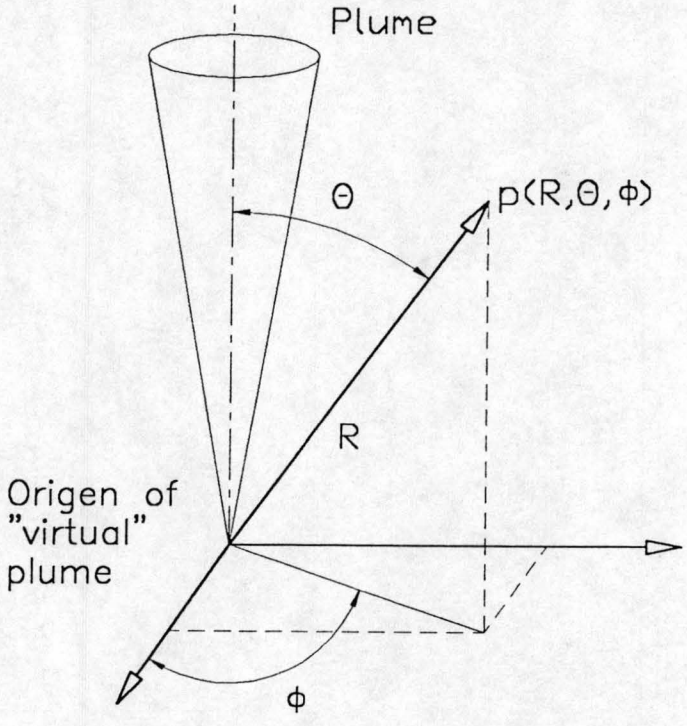

Figure C-2. Definition sketch for entrainment of ambient air by plume.

Let

$$\psi(R,\theta)=F(R)\times G(\theta) \qquad \ldots (C\text{-}6)$$

Substitute equation (C-6) with its relevant derivatives into equation (C-5) and re-arrange terms to find

$$\left(R^2 F'' + 2RF'\right)/F = -\left[G'' + \frac{\cos\theta}{\sin\theta}G'\right]/G = \lambda^2 \qquad \ldots (C\text{-}7)$$

with λ^2 an arbitrary real constant. With $\lambda^2 = n(n+1)$, equation (C-7) is separated into two ordinary differential equations,

$$R^2 F'' + 2RF' - n(n+1)F = 0$$

that is Euler's differential equation, with solution

$$F(R) = a_1 R^n + \frac{a_2}{R^{n+1}} \qquad \ldots (C\text{-}8)$$

and

$$G'' + \frac{\cos\theta}{\sin\theta}G' + n(n+1)G = 0$$

that is Legendre's differential equation, with solution

$$G(\theta) = c_1 P_n(\cos\theta) + c_2 Q_n(\cos\theta) \qquad \ldots (C\text{-}9)$$

with $P_n(\cos\theta)$ and $Q_n(\cos\theta)$ Legendre functions of degree n. Since finite solutions on the domain $0 \le \theta \le \pi$ are required, $c_2 = 0$, since Q_n is unbounded in this region. Furthermore, $R^{-(n+1)}$ has a singular point at $R = 0$ that renders it unfit for use, and it follows that $a_2 = 0$. Thus the only permissible solution left is

$$\psi(R,\theta) = A_n R^n P_n(\cos\theta) \qquad \ldots (C\text{-}10)$$

Taylor [58TA1] has shown that as far as the inflow of ambient air is concerned, the plume may be represented by a line-sink along the $\theta = 0$ axis. The sink strength is chosen to match the entrainment of atmospheric air by the plume. Hence, on the $\theta = 0$

axis, $\psi(R, 0)$ must match the centreline velocity of a plume as predicted by Taylor, i.e. $v_0 \propto z^{1/3}$. This gives a sink strength proportional to $z^{2/3}$ [58TA1], thus

$$\psi(R,0) = \int_0^R \frac{a\xi^{2/3}}{4\pi}\cos\theta \, d\xi = \frac{3a}{20\pi}R^{5/3} \qquad \text{... (C-11)}$$

with ξ a dummy variable. By inspection, it follows that n = 5/3, since equations (C-10) and (C-11) must be identical.

The above equation describes the flow field arising due to the entrainment of ambient air by a plume with its source in an unlimited three dimensional space. For a plume originating from a source within an infinite horizontal plane, the flow field is obtained by reflecting the plume in this plane. Hence, the impervious plane is converted into a plane of symmetry, but due to the frictionless nature of potential flow, the two cases are identical. Hence, invoking the linearity of the La Place equation, the solution for this flow field is immediately written, making use of superposition

$$\psi(R,\theta) = A_n R^{5/3}\left[P_{5/3}(\cos\theta) + P_{5/3}(-\cos\theta)\right] \qquad \text{... (C-12)}$$

Invoking some of the identities for Legendre functions, the above equation may be written in the form suggested by Taylor [58TA1] for $A_n = 1$.

$$\psi(R,\theta) = R^{5/3}\frac{d}{d\theta}\left[P_{2/3}(\cos\theta) + P_{2/3}(-\cos\theta)\right] \qquad \text{... (C-13)}$$

C.4.2 EFFECT OF THE TOWER INLET

The tower inlet may be represented by a point sink of strength M, where M is chosen such that the resulting mass flow matches the air flow rate through the tower. The stream function for a point sink is simply

$$\psi(R,\theta,\phi) = -\frac{M}{4\pi}\cos\theta \qquad \ldots (C\text{-}14)$$

C.4.3 COMBINED EFFECT OF TOWER INLET AND PLUME

The final solution for the air flow pattern induced by the tower and its plume in the vicinity of the tower is found through superposition

$$\psi(R,\theta,\phi) = -\frac{M}{4\pi}\cos\theta + A\,R^{5/3}\frac{d}{d\theta}\left[P_{2/3}(\cos\theta) + P_{2/3}(-\cos\theta)\right] \qquad \ldots (C\text{-}15)$$

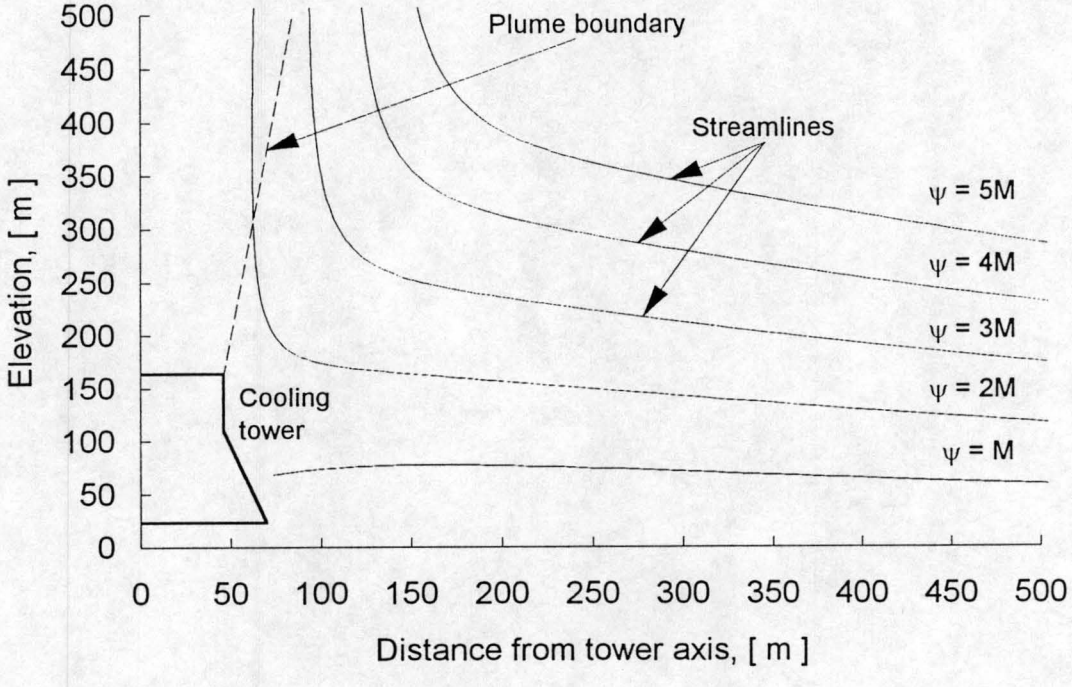

Figure C-3. Streamlines for potential flow in the vicinity of tower.

with the subscript n dropped in the coefficient A_n. The streamlines of the flow pattern described by equation (C-14) is shown in figure C-3. Note that the entrainment by the plume soon dominates the inlet effects, and that the air entering the tower comes from

relatively close to the ground. Even relatively close to the tower, the streamlines are essentially straight, a fact that is later exploited in numerical flow analysis.

The derivation above was limited to the air flow field induced by a natural draft cooling tower and its plume in an adiabatic atmosphere. A temperature inversion will distort this flow pattern, since the inversion will inhibit vertical movement of the plume. However, this should pose no serious problems, since with Fox's model, it is possible to predict the plume's centreline velocity for any atmospheric condition. This velocity is then used as a boundary condition. Thus, although the mathematics may become complex, the same general principle of matching the sink strength to the plume velocity is still applicable.

APPENDIX D

LISTING OF THE PHOENICS COMMUNICATION FILES FOR KENDAL NATURAL DRAFT DRY-COOLING TOWER SIMULATION

D.1 STANDARD Q1.DAT FILE FOR KENDAL TOWER

```
**************************************************************
TALK=T
RUN(1,1)
VDU=T4107
**************************************************************
DATE:          07 - 02 - 1992
CREATED by:    J.E. Hoffmann
**************************************************************
```

GROUP 1. Run title and other preliminaries

```
TEXT(NATURAL DRAUGHT DRY-COOLING TOWER)
**************************************************************
This run illustrates the buoyancy induced flow arising through a natural draft dry-
cooling tower.  The tower shell is cylindrical at the outlet.
**************************************************************
```

NOMENCLATURE

Afr	Frontal area of heat exchanger
Aratio	Ration of open area to total inlet area
Atube	Combined water side area of all tubes
Anu	Coefficient in correlation for heat transfer coefficient
Ary	Coefficient in correlation for pressure loss coefficient
Bnu	Exponent in correlation for heat transfer coefficient
Bry	Exponent in correlation for pressure loss coefficient
Cpair	Specific heat of air
Cpwtr	Specific heat of liquid water
Fcor	LMTD correction factor for crossflow heat exchanger
GAMMA	Isentropic compression exponent for air
GHwtr	Water side heat transfer coefficient
GRAV	Gravitational acceleration
Hin	Tower inlet height
Hout	Tower exit height
Kair	Linear heat transfer coefficient of air
Kstr	Tower support struts pressure loss coefficient
MUair	Dynamic viscosity of air
Mwtr	Water mass flow rate
NY	Number of grid cells in radial direction
NZ	Number of grid cells in axial direction
Patm	Atmospheric pressure

```
          PI              Mathematical constant
          PRair           Air Prandtl number to power 1/3
          Rair            Gas constant for air
          Rin             Tower inlet radius
          RHOatm          Density of atmospheric air
          Rout            Tower exit radius
          THETA           Angle spanning sector of tower under investigation
          Tin             Inlet water temperature
*****************************************************************
          DECLARATION OF VARIABLES
          SECTION 1:      Declare integers
INTEGER(NYamb,NYtow,NZexc,NZin,NZtow,NZplm)
          SECTION 2:      General constants
REAL(GRAV,PI)
          SECTION 3:      Variables describing tower geometry
REAL(Afr,Aratio,Hin,Hout,Rin,Rout,THETA)
          SECTION 4:      Air and water properties
REAL(GAMMA,Cpair,Cpwtr,Kair,MUair,PRair,Rair)
          SECTION 5:      Atmospheric conditions
REAL(Patm,RHOatm,Tatm)
          SECTION 6:      Transport coefficients and correlations
REAL(Atube,Anu,Bnu,Ary,Bry,Fcor,GHwtr,Kstr)
          SECTION 7:      Station operation
REAL(Mwtr,Tin)
*****************************************************************
ALLOCATION OF VARIABLES
1.        Integers
NYamb=20; NYtow=30
NZin=10; NZexc=NZin+1; NZtow=20; NZplm=10
2.        General constants
GRAV=-9.8; PI=3.14159
3.        Tower geometry
Afr=; Aratio=Afr/(pi*Rin**2); THETA=PI/12.0
Hin=25.4; Hout=165.0
Rin=72.25; Rout=51.050
4.        Air and water properties
GAMMA=1.4; Cpair=1004.31; Cpwtr=4184.0; Rair=287.08
Kair=0.0516; MUair=1.868e-5; PRair=0.892
5.        Atmospheric conditions
Patm=84600.0; Tatm=15.6+273.15; RHOatm=Patm/Rair/Tatm
6.        Transport coefficients, etc
Atube=*****
Anu=*****; Bnu=*****
Ary=*****; Bry=*****
GHwtr=*****; Kstr=*****
7.        Station operation
Mwtr=*****; Tin=*****
*****************************************************************
```

GROUP 2. Transience; time-step specification

STEADY=T

GROUP 3. X-direction grid specification

GROUP 4. Y-direction grid specification

NY=NYamb+NYtow

YVLAST=500.0

GROUP 5. Z-direction grid specification

NZ=NZin+NZtow+NZplm

ZWLAST=500.0

GROUP 6. Body-fitted coordinates or grid distortion

BFC=T

NONORT=T

Set coordinates for body fitted grid

****

Domain 1A. Tower inlet

setpt(1,1,1,0.0,0.0,0.0); setpt(2,1,1,0.0,0.0,0.0)

setpt(1,1,11,0.0,0.0,24.5); setpt(2,1,11,0.0,0.0,24.5)

setpt(1,31,1,0.0,72.25,0.0); setpt(2,31,1,0.0,72.25,0.0)

setpt(1,31,11,0.0,72.25,24.5); setpt(2,31,11,0.0,72.25,24.5)

South border

domain(1,2,1,1,1,11)

setlin(xc,0.0); setlin(yc,0.0); setlin(zc,zl*lnk)

High border

domain(1,2,1,31,11,11)

setlin(xc,0.0); setlin(yc,yl*lnj); setlin(zc,Hin)

North border

domain(1,2,31,31,1,11)

setlin(xc,0.0); setlin(yc,Rin); setlin(zc,zl*lnk)

Low border

domain(1,2,1,31,1,1)

setlin(xc,0.0); setlin(yc,yl*lnj); setlin(zc,0.0)

Get corner coordinates

domain(1,2,1,31,1,11)

magic(T)

****

Domain 1B. Atmosphere adjacent to tower inlet

setpt(1,51,1,0.0,500.0,0.0); setpt(2,51,1,0.0,500.0,0.0)

setpt(1,51,11,0.0,500.0,24.5); setpt(2,51,11,0.0,500.0,24.5)

High border

domain(1,2,31,51,11,11)

setlin(xc,0.0); setlin(yc,yf+(yl-yf)*lnj); setlin(zc,Hin)

North border

domain(1,2,51,51,1,11)

setlin(xc,0.0); setlin(yc,500.0); setlin(zc,zf+(zl-zf)*lnk)

Low border

domain(1,2,31,51,1,1)

setlin(xc,0.0); setlin(yc,yf+(yl-yf)*lnj); setlin(zc,0.0)

Get corner coordinates

domain(1,2,31,51,1,11)

```
magic(T)
************************************************************
```

Domain 2A: Cooling tower

Define hyperbolic shell profile

```
setpt(1,31,12,0.0,69.020,31.525); setpt(2,31,12,0.0,69.020,31.525)
setpt(1,31,13,0.0,65.961,38.550); setpt(2,31,13,0.0,65.961, 38.550)
setpt(1,31,14,0.0,63.101,45.575); setpt(2,31,14,0.0,63.101,45.575)
setpt(1,31,15,0.0,60.469,52.600); setpt(2,31,15,0.0,60.469,52.600)
setpt(1,31,16,0.0,58.095,59.625); setpt(2,31,16,0.0,58.095,59.625)
setpt(1,31,17,0.0,56.103,66.650); setpt(2,31,17,0.0,56.103,66.650)
setpt(1,31,18,0.0,54.255,73.675); setpt(2,31,18,0.0,54.255,73.675)
setpt(1,31,19,0.0,52.854,80.700); setpt(2,31,19,0.0,52.854,80.700)
setpt(1,31,20,0.0,51.839,87.725); setpt(2,31,20,0.0,51.839,87.725)
setpt(1,31,21,0.0,51.233,94.750); setpt(2,31,21,0.0,51.233,94.750)
setpt(1,31,22,0.0,51.051,101.775); setpt(2,31,22,0.0,51.051,101.775)
setpt(1,31,23,0.0,51.050,108.800); setpt(2,31,23,0.0,51.050,108.800)
setpt(1,31,24,0.0,51.050,115.825); setpt(2,31,24,0.0,51.050,115.825)
setpt(1,31,25,0.0,51.050,122.850); setpt(2,31,25,0.0,51.050,122.850)
setpt(1,31,26,0.0,51.050,129.875); setpt(2,31,26,0.0,51.050,129.875)
setpt(1,31,27,0.0,51.050,136.900); setpt(2,31,27,0.0,51.050,136.900)
setpt(1,31,28,0.0,51.050,143.925); setpt(2,31,28,0.0,51.050,143.925)
setpt(1,31,29,0.0,51.050,150.950); setpt(2,31,29,0.0,51.050,150.950)
setpt(1,31,30,0.0,51.050,157.975); setpt(2,31,30,0.0,51.050,157.975)
setpt(1,31,31,0.0,51.050,165.000); setpt(2,31,31,0.0,51.050,165.000)
```

On central Z-axis

```
setpt(1,1,31,0.0,0.0,Hout); setpt(2,1,31,0.0,0.0,Hout)
```

South border

```
domain(1,2,1,1,11,31)
setlin(xc,0.0); setlin(yc,0.0); setlin(zc,zf+(zl-zf)*lnk)
```

High border

```
domain(1,2,1,31,31,31)
setlin(xc,0.0); setlin(yc,yf+(yl-yf)*lnj); setlin(zc,Hout)
```

Get corner coordinates

```
domain(1,2,1,31,11,31)
magic(T)
************************************************************
```

Domain 2B. Atmosphere adjacent to tower shell

```
setpt(1,51,31,0.0,500.0,120.0); setpt(2,51,31,0.0,500.0,120.0)
```

High border

```
domain(1,2,31,51,31,31)
setlin(xc,0.0); setlin(yc,yf+(yl-yf)*lnj); setlin(zc,Hout)
```

North border

```
domain(1,2,51,51,11,31)
setlin(xc,0.0); setlin(yc,500.0); setlin(zc,zf+(zl-zf)*lnk)
```

Get corner coordinates

```
domain(1,2,31,51,11,31)
magic(T)
************************************************************
```

Domain 3A. Plume

```
setpt(1,1,51,0.0,0.0,300.0); setpt(2,1,51,0.0,0.0,300.0)
setpt(1,31,51,0.0,29.0,300.0); setpt(2,31,51,0.0,29.0,300.0)
        South border
domain(1,2,1,1,31,51)
setlin(xc,0.0); setlin(yc,0.0); setlin(zc,zf+(zl-zf)*lnk)
        High border
domain(1,2,1,31,51,51)
setlin(xc,0.0); setlin(yc,yf+(yl-yf)*lnj); setlin(zc,300.0)
        North border
domain(1,2,31,31,31,51)
setlin(xc,0.0); setlin(yc,Rout); setlin(zc,zf+(zl-zf)*lnk)
        Get corner coordinates
domain(1,2,1,31,31,51)
magic(T)
```

****

Domain 3B. Atmosphere adjacent to plume

```
setpt(1,51,51,0.0,500.0,300.0); setpt(1,51,51,0.0,500.0,300.0)
        High border
domain(1,2,31,51,51,51)
setlin(xc,0.0); setlin(yc,yf+(yl-yf)*lnj); setlin(zc,300.0)
        North border
domain(1,2,51,51,31,51)
setlin(xc,0.0); setlin(yc,500.0); setlin(zc,zf+(zl-zf)*lnk)
        Get corner coordinates
domain(1,2,31,51,31,51)
magic(T)
```

****

```
        Change from Cartesian to Cylindrical Polar coordinates
domain(2,2,1,51,1,51)
setlin(xc,yc*sin(theta)); setlin(yc,yc*cos(theta))
```

****

GROUP 7. Variables stored, solved & named

```
DEN1=40
NAME(DEN1)=DENS
SOLVE(V1,W1,H1)
SOLUTN(P1,Y,Y,Y,N,N,N)
STORE(DENS)
```

GROUP 8. Terms (in differential equations) & devices

```
TERMS(H1,N,Y,Y,N,Y,N)
```

GROUP 9. Properties of the medium

```
PRESS0=Patm
RHO1B=1.0/Rair; RHO1C=1.0/GAMMA; RHO1=GRND5; DRH1DP=GRND5
TMP1A=0.0; TMP1B=1.0; TMP1=GRND2
PRNDTL(H1)=0.707; ENUL=1000.0*MUair
```

GROUP 10. Inter-phase transfer processes and properties

GROUP 11. Initialization of variable or porosity fields

```
RESTART(ALL)
FIINIT(P1)=0.0; FIINIT(V1)=0.0; FIINIT(W1)=0.0; FIINIT(H1)=Tatm
```

FIINIT(DENS)=RHOatm

Set small values for variables in tower to speed up convergence

PATCH(TOW,INIVAL,1,1,1,NYtow,1,NZ,1,1)
INIT(TOW,W1,0.0,2.0); INIT(TOW,H1,0.0,Tatm+30.0)

Set porosities for shell and ground to zero

CONPOR(0.0,NORTH,1,1,-NYtow,-NYtow,NZin+1,NZin+NZtow)
CONPOR(0.0,LOW,1,1,1,NY,-1,-1)

Set porosity for heat exchanger

CONPOR(0.43,LOW,1,1,1,NYtow,NZexc,NZexc)

GROUP 12. Convection and diffusion adjustments

GROUP 13. Boundary conditions and special sources

Inflow of ambient air

PATCH(INLET,NORTH,1,1,NY,NY,1,NZ,1,1)
COVAL(INLET,P1,FIXP,0.0); COVAL(INLET,V1,ONLYMS,SAME)
COVAL(INLET,W1,ONLYMS,SAME); COVAL(INLET,H1,ONLYMS,Tatm)

Pressure drop at tower support struts

PATCH(STRUTS,NORTH,1,1,NYtow,NYtow,1,NZin,1,1)
COVAL(STRUTS,V1,GRND,0.0)

Heat transfer and pressure loss at heat exchanger

PATCH(EXCHGR,LOW,1,1,1,NYtow,NZexc,NZexc,1,1)
COVAL(EXCHGR,V1,FIXVAL,0.0); COVAL(EXCHGR,W1,GRND1,0.0)
COVAL(EXCHGR,H1,GRND3,GRND3)

Exit of plume

PATCH(EXIT,HIGH,1,1,1,NY,NZ,NZ,1,1)
COVAL(EXIT,P1,FIXP,0.0)

Buoyancy activated over entire domain

PATCH(BUOY,PHASEM,1,1,1,NY,1,NZ,1,1)
COVAL(BUOY,V1,FIXFLU,GRND2); COVAL(BUOY,W1,FIXFLU,GRND2)

GROUP 14. Downstream pressure for PARAB=.TRUE.

GROUP 15. Termination of sweeps

LSWEEP=125

GROUP 16. Termination of iterations

LITER(P1)=50

GROUP 17. Under-relaxation devices

RELAX(V1,FALSDT,0.3); RELAX(W1,FALSDT,0.3)
RELAX(H1,FALSDT,0.3); RELAX(P1,LINRLX,0.2)

GROUP 18. Limits on variables or increments to them

VARMAX(DENS)=RHOatm
VARMIN(H1)=Tatm; VARMAX(H1)=Tin

GROUP 19. Data communicated by satelite to GROUND

USEGRD=T

Variables for use in GXBUOY

RSG1=RHOatm; RSG10=GRAV

User defined variables transfered to GROUND

IG(1)=NYtow; IG(2)=NZexc
RG(1)=Mwtr; RG(2)=Tin; RG(3)=Cpwtr; RG(4)=Afr; RG(5)=Atube
RG(6)=Tatm; RG(7)=Patm; RG(8)=Cpair; RG(9)=MUair; RG(10)=Kair
RG(11)=PRair; RG(12)=Anu; RG(13)=Bnu; RG(14)=Fcor; RG(15)=Ary
RG(31)=Bry; RG(17)=Kstr; RG(18)=GHwtr; RG(19)=THETA; RG(20)=Aratio

GROUP 20. Preliminary print-out
GROUP 21. Print-out of variables
GROUP 22. Spot-value print-out
GROUP 23. Field print-out and plot control
GROUP 24. Dumps for restarts

STOP

D.2 GROUND.FOR SUBROUTINE FOR KENDAL COOLING TOWER SIMULATION

The coding presented here is compressed in such a way that only actual additions to the original empty GROUND.FOR subroutine is given. The user is referred to the PHOENICS REFERENCE MANUAL to ascertain where each addition fits into the larger GROUND.FOR file. In the listing, it will be indicated when some of the original coding has been omitted.

```
C       FILE NAME GROUND.DRY----------7 FEBRUARY 1992
C       THIS IS THE MAIN PROGRAM OF EARTH
C
C       (C) COPYRIGHT 1984, LAST REVISION 1987.
C       CONCENTRATION HEAT AND MOMENTUM LTD. ALL RIGHTS
C       RESERVED.
C       This subroutine and the remainder of the PHOENICS code are proprietary
C       software owned by Concentration Heat and Momentum Limited, 40 High
C       Street, Wimbledon, London SW19 5AU, England.
C
C
C   PROGRAM MAIN
C
---*****************************************************************---
                              MATERIAL OMITTED
---*****************************************************************---
C
C       USER SECTION STARTS:
C
C 1  Set dimensions of data-for-GROUND arrays here. WARNING: the
C    corresponding arrays in the MAIN program of the satellite
C    and EARTH must have the same dimensions.
        COMMON/LGRND/LG(20)/IGRND/IG(20)/RGRND/RG(100)
        COMMON/CGRND/CG(10)
        REAL Kair,Khe,Kstr,LMTD,MUair,Mwtr,NU
        LOGICAL LG
        CHARACTER*4 CG
C
C 2     User dimensions own arrays here, for example:
C       DIMENSION UUH(10,10),UUC(10,10),UUX(10,10),UUZ(10)
C
        DIMENSION GHair(30),GQtow(30),Gair(30),GArea(30,2),GUex(30),
        DIMENSION GMair(30),GTair(30),GTwtr(30)
C
C       Variables transfered from SATLITE to GROUND
```

```
C       Note that the line continuation mark should be in column 6, with the actual
C       FORTRAN statement starting in column 7.
C
        EQUIVALENCE(NYtow,IG(1)),(NZexc,IG(2))
        EQUIVALENCE(Mwtr,RG(1)),(Tin,RG(2)),(Cpwtr,RG(3)),
       *(Afr,RG(4)),(Atube,RG(5)),(Tatm,RG(6)),(Patm,RG(7)),
       *(Cpa,RG(8)),(MUair,RG(9)),(Kair,RG(10)),(PRair,RG(11)),
       *(Anu,RG(12)),(Bnu,RG(13)),(Fcor,RG(14)),(Ary,RG(15)),
       *(Bry,RG(31)),(Kstr,RG(17)),(GHwtr,RG(18)),(THETA,RG(19)),
       *(Aratio,RG(20))
C
C 3  User places his data statements here, for example:
C    DATA NXDIM,NYDIM/10,10/
C
---*****************************************************************---
                              MATERIAL OMITTED
---*****************************************************************---
C
C--- GROUP 13. Boundary conditions and special sources
C
  13    CONTINUE
        GO TO (130,131,132,133,134,135,136,137,138,139,1310,
        11311,1312,1313,1314,1315,1331,1317,1318,1319,1320,1331),ISC
 130    CONTINUE
C------------------- SECTION  1 ------- coefficient = GRND
C***
C***  Tower support struts pressure loss coefficient
C***
        CALL ONLYIF(V1,V1,'STRUTS')
        CALL FN31(CO,AUX(DEN1),V1,0.0,0.5*Kstr)
        CALL FN40(CO)
        RETURN
 131    CONTINUE
C------------------- SECTION  2 ------- coefficient = GRND1
C***
C***  Heat exchanger pressure loss coefficient
C***
C***  Khe=Ary*Ry^Bry with Ry=Gair/mu
C***
        CALL ONLYIF(W1,W1,'EXCHGR')
        L0CO=L0F(CO)
        L0W1=L0F(W1)
        L0RH=L0F(AUX(DEN1))
        DO 3100 IY=1,NYtow
                Gair(IY)=F(L0RH+IY)*F(L0W1+IY)
                Ry=Gair(IY)/MUair
                Khe=Ary*Ry**Bry
                F(L0CO+IY)=0.5*Gair(IY)*Khe
 3100   CONTINUE
```

```
      RETURN
  132 CONTINUE
C------------------ SECTION  3 ----- coefficient = GRND2
      RETURN
  133 CONTINUE
C------------------ SECTION  4 ----- coefficient = GRND3
C***
C***  Overall heat transfer coefficient for heat exchanger
C***
C***  Q = Cmin * EPSI * (Twi - Tai), with
C***  UA=1/(1/(GHair*Aair)+1/(GHwtr*Awtr))
C***  where
C***  GHair*Aair=Kair*PRair^(1/3)*Afr*Ny
C***  with
C***  Ny=Anu*Ry^Bnu where Ry=Gair/MUair
C***  and
C***  NTU = UA/Cmin
C***
      CALL ONLYIF(H1,H1,'EXCHGR')
      L0CO=L0F(CO)
      L0W1=L0F(W1)
      L0RH=L0F(AUX(DEN1))
      CALL GTIZYX(10,IZ,GArea,NYtow,2)
      DO 3200 IY=1,NYtow
            Gair(IY)=F(L0RH+IY)*F(L0W1+IY)
            Ry=Gair(IY)/MUair
            NU=Anu*Ry**Bnu
            GHair(IY)=Kair*PRair*NU*Aratio*GArea(IY,1)*
     *      (154.0/156.0)
            Awtr=(Atube/Afr)*Aratio*GArea(IY,1)
            GUex(IY)=1.0/(1.0/GHair(IY)+1.0/(GHwtr*Awtr))/
     *      GArea(IY,1)
            IF (Mwtr*Cpwtr).GE.(GMair*Cpa) THEN
                  Cmin=Mwtr*Cpwtr
            ELSE
                  Cmin=GMair*Cpa
            END IF
            GNTU=GUex/Cmin
            GEPSI=
            F(L0CO+IY)=Cmin*GEPSI
 3200 CONTINUE
      RETURN
  134 CONTINUE
---*****************************************************************---
                        MATERIAL OMITTED
---*****************************************************************---
C
C------------------ SECTION 15 --------- value = GRND3
C***
```

```
C***  Q=Cmin * EPSI * (Twi - Tai)
C***  For use by PHOENICS; VAL=Twi
C***
      CALL ONLYIF(H1,H1,'EXCHGR')
      L0VAL=L0F(VAL)
      DO 1350 IY=1,NYtow
      F(L0VAL+IY)=Tin
 1350 CONTINUE
      RETURN
 1315 CONTINUE
C------------------ SECTION 31 --------- value = GRND4
C
---*****************************************************************---
                          MATERIAL OMITTED
---*****************************************************************---
C
C--- GROUP 19. Special calls to GROUND from EARTH
C
  19 GO TO (191,192,193,194,195,196,197,198),ISC
 191 CONTINUE
C   * ------------------ SECTION 1 ---- START OF TIME STEP.
    RETURN
 192 CONTINUE
C   * ------------------ SECTION 2 ---- START OF SWEEP.
C***
C***  Initialize arrays containing air and water outlet temperatures
C***
    IF (ISWEEP.GT.FSWEEP) RETURN
    L0W1=L0F(W1)
    L0RH=L0F(AUX(DEN1))
    DO 1920 IY=1,NYtow
      Gair(IY)=F(L0W1+IY)*F(L0RH+IY)
      GTair(IY)=Tatm+30.0
      GTwtr(IY)=Tin-2.0*30.0*(Cpa/Cpwtr)*(Afr/Mwtr)
 1920 CONTINUE
    RETURN
 193 CONTINUE

C
---*****************************************************************---
                          MATERIAL OMITTED
---*****************************************************************---
C   * ------------------ SECTION 6 ---- FINISH OF IZ SLAB.
C***
C***  Calculating air mass flow rate and heat rejection rate for cell
C***
    IF (IZ.NE.NZexc) RETURN
    L0W1=L0F(W1)
    L0RH=L0F(AUX(DEN1))
```

```
      L0H1=L0F(H1)
      CALL GTIZYX(10,NZexc,GArea,NYtow,2)
      DO 1960 IY=1,NYtow
        GTair(IY)=F(L0H1+IY)
        Gair(IY)=F(L0W1+IY)*F(L0RH+IY)
        GMair(IY)=Gair(IY)*Aratio*GArea(IY,1)
        GQtow(IY)=GMair(IY)*Cpa*(F(L0H1+IY)-Tatm)
        GTwtr(IY)=Tin-GQtow(IY)/Cpwtr/(Mwtr*Aratio*GArea(IY,1)/Afr)
 1960 CONTINUE
      RETURN
  197 CONTINUE
C   * ------------------ SECTION 7 ---- FINISH OF SWEEP.
C***
C***  Heat rejected and mass flow for tower
C***
      IF (ISWEEP.NE.LSWEEP) RETURN
      GAsum=0.0
      GMsum=0.0
      GQsum=0.0
      GTsum=0.0
      CALL GTIZYX(10,NZexc,GArea,NYtow,2)
      DO 1970 IY=1,NYtow
        GAsum=GAsum+Garea(IY,1)
        GMsum=GMsum+GMair(IY)
        GQsum=GQsum+GQtow(IY)
        GTsum=GTsum+GTwtr(IY)*GArea(IY,1)
 1970 CONTINUE
      GMflow=GMsum*PI/THETA
      GQtowr=GQsum*PI/THETA
      GQwatr=GTsum/NYtow/GAsum
      WRITE(LUPR1,'(" Air mass flow rate through tower = ",
     *f15.5,"  kg/s")'),GMflow
      WRITE(LUPR1,'(" Amount of heat rejected by tower = ",
     *f15.5,"  Watt")'),GQtowr
      WRITE(LUPR1,'(" Mass mean cold water temperature = ",
     *f15.5," K")'),GTwatr
      RETURN
  198 CONTINUE
C---*****************************************************************---
                              MATERIAL OMITTED
C---*****************************************************************---
C
C--- GROUP 24. Dumps for restarts
C
   24 CONTINUE
      RETURN
      END
C*****************************************************************
```

APPENDIX E

TOWER PERFORMANCE DATA MEASURED AT KENDAL, AND THE CORRESPONDING PERFORMANCE PREDICTIONS BY PHOENICS

Table E-1. Actual tower performance data measured on 9 August 1990 at Kendal.

Time	T_{atm} [°C]	T_{aim} [°C]	T_{wi} [°C]	T_{wo} [°C]
01:00	10.29	13.42	39.21	29.84
02:00	8.03	13.19	37.41	28.29
03:00	8.25	12.72	37.60	28.50
04:00	7.88	11.90	37.67	28.14
05:00	7.65	11.85	36.96	27.55
06:00	6.99	12.52	37.74	28.45
07:00	7.64	12.48	38.37	28.85
08:00	13.34	13.97	43.76	31.98
09:00	17.13	14.44	44.57	32.56
10:00	18.62	15.94	45.04	33.75
11:00	19.91	17.24	42.39	33.19
12:00	21.48	18.12	43.16	33.80
13:00	22.14	19.16	44.36	35.26
14:00	23.35	19.96	45.22	35.74
15:00	23.55	20.41	45.52	36.18
16:00	23.59	20.75	45.39	36.12
17:00	22.29	20.68	45.52	36.23
18:00	18.46	19.77	45.11	35.75
19:00	16.29	19.21	50.50	38.16
20:00	14.96	18.53	46.15	35.69
21:00	13.28	17.06	43.00	33.75
22:00	13.48	16.08	43.07	33.50
23:00	12.77	15.37	42.71	32.86
24:00	11.98	15.03	41.18	31.60

Table E-2. Predicted performance (PHOENICS) of the Kendal towers in a stratified atmosphere.

Time	T_{ai} [°C]	T_{wi} [°C]	T_{wo} [°C]	m_a [kg/s]
01:00	12.26	37.14	28.40	32215.36
02:00	12.17	37.04	28.30	32230.51
03:00	13.32	38.27	29.53	32076.73
04:00	13.26	38.21	29.47	32081.20
05:00	12.55	37.45	28.71	32177.80
06:00	15.25	40.34	31.60	31833.94
07:00	14.49	39.52	30.78	31931.98
08:00	14.89	39.95	31.21	31876.84
09:00	16.10	41.25	32.51	31727.15
10:00	18.10	43.38	34.64	31472.34
11:00	19.87	45.29	36.55	31263.18
12:00	20.79	46.26	37.52	31143.35
13:00	21.44	46.96	38.22	31061.65
14:00	22.51	48.10	39.36	30935.42
15:00	22.52	48.11	39.37	30933.85
16:00	22.46	48.05	39.31	30943.26
17:00	20.88	46.36	37.62	31139.69
18:00	18.65	43.97	35.23	31405.19
19:00	17.75	43.01	34.27	31518.14
20:00	17.10	42.32	33.58	31602.00
21:00	15.15	40.23	31.49	31844.93
22:00	15.32	40.41	31.67	31822.42
23:00	14.45	39.48	30.74	31933.08
24:00	14.91	39.97	31.23	31873.54

Table E-3. Estimated tower performance with ground temperature as air inlet temperature. This is the equivalent adiabatic case for table E-2.

Time	T_{ai} [°C]	T_{wi} [°C]	T_{wo} [°C]	$\dot{m}_a$ [kg/s]
01:00	10.29	35.05	26.31	31993.03
02:00	8.03	32.62	23.88	32038.44
03:00	8.26	32.86	24.12	31727.46
04:00	7.88	32.46	23.72	31668.61
05:00	7.65	32.21	23.47	31436.81
06:00	6.99	31.51	22.77	31220.74
07:00	7.64	32.20	23.46	31599.13
08:00	13.34	38.29	29.55	32151.12
09:00	17.13	42.35	33.61	32268.00
10:00	18.62	43.93	35.19	31966.42
11:00	19.91	45.31	36.57	31662.29
12:00	21.48	47.00	38.26	31678.69
13:00	22.14	47.70	38.96	31581.69
14:00	23.35	49.00	40.26	31407.50
15:00	23.55	49.21	40.47	31512.83
16:00	23.59	49.25	40.51	31386.50
17:00	22.29	47.87	39.13	31321.57
18:00	18.46	43.78	35.04	31446.90
19:00	16.29	41.45	32.71	31439.59
20:00	14.96	40.02	31.28	31447.73
21:00	13.28	38.23	29.49	31732.29
22:00	13.48	38.44	29.70	31644.61
23:00	12.77	37.69	28.95	31857.88
24:00	11.98	36.84	28.10	31597.69

APPENDIX F

PROPERTIES OF FLUIDS

F.1 DRY AIR AT 101325 Pa AND FOR RANGE 220 K < T < 380 K

Density, in kg/m^3

$$\rho = \frac{p}{R\,T} \qquad \text{... (F.1-1)}$$

with p in Pascal, T in Kelvin and R = 287.08 J/kg K.

Specific heat, in J/kg K

$$c_p = 1.045356\times10^{3} - 3.161783\times10^{-1}\,T + 7.083814\times10^{-4}\,T^2 - 2.705209\times10^{-7}\,T^3$$

... (F.1-2)

Dynamic viscosity in kg/s m

$$\mu = 2.287973\times10^{-6} + 6.259793\times10^{-8}\,T - 3.131956\times10^{-11}\,T^2 + 8.150380\times10^{-15}\,T^3$$

... (F.1-3)

Thermal conductivity in W/K m

$$k = -4.937787\times10^{-4} + 1.018087\times10^{-4} - 4.627937\times10^{-8}\,T^2 + 1.250603\times10^{-11}\,T^3$$

... (F.1-4)

F.2 SATURATED WATER LIQUID FOR 273.15 K < T < 380 K

Density in kg/m^3

$$\rho = \left[1.49343\times10^{-3} - 3.7164\times10^{-6}\,T + 7.09782\times10^{-9}\,T^2 - 1.90321\times10^{-20}\,T^6\right]^{-1} \quad \ldots (F.2\text{-}1)$$

Specific heat in J/kg K

$$c_p = 8.15599\times10^{3} - 2.80627\times10^{1}\,T + 5.11283\times10^{-2}\,T^2 - 2.17582\times10^{-13}\,T^6 \quad \ldots (F.2\text{-}2)$$

Dynamic viscosity in kg/m s

$$\mu = 2.414\times10^{-5}\,10^{247.8/(T-140)} \quad \ldots (F.2\text{-}3)$$

Thermal conductivity in W/m K

$$k = -6.14255\times10^{-1} + 6.9962\times10^{-3}\,T - 1.01075\times10^{-5}\,T^2 + 4.74737\times10^{-12}\,T^4 \quad \ldots (F.2\text{-}4)$$

Latent heat of vaporization in J/kg

$$i_{fg} = 3.4831814\times10^{6} - 5.8627703\times10^{3}\,T + 1.2139568\times10^{1}\,T^2 - 1.40290431\times10^{-2}\,T^3 \quad \ldots (F.2\text{-}5)$$